Hybrid Adsorption + Liquefaction Process for Post-Combustion CO_2 Capture

by

Sunny Jitendra Pawar

A thesis submitted in partial fulfillment of the requirements for the degree of

Master of Science

in

Chemical Engineering

Department of Chemical and Materials Engineering
University of Alberta

Abstract

Greenhouse gas (GHG) emissions reduction through carbon capture and storage (CCS) will be pivotal in achieving the world's net zero emissions target by 2050. However, we have a long way to go before CCS is implemented at scale worldwide. Emerging technologies such as adsorption-based CO_2 capture have shown promise in treating flue gas streams with relatively high CO_2 partial pressures, such as the cement or steel industry. Despite their competitive advantages in energy efficiency in gas separation applications, they struggle to meet the scalability requirements compared to mature technologies like physical solvent absorption. In low CO_2 partial pressures, even with the best possible adsorbents, the capture costs for pressure-vacuum swing adsorption (PVSA) processes are significantly higher than the Mono-ethanolamine (MEA) absorption-based processes. Hence, it is imperative to explore and evaluate scalable and economically viable alternative options, which is critical in determining the success of CCS in cutting emissions.

This study aims to assess the effectiveness of a hybrid process that combines pressure-vacuum swing adsorption (PVSA) with liquefaction to determine if it is cost-effective and energy-efficient in capturing CO_2. Modelling and optimization studies are conducted for both processes independently to test the performance limits. The dynamic adsorption process is simulated using detailed first principles models consisting of a system of coupled partial differential equations of mass, heat and momentum transfer solved numerically in space and time. The liquefaction process is simulated using Aspen Plus® from AspenTechnology, a commercial process simulation software using the Peng-Robinson (PR) thermodynamics property package.

The hybrid process is optimized by minimizing the capture cost by constraining the recovery to at least 90 mol % of the CO_2 at a purity of 95 mol % from the overall process. The flue gas streams with CO_2 composition ranging from 3.5 - 30 mol %, representative of emissions from Natural-gas combined cycle (NGCC) power plants, coal-fired power plants, and cement and steel kilns, are studied. The variant of the PVSA process studied is a 4-step Light product pressurization (LPP) cycle. The performance of these processes for commercially available adsorbent materials like Zeolite 13X is studied. The liquefaction uses compression and refrigeration to purify CO_2 up to 95 mol %.

The hybrid process reduces the overall specific energy consumption and, thus, capital and operational costs by more than 50 % compared to a standalone PVSA process in the low CO_2 partial pressure ranges. It leverages the ability of the pressure-vacuum swing adsorption process to recover CO_2 at a high rate in the low CO_2 partial pressure ranges. In contrast, the liquefaction process takes the load of purifying it from an intermediate purity of 40-75 mol % to the desired purity of 95 mol % to deliver it at conditions suitable for transport and storage. The hybrid process reduces the number of parallel PVSA trains required to process the same amount of flue gas, thus improving the scalability of the process.

Preface

The models used for simulating pressure-vacuum swing adsorption (PVSA) processes, along with the costing and column scheduling models, were obtained from Dr. Sai Gokul Subraveti, an alumnus of the laboratory. These models were modified to evaluate the PVSA process performance and optimize it at reduced purity levels by the author. The author developed models for the liquefaction unit and its costing framework in Aspen Plus® and Aspen Process Economic Analyzer® software.

To my parents, mentors, and friends who always encouraged me to keep an inquisitive mind.

Acknowledgements

I want to thank my research supervisor, Dr. Arvind Rajendran, for believing in me and allowing me to learn and contribute to his research. Thank you for extending all possible support at every critical milestone from admission to graduation. His technical and non-technical discussions were precious and helped me broaden my horizons and think big.

I thank our colleagues at SINTEF Energy Research, Dr. Sai Gokul Subraveti, Dr. Simon Roussanaly and Dr. Rahul Anantharaman, for collaborating with us on this work by providing key inputs and feedback. I am grateful to adjunct professor Mr. William Pick for his support in reviewing our work and suggesting possible ways of improving our processes. Thank you to Dr. Jim Sawada for teaching us the art of storytelling through speechcraft workshops; this was very helpful when preparing for presentations at research conferences and events. I want to thank my colleagues Anjana, Bhubesh, Chinmay, Evelyn, Gwyn, Henry, Lauren, Nick, Noelie, Shanmuk, Sripradha, Harsha, Ravi and Yoga for making work fun, collaborating and providing honest feedback during mock presentations. I will cherish the memories made during our meetings at the university club.

I acknowledge the funding from our industry partner, Benchmark International's Oxygen Solutions Inc. (OSI), and funding agencies Future Energy Systems (FES) and NSERC Alliance Grant. I thank Josh Tolley for helping us with the industrial visits to OSI and showing us how large-scale oxygen concentrators are built at their Edmonton facility. I acknowledge the Digital Research Alliance of Canada, formerly Compute Canada, for providing the computational resources used in this study.

I want to thank Shanmuk, Harsha, Ravi, and Devavrat for our time together during lunch hours, on the weekends at the temple, exploring restaurants and the occasional road trips to the Rocky Mountains. I am eternally grateful to my parents and relatives for their unconditional love, support and trust, without which this degree would not have been possible.

Table of Contents

List of Tables

List of Figures

Chapter 1

Introduction

The imperative for carbon capture and storage (CCS) lies in the pressing global challenge of mitigating climate change. Carbon dioxide (CO_2) emissions, primarily from burning fossil fuels, continue to drive a dangerous rise in atmospheric greenhouse gases, intensifying the effects of global warming [1]. As the Paris Agreement outlines, the urgent need to limit global temperature increases to below 2°C reduce CO_2 eminently [2]. CCS technology is critical to these efforts by capturing CO_2 emissions from industrial processes and power generation, preventing their release into the atmosphere. This helps curtail the warming effect and offers opportunities for CO_2 storage and CO_2 utilization in producing valuable products, contributing to the circular carbon economy [3].

1.1 Post-combustion CO_2 Capture

Carbon capture and storage (CCS) is not a new concept, and it has been practiced in the oil and gas industry for several decades, with the captured CO_2 used for applications like enhanced oil recovery or sent for geological sequestration. The technology of choice is a solvent-based absorption process wherein flue gas containing CO_2 is contacted with the amine-based solvent counter-currently in the absorption tower [4]. As the gas flows upwards, CO_2 is preferentially absorbed into the solvent while the other gases exit the top of the tower. The solvent, now saturated with CO_2, leaves the bottom of the absorption tower and needs to be regenerated before it can be recycled back to the absorption tower for continuous operation. Solvent regeneration occurs in the stripping tower, where the solvent is heated to a higher temperature, most commonly using steam as the heating utility. CO_2 is stripped from the solvent and exits the top of the stripper. The regenerated solvent is recycled back to the absorption tower, with some heat recovered through heat integration. Figure 1.1 illustrates a typical amine absorption-based post-combustion CO_2 capture process.

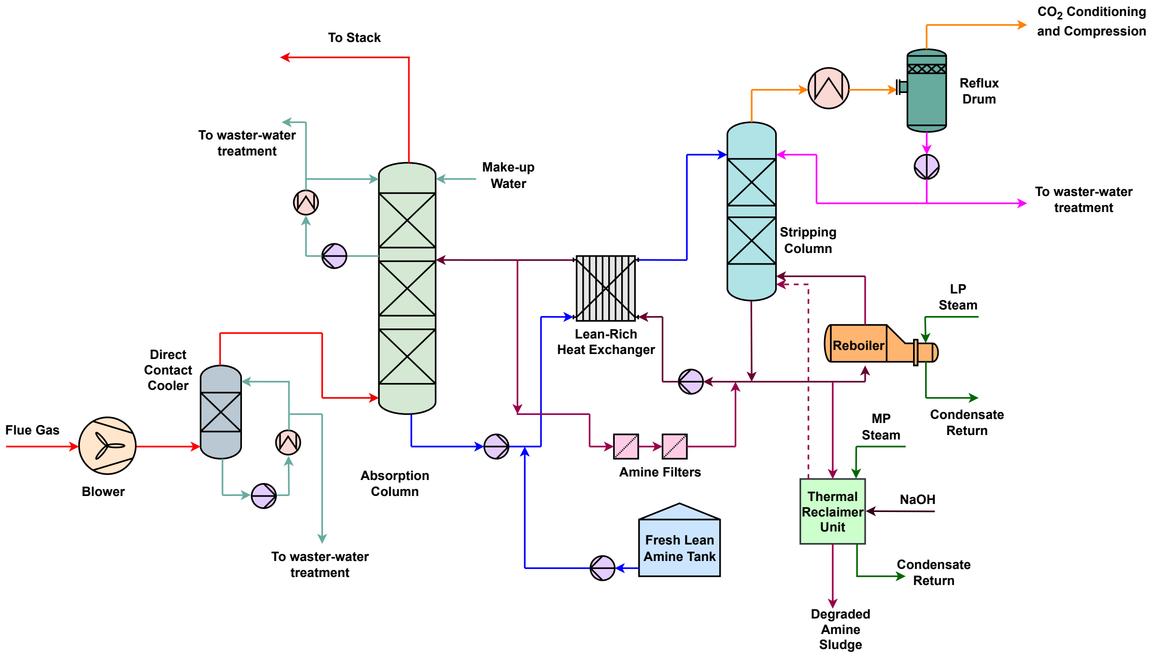

Figure 1.1: Amine absorption based CO_2 capture process

Two commercial-scale CO_2 capture projects have been operational for over a decade in power generation [5]. The Boundary Dam project in Saskatchewan, Canada, and the Petronova project in Thompson, Texas, are prime examples of CO_2 capture plants retrofitted to coal-fired power plants using the proprietary amine-solvent absorption process. Despite being commonly referred to as a mature technology for CO_2 capture, the amine-based absorption process has experienced several operational challenges. Even after a decade of operations, the Boundary Dam project has struggled to reach its design capacity of over a million tonnes per year. Problems like amine-solvent degradation, clogging of column internals by fly ash brought in by the flue gas, and excessive corrosion in the rich-amine to lean-amine heat recovery exchangers have interrupted operations and increased maintenance costs [6]. Over the years, several improvements in amine-scrubbing technology have focused on reducing the specific energy penalty associated with CO_2 capture from 5.5 to 2.6 MJ/tonne of CO_2 captured [7]. The cost of CO_2 capture is highly contestable and subject to vary with several factors such as the partial pressure of CO_2 in the flue gas, cost of energy and the size of the capture plant, amongst others. The CO_2 avoided cost for pulverized coal (PC) power plants with 12 mol % CO_2 is reported to be \$50-55 per metric tonne of CO_2 avoided, and for a natural gas combined cycle (NGCC) power plant with 4 mol % CO_2 to be \$62-70 per metric tonne of CO_2 avoided [8].

1.2 Adsorption Processes for Post-combustion CO_2 Capture

Adsorption processes for post-combustion CO_2 capture are crucial to carbon capture and storage (CCS) technologies [9]. These processes involve using solid adsorbents to capture and separate CO_2 from the flue gas generated during combustion.

The heart of the adsorption process is the adsorbent, typically a solid substance with a high affinity for CO_2. Common adsorbents used in post-combustion capture include activated carbon, zeolites, metal-organic frameworks (MOFs), and amine-modified materials [9]. Adsorption occurs when CO_2 molecules in the flue gas adhere to the surface of the adsorbent through physical or chemical interactions. In physical adsorption, CO_2 molecules are attracted to the adsorbent's surface by weak Van der Waals forces. In contrast, chemical adsorption involves the formation of chemical bonds between CO_2 and the adsorbent.

In a typical post-combustion capture setup, a packed adsorption column is used. The flue gas passes through this column, and the CO_2 selectively adheres to the adsorbent while the other gases (mainly nitrogen) pass through. The CO_2-loaded adsorbent must be periodically regenerated to release the captured CO_2 for storage or utilization. This involves changing the conditions within the column, such as temperature and pressure, to desorb the CO_2 from the adsorbent. The regenerated adsorbent can then be reused for further CO_2 capture. Depending on the technique used to regenerate the adsorbent, there can be two methods: pressure/vacuum swing adsorption (P/VSA) and temperature swing adsorption (TSA). PSA relies on changing the pressure within the adsorption column to control the adsorption and desorption processes. When the pressure is lowered, CO_2 is desorbed; when it's increased, CO_2 is adsorbed. VSA is similar to PSA but operates under vacuum conditions, which can reduce energy requirements for regeneration.

1.3 Motivation

Adsorption-based CO_2 capture processes have been studied extensively to evaluate if they are cost-effective in treating a variety of flue gas compositions. The standalone PVSA process has shown promise in competing with the solvent-based absorption process in the high CO_2 partial pressure ranges (20 mol % CO_2 and above). However, in the low CO_2 partial pressure ranges (under 10 mol % CO_2), even with the best adsorbent, the CO_2 avoided costs are considerably higher than the solvent-based absorption process. Also, in terms of scaling up the process, there are limitations in the practical implementation of a large number of parallel PVSA trains required to treat a given volume of flue gas due to the complexity and the large footprint of the overall plant [10].

One of the ways to address the challenges in the low CO_2 partial pressure ranges is by considering hybrid processes [11]. In the hybrid approach, the PVSA unit acts as a pre-concentration unit, while the liquefaction unit takes the purification load. By leveraging the ability of the liquefaction unit to produce high-purity CO_2 as a liquid, we can combine the additional compression stage otherwise required in a standalone PVSA process for delivering product CO_2 at high pressure. The reduced purification load on the PVSA unit offers the opportunity to reduce the number of parallel PVSA trains required to treat a given volume of flue gas. This approach can also produce high-purity CO_2 product without requiring additional energy, thus allowing us to minimize impurities and meet the product specifications expected in the downstream transport and storage stages.

In this work, we explore how much the CO_2 avoided cost can be reduced using low-cost commercially available adsorbents like Zeolite 13X by reducing the purity constraints on the PVSA unit while maintaining the high recovery constraint on the overall hybrid adsorption-liquefaction process. The variant of the PVSA process, the 4-step LPP cycle, is studied by carrying out detailed techno-economic optimizations. The cost implications of using liquefaction as the downstream purification unit are explored.

1.4 Thesis Outline

This work aims to study the cost-effectiveness of a hybrid adsorption + liquefaction process for post-combustion CO_2 capture focused on the low CO_2 partial pressure ranges.

Chapter 3 considers the standalone PVSA process performance under reduced purity constraints. Details about the PVSA cycle design studied and the modelling of adsorption equilibria and the PVSA process dynamics are provided. Information on the optimization framework is included. Results of the energy and cost evaluation are presented.

Chapter 4 considers the standalone liquefaction process performance. Details on the pure component phase diagrams for CO_2 and N_2 and the binary isothermal VLE data for the CO_2-N_2 system are provided. The thermodynamic models used in the process simulations and details on the model flow sheeting and heat integration are discussed. Results of the energy and cost evaluation are presented.

Chapter 5 considers the Hybrid Adsorption + Liquefaction process performance.

An overview of the proposed hybrid process is provided, followed by the modelling approach for the hybrid processes. Lastly, the performance of the hybrid process is compared with standalone PVSA processes.

Chapter 2

Literature Review

This chapter briefly reviews the adsorbent materials important for CO_2 capture processes. Adsorbent characteristics desirable for designing effective cyclic adsorption processes, such as adsorption working capacity, kinetics, and ease of regeneration, are highlighted. Two classes of porous materials, Zeolite and Metal-Organic Frameworks (MOFs), and their suitability for adsorption-based CO_2 capture processes are discussed. Two types of gas-solid contactor configurations popular in adsorption processes are discussed, along with their merits and demerits. The performance of pressure-vacuum swing adsorption processes in CO_2 applications, in terms of achievable CO_2 purity-recovery levels and the associated energy requirements as reported in the literature, is discussed. Towards the end, developments in hybrid processes for CO_2 capture applications are highlighted.

2.1 Adsorbent Materials for CO_2 Capture

Adsorption is a process where gas molecules are held by forces emanating from a solid surface. The attraction between the adsorbate molecules and the adsorbent can be classified into two types based on the nature of the forces involved: physical and chemical adsorption. Physical adsorption occurs when van der Waals forces attract the adsorbate molecules to the sorbent surface. This results in a low heat of adsorption (10-40 kJ/mol) [12]. This type of adsorption is known as physisorption, and the sorbents are called physisorbents. Because the forces involved are relatively weak, this type of adsorption is easily reversible.

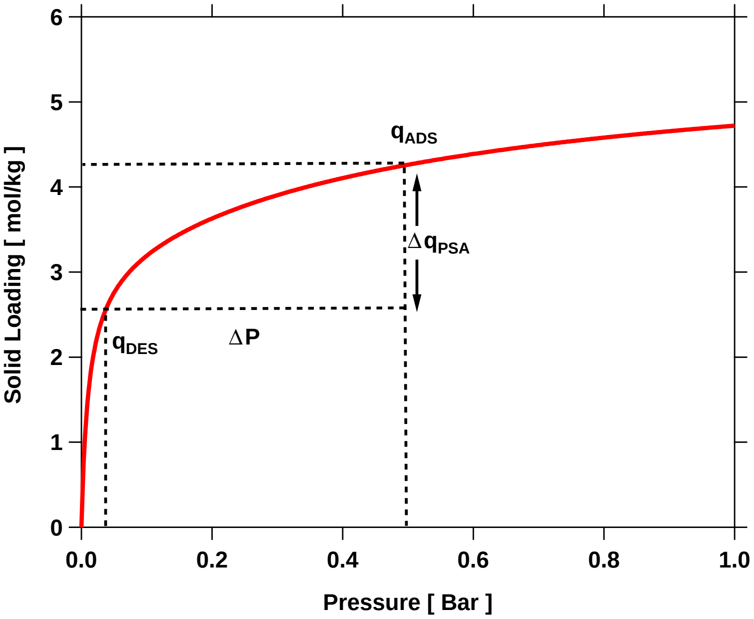

(a) Pressure Swing Adsorption

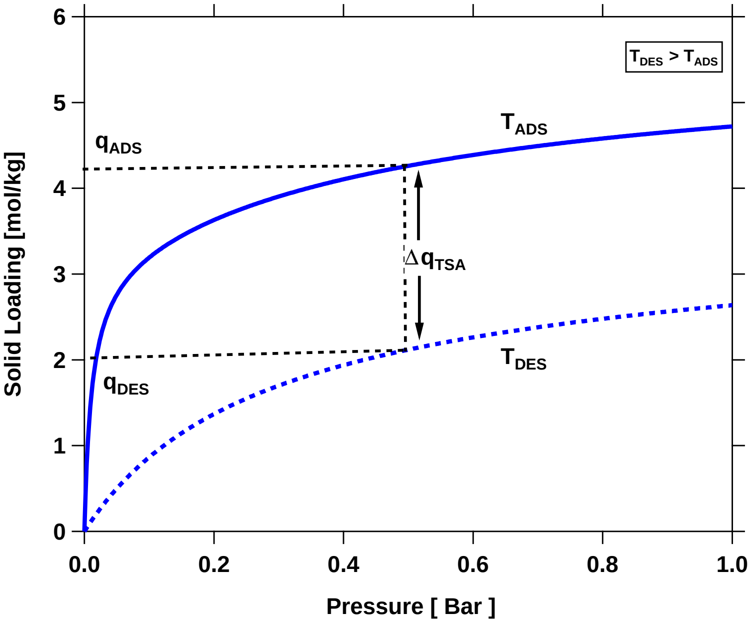

(b) Temperature Swing Adsorption

Figure 2.1: Concept of CO_2 working capacity in the context of Pressure Swing Adsorption and Temperature Swing Adsorption processes.

Chemical adsorption involves additional forces that bind the absorbed molecules to the solid surface. These forces are approximately equivalent to the heat of the adsorption (100 kJ/mol). This binding involves exchanging or sharing electrons or possibly atoms, leading to the formation of molecules or radicals. Sorbents in this category are called chemisorbents. Chemical adsorption is less easily reversible than physical adsorption, and regeneration may pose more significant challenges.

Choosing appropriate sorbents, whether physical or chemical, is a critical aspect that requires careful consideration. This process is inherently complex as the selected sorbent materials must meet multiple critical criteria to align with economic and performance requirements under typical post-combustion operating conditions, specifically low CO_2 pressure, typically up to 0.3 bar.

CO_2 Working Capacity: CO_2 adsorption capacity is a crucial factor in the design of a capture system. It refers to the equilibrium adsorption capacity of a sorbent, representing the amount of CO_2 adsorbed at thermodynamic equilibrium. Equilibrium is achieved when the rate of CO_2 molecules adsorbing onto a surface equals the rate at which they desorb. The significance of this lies in its direct impact on the capital cost of the capture system, as it determines the quantity of adsorbent required and, consequently, the volume of the adsorber vessel. Therefore, a sorbent with a high CO_2 adsorption capacity minimizes the amount of sorbent needed and reduces the size of the process equipment. In this context, ideal adsorbent materials should display a steep-sloped CO_2 adsorption isotherm, indicating a favourable CO_2 adsorption capacity, particularly at low CO_2 partial pressure. While comparing various adsorbents, the equilibrium CO_2 adsorption capacity is a valuable metric; however, its sole consideration does not provide a complete understanding of their practical suitability in real cyclic processes. In practice, a more meaningful assessment involves evaluating the performance based on the CO_2 working capacity—specifically, the amount of CO_2 that can be captured throughout an entire adsorption/desorption cycle [13]. CO_2 working capacity refers to the difference in the quantity of CO_2 adsorbed during the adsorption and desorption steps [14]. In this context, it is recommended that an optimal CO_2 adsorbent should demonstrate a CO_2 working capacity within the range of 3 - 4 mmol/g to be competitive with an established mono-ethanolamine (MEA) absorption process [15]. Figure 2.1 explains the concepts of CO_2 working capacity for PSA and TSA processes using an adsorption isotherm. The CO_2 working capacity $\Delta \mathrm{q}_{PSA}$ for PSA processes is the difference between the CO_2 loading at the adsorption pressure q_{ADS} and the desorption pressure q_{DES} . For TSA processes, the CO_2 working capacity $\Delta \mathrm{q}_{TSA}$ is the difference between the CO_2 loading at the adsorption temperature T_{ADS} and the desorption temperature T_{DES}.

Adsorption Kinetics: Fast adsorption kinetics are crucial for an effective CO_2 sorbent because kinetics govern the cycle time of the dynamic adsorption process. The quicker the CO_2 can adsorb and desorb, the more cost-effective the capture process becomes [16]. Under isothermal conditions, a sorbent with fast kinetics provides steep CO_2 breakthrough curves (i.e., CO_2 concentration in the effluent stream as a function of time). In contrast, slow kinetics yields dispersed breakthrough curves, thus remarkably impacting the amount of sorbent required [17].

Ease of Regeneration: An ideal sorbent should feature milder conditions for regeneration, aiming to minimize the capture cost. In a temperature swing adsorption process, the necessary regeneration energy can be quantified by the heat of adsorption, which ideally should be as low as possible. For PSA processes, regeneration should be possible at reasonable pressure levels. Very low vacuum pressures lead to more parasitic energy and additional processing equipment.

2.1.1 Zeolites

Zeolites are structured microporous crystalline substances composed of silicon, aluminum, and oxygen. More precisely, the crystals consist of TO_4 tetrahedra (where T = Si or Al), creating a framework of channels and cavities that result in a well-defined porous structure characterized by a very high specific surface area [18]. Among the spectrum of available sorbent materials, zeolites are highly promising for post-combustion CO_2 capture. They showcase substantial adsorption capacities coupled with swift adsorption kinetics, particularly under mild operating conditions (0-100°C and 0.1-1 bar CO_2) commonly found in post-combustion flue gases and biogas. Zeolites are also considered better-performing CO_2 adsorbents, demonstrating excellent regenerability. Notably, their CO_2 adsorption isotherms typically exhibit minimal changes even after undergoing extensive adsorption/desorption cycling [19].

Zeolites possess an interesting characteristic in that their unique properties, including chemical composition, pore size, and architecture, directly influence their CO_2 adsorption performance [19]. Analysis of the chemical compositions of zeolites suggests cations such as Na^+ and Li^+ in the silicate structure induce a negative charge in the zeolite framework. The imparted negative charge enables zeolites to adsorb CO_2 to varying extents, depending on the quantity and nature of the cations present [20]. Similarly, the Si/Al ratio is a crucial factor influencing CO_2 adsorption performance. It is widely acknowledged that zeolites with a low Si/Al ratio, indicating a higher number of extra-framework cations in the lattice, are considered the most effective for CO_2 capture [21].

Numerous studies are directed toward substituting the cations initially present in the zeolite framework with alkali cations like Na, Rb, Li, Cs, and K. This substitution aims to improve further the CO_2 adsorption capacity [22]. While zeolites with low silica content can offer high CO_2 adsorption capacity and selectivity at low pressures, they exhibit poor tolerance to moisture. This limitation significantly impedes CO_2 capture, as water vapour is preferentially adsorbed instead of CO_2 [22]. This challenge has spurred various research endeavours aimed at exploring the CO_2 adsorption capabilities of hydrophobic zeolites characterized by a high silica content, including the MWW zeotype and NaZSM-5 [23, 24].

2.1.2 Metal Organic Frameworks (MOFs)

Metal-organic frameworks (MOFs) are porous crystalline materials of metallic species and organic ligands. They have shown significant promise for CO_2 post-combustion capture, in terms of CO_2 adsorption capacity and outstanding recycling stability with negligible reduction in their capture performances over repeated adsorption/desorption cycles [25]. Due to the adaptability of utilizing nearly all metals and a diverse array of organic species, it is possible to synthesize many MOFs with distinct properties, including varying pore sizes and structures [26]. By carefully choosing the organic ligands and metallic species, it is feasible to finely tune these features, allowing for the creation of MOFs with high surface areas (up to 3000 m^2/g) and specific pore sizes [27]. Specifically, MOFs featuring pore dimensions compatible with the kinetic diameter of CO_2 molecules and incorporating polar functional groups within the pores (such as -OH, -N=N-, -NH_2, and -N=C(R)-) that can interact with the quadrupole moments of CO_2 molecules tend to exhibit higher CO_2 adsorption capacity [27].

Despite their advantageous CO_2 adsorption properties, MOFs, unfortunately, are easily susceptible to poisoning by H_2S, SO_x, and NO_x, even at trace levels [18]. They display a strong affinity for these species, which are preferentially adsorbed on the available sites, necessitating their complete removal from the flue gas before introduction to the adsorption bed to prevent a significant reduction in CO_2 adsorption capacity. While MOFs show great potential for post-combustion capture, their production and utilization costs remain relatively high compared to commercially available sorbents [25]. Indeed, the synthesis and characterization of MOFs with costly linkers have been primarily tested at the laboratory scale, typically on the milligram scale [28]. Furthermore, due to the reliance on expensive and often toxic solvents, the current MOF synthesis methods are generally challenging to scale up in an environmentally friendly manner [28]. Only recently, a zinc-based MOF called CALF-20 with high CO_2 capacity and resilience to water was synthesized. It can be synthesized in a single step, and its production can be scaled up to a kilogram scale [29]. A Vancouver-based company by the name Svante Technologies Inc. has collaborated with BASF to scale up from laboratory scale to industrial scale [30]. Svante has implemented CALF-20 into their proprietary rotary TSA processes for post-combustion CO_2 capture [31]. Svante has secured agreements with BASF for commercial supply of CALF-20 [32]. BASF claims they are equipped to scale up the production of CALF-20 to a tonne scale.

2.2 Gas-Solid Contactor Configuration

The development of adsorbent materials should advance closely with the gas-solid contactor configuration and regeneration mode [33]. Hence, to ensure the effectiveness of the chosen sorbent, it is imperative to channel efforts into developing an appropriate gas-solid contacting system. This system is pivotal in determining process efficiency, footprint, and overall capture costs [34].

Different gas-solid adsorbers have been proposed for adsorption-based CO_2 capture processes, such as fixed-bed and moving-bed. Due to its straightforward and uncomplicated design, the fixed bed configuration has been extensively studied at the laboratory scale. Several papers have reported assessments of various sorbent types, incorporating different regeneration modes [34]. Nevertheless, there has been a recent exploration of alternative adsorber configurations, given the significance of the gas-solid contacting system within the broader context of post-combustion capture processes. Indeed, the effectiveness and affordability of any post-combustion CO_2 capture technology on a global scale depends mainly on the simplicity of retrofitting it to existing plants, ease of operation, and the total footprint.

2.2.1 Fixed-beds

The fixed bed contactor, characterized by its simplicity in the gas-solid configuration, operates by directing flue gas through a packed bed containing relatively large-sized sorbent particles. A notable feature of the fixed bed adsorber is its near plug-flow behaviour, assuming minimal axial dispersion. This results in the bed becoming saturated along its entire length, from the feed point to the outlet, thereby enabling the separation of CO_2 from other gases by adsorption until the bed approaches saturation.

The primary disadvantage of employing a fixed-bed configuration for adsorption-based processes in CO_2 post-combustion capture is the relatively high-pressure drops, even at moderate flow rates. This leads to a significantly large footprint due to the limitation of using high gas velocities in adsorption and regeneration steps [35]. As extensively discussed by Yang et al. [36], the primary challenges for CO_2 capture from conventional power plants include large volumetric flue gas flow rates. For instance, a substantial volumetric flue gas flow rate requires the adsorption process to be designed to achieve a reasonable number of parallel trains and appropriately sized columns. The flue gas in typical power plants operates close to atmospheric pressure. After suitable integration, the estimated pressure drop available at the CO_2 adsorption column is approximately 0.2 bar. Any increase beyond this value would incur additional fan-blowing costs to elevate the flue gas pressure, resulting in a significant energy penalty.

To minimize the pressure drop in fixed beds for post-combustion CO_2 capture, it is necessary to use relatively coarse sorbent particles. For instance, to maintain the total pressure drop below 0.2 bar, it can be estimated that, for a bed height of 3 m and a superficial gas velocity of about 1 m/s, the sorbent particles must have a size of at least 2 mm. At higher velocities, such as 1.5 m/s and above, the particles must be even coarser, exceeding 5 mm [36]. However, this approach increases heat and mass transfer resistances, impeding the CO_2 working adsorption capacity and kinetics. Large-sized fixed beds inherently exhibit poor heat transfer coefficients due to low surface area-to-volume ratios. The result of these limitations in mass and heat transfer is the dispersion of the adsorption front as it travels through the bed. This causes the CO_2 to break through at the bed outlet with a substantial portion of the bed still unsaturated, resulting in high values of the length of the unused bed. Moreover, due to the exothermic nature of the adsorption process, the heat generated during CO_2 adsorption induces a heat front that travels through the bed, akin to the movement of the adsorption front. The resulting increase in bed temperature negatively impacts the adsorption equilibrium, leading to a decrease in adsorption capacity. Consequently, more frequent inlet and outlet valve switching becomes necessary as each cycle captures only a small amount of CO_2.

Various solutions have been suggested to address the inherent thermal limitations of fixed-bed adsorbers. One viable approach involves incorporating a heat exchanger into the adsorber to remove the generated heat [34] efficiently. However, this solution may cause increased heating/cooling time due to the poor heat transfer coefficients in fixed beds. Specialized structured contactor configurations have been explored as promising alternatives to conventional fixed beds. While the conventional method of reducing mass transfer resistances would involve minimizing particle size, an alternative approach has been investigated. This involves the development of innovative non-particulate adsorbent structures. Various structures with adjustable shape, cell density, and wall thickness have been explored for CO_2 capture. These structures are characterized by reduced pressure drop, heat transfer resistance, and enhanced mass transfer kinetics due to a shorter diffusion path than standard fixed bed adsorbers [37]. Given these advantages, the cycle time can be significantly reduced and productivity increased, enabling more expensive and sophisticated sorbents to be used while maintaining the competitiveness of the CO_2 capture process. However, when working with structured adsorbents, various trade-offs should be carefully considered [37]. Indeed, on the one hand, the aim is to maximize the external surface area per unit volume of adsorbent to enhance kinetic properties. This can be achieved by minimizing the wall thickness and spacing. On the other hand, a thinner wall thickness, indicating a shorter diffusion path, results in a lower adsorbent loading, leading to a low effective sorbent bulk density. In other words, the inert support structure occupies a significant portion of the adsorber volume. Consequently, achieving a high voidage is linked to faster kinetics, but it simultaneously yields a lower working capacity due to the reduced bed density. Similarly, small spacing between adjacent sheets or channels increases pressure drop.

In summary, fixed bed adsorbers are generally well-suited for pressure swing processes, involving regeneration through pressure reduction, rather than temperature swing processes, which involve regeneration through temperature increase. This particularly applies to physisorbents with low adsorption enthalpy, as they are less sensitive to temperature variations.

2.2.2 Moving-beds

An alternative gas-solid system for adsorption-based CO_2 capture processes is the moving bed. In this setup, adsorbent particles are transported through different sections/columns, all operated at fixed conditions specific to their intended purpose (adsorption, desorption, or heating/cooling). This design reduces the pressure drop compared to an equivalent fixed bed. Simultaneously, it preserves the plug-flow nature of a fixed bed adsorber, enabling steady-state operation. Additionally, this configuration allows for the adsorption front to be fixed in position, provided the rate of particle movement in one direction aligns with the opposite direction of the adsorption front.

However, the main drawback of this configuration is its increased complexity, as it involves moving particles between interconnected beds. This limitation restricts the feasibility of conducting pressure swing processes. Conversely, the moving bed configuration addresses a significant drawback of temperature swing processes in fixed bed adsorbers (with the sorbent packed in large columns). Specifically, it overcomes the prolonged cycle time associated with heating/cooling steps, thus significantly enhancing the productivity of the separation process [38].

A moving bed system for CO_2 capture, known as the Kawasaki CO_2 Capture System (KCC), has been developed by Kawasaki Heavy Industries. This system is designed to be suitable for large-scale plants [39]. The KCC scheme, characterized by the counter-current movement of gas and solids, comprises three primary components:

(i) Adsorber: In this component, CO_2 is captured by an amine-impregnated porous material.

(ii) Desorber: Low-grade steam (110°C) is utilized as purging gas in the desorber to release the captured CO_2.

(iii) Sorbent Dryer: Warm air is employed in the sorbent dryer to eliminate the water accumulated in the sorbent.

2.3 Performance of adsorption-based CO_2 capture processes

The US Department of Energy (DOE) suggests for any post-combustion CO_2 capture technology to be an effective decarbonization solution should meet a performance target of at least 95% CO_2 purity with a 90% recovery [40]. In this context, the performance of adsorption-based CO_2 capture processes must meet these requirements and with lower energy consumption and high productivity to demonstrate their competitiveness with alternative post-combustion CO_2 capture technologies.

Pressure vacuum swing adsorption (PVSA) processes

A study by Haghpanah et al. analyzed six different VSA cycle configurations with Zeolite 13X as the adsorbent to capture CO_2 from dry flue gas with a composition 15% CO in N_2 [41]. They optimized the VSA cycles using a genetic algorithm to obtain purity-recovery and energy-productivity Pareto fronts. They assessed the cycles' ability to produce high-purity CO_2 at high recovery and ranked configurations that satisfied 90% purity-recovery constraints according to their energy-productivity Pareto fronts. The study found that a 4-step VSA cycle with light product pressurization resulted in the minimum energy penalty of 131 kWh/tonne CO_2 captured at the productivity of 0.57 mol CO_2/m^3 adsorbent/s. The minimum energy consumption required to achieve 95 and 97% purities at 90% recoveries was 154 and 186 kWh/-tonne CO_2 captured, respectively. They also showed that a significant increase in productivity could be achieved with only a marginal increase in energy consumption.

In another study, Hagapanah et al. explored a four-step PVSA process incorporating feed pressurization through Genetic Algorithm (GA) optimizations [42]. Their findings indicated that the minimum energy consumption for the four-step PVSA cycle while adhering to a 90% purity-recovery constraint, occurs when operating in the Vacuum Swing Adsorption (VSA) mode with a low evacuation pressure (P_L) of 0.02 bar. This optimal condition resulted in a minimal energy requirement of 149 kWh/tonne of captured CO_2 and a productivity of 0.49 mol CO_2/m^3 adsorbent/s. The study concluded that pressurizing the feed in a four-step cycle is not advantageous due to the associated high energy penalty. In instances where a higher P_L is a requirement for the four-step PVSA process with feed pressurization, it becomes necessary to pressurize the feed to meet the purity-recovery constraint. Despite the energetic drawbacks, the study suggested that pressurizing the feed while maintaining P_L in the 0.02–0.03 bar range allows for a notable eight-fold increase in productivity. Importantly, energy consumption increased at approximately half that rate. Consequently, the combination of feed pressurization and a low evacuation pressure presents an opportunity for a substantial reduction in plant size and capital cost, albeit at the expense of an energy penalty.

Zhang et al. simulated a Vacuum Swing Adsorption (VSA) process using a 3-bed, 9-step cycle that alternated between 1 and 0.05 bar, including heavy reflux (HR) and light-end pressure equalization (PE) steps. They also presented results from a 3-bed, 6-step cycle without HR and with two light-end PE steps. In both setups, zeolite 13X was employed, and the experiments utilized dry flue gas containing 12% CO_2 and 88% N_2 [43]. CO_2 purity and recovery of 83% was achieved, and power consumption of 124 kWh/tonne of CO_2 captured was reported from the 3-bed, 6-step cycle without HR. For the 3-bed, 9-step cycle with HR, a purity of 95% and a recovery of 70% was achieved. In another study, they presented an experimental investigation of a 3-bed, 6-step cycle that incorporated heavy reflux (HR) step [44]. In this cycle, they attained a purity of 95.2% and a recovery of 66.9%, accompanied by a power consumption of 290.4 kWh/tonne of CO_2 captured. Xiao et al. simulated a 3-bed, 9-step cycle with two pressure equalization (PE) steps at an evacuation pressure of 0.03 bar. In this setup, they reported a purity of 92.5%, a recovery of 75%, and a power consumption of 152 kWh/tonne of CO_2 captured [45]. Agarwal et al. introduced 2-bed, 6-step, and 2-bed, 8-step cycles incorporating both light and heavy refluxes (dual reflux) utilizing zeolite 13X [46]. Using a superstructure-based approach, they fine-tuned the 2-bed, 6-step cycle to optimize CO_2 recovery. The optimized cycle achieved a CO_2 purity of 95% and a recovery of 80%, with a power consumption of 637 kWh/tonne for captured CO_2. They imposed a constraint on the evacuation pressure, limiting it to 0.5 bar, leading to the pressurization of the flue gas up to 6 bar. Another alternative, the 2-bed, 8-step cycle, demonstrated the minimum power consumption of 465 kWh/tonne for captured CO_2 at 90% purity and 85% recovery. Liu et al. simulated a two-stage Vacuum Swing Adsorption (VSA) process using 5A zeolite for CO_2 capture from a dry flue gas with 15% CO_2 and 85% N_2. Their simulation involved a 3-bed, 5-step cycle with heavy reflux (HR) and light reflux (LR) steps for the first stage and a 2-bed, 6-step cycle with LR and pressure equalization (PE) steps for the second stage. The results showed a CO_2 purity of 96%, a recovery of 91%, a power consumption of 179.4 kWh/tonne for captured CO_2, and a productivity of 0.1 mol CO_2/m^3 adsorbent/s [47].

2.4 Hybrid processes in CO_2 capture

Standalone separation technologies, such as absorption, membranes, cryogenic, and adsorption for CO_2 capture applications, have been studied extensively and are known to impose a significant energy penalty and thus result in high capture costs [48]. To overcome the challenges of standalone CO_2 capture technologies, hybrid processes, which combine two or more standalone technologies, are being proposed to be effective for industrial decarbonization. By leveraging the abilities of individual technologies in the operational range where they are the most effective, the hybrid process's performance could be superior to standalone technologies.

Song et al. comprehensively review recent advancements in hybrid processes for CO_2 capture applications [49]. They present the existing challenges with current standalone CO_2 capture processes and also compare the performance of various combinations of hybrid processes such as membrane-absorption [50], adsorption-cryogenics [51], membrane-cryogenics [52] amongst others. The author could find only one work in the literature that focused on evaluating the hybrid adsorption combined with the liquefaction process for CO_2 capture applications. In that work, Fong et al. concluded that a hybrid process comprising of a VSA process combined with a cryogenic process could result in energy savings and thus compete with an MEA-based amine absorption process for coal flue gas capture applications [51]. They, however, did not provide any cost estimates for the hybrid process.

With the growing push for decarbonization in the industrial sector, only recently, companies involved in gas separation applications are starting to offer solutions for post-combustion CO_2. Air Liquide, a French multinational company, has developed a suite of hybrid CO_2 capture technologies called CryoCap™ for pre-combustion, post-combustion and oxyfuel combustion applications. These are hybrid processes that combine PSA technology with cryogenic technology for gas compositions > 15 mol % CO_2 [53]. Linde Plc, another multinational company, is offering solutions for a variety of CO_2 capture applications through its hybrid technology called HISORP-CC®, which is a combination of PSA, membrane and cryogenic technologies [54].

2.5 Summary

Exploring alternative options for reducing the cost of CO_2 capture is crucial to enable rapid deployment of carbon capture technologies on a large scale. To demonstrate the competitiveness of adsorption-based CO_2 capture processes, research efforts are focused on advancing the performance of adsorbent materials as well as on designing and optimizing adsorption cycles. Continuous improvements in the gas-solid contactor designs are important to maximize the productivity of adsorption processes. Hybrid processes are being developed as alternative options over standalone technologies as they as expected to perform better in terms of the energy penalty. However, the cost of capture determines the economic viability of carbon capture technology, and thus research efforts must be directed toward integrated techno-economic assessments to establish the suitability of these processes.

Chapter 3

Standalone PVSA Process Performance

3.1 Introduction

Adsorption-based gas separation processes exhibit a distinctive cyclic nature, characterized by repetitive adsorption and desorption cycles. In these processes, a solid adsorbent selectively captures specific gas molecules on its surface during the adsorption phase. This accumulation of gas molecules is then reversed in the desorption phase, where the adsorbent is regenerated by releasing the captured gases. The cyclic nature of these processes is essential for carrying out the separation in a practical application. During adsorption, the target gas is separated from the mixture, and in the subsequent desorption, the adsorbent is regenerated for the next adsorption cycle. This cyclic operation allows for the continuous separation of gases, making it a crucial aspect of various industrial applications, such as natural gas purification, carbon capture, and air separation. The optimization of these cyclic processes plays a vital role in enhancing their overall performance and economic viability in diverse industrial settings.

Proper design and optimization of adsorption-based gas separation processes are imperative for achieving the desired separation performance and making the separation cost-effective. This intricate process involves a thorough understanding of the interplay between adsorbent properties, gas-phase characteristics, and operating parameters. Thus, a systematic design begins with the selection of an appropriate adsorbent tailored to the target gas species, along with a workable cycle design configuration that can meet the desired separation performance. Parameters such as temperature, pressure, and flow rates are then meticulously optimized to enhance the adsorption and desorption kinetics. Furthermore, the cyclic nature of adsorption processes necessitates the careful consideration of cycle time and operation conditions to achieve optimal productivity. Additionally, optimization involves balancing the trade-offs between factors such as adsorption capacity, selectivity, and energy consumption in order to minimize the cost associated with the separation.

Continuous advancements in materials science and process engineering contribute to the ongoing refinement of these systems. Overall, a systematic approach to design and optimization is crucial for ensuring the efficacy and sustainability of adsorption-based gas separation processes in addressing the diverse challenges posed by industrial gas separation applications. In this chapter, the cost reduction potential of a 4-step PVSA process at reduced purity levels is studied using a techno-economic optimization framework.

3.2 Systematic Design of PVSA Capture Unit

The framework used in this work was developed by Subraveti et al. [55] and is illustrated in Fig. 3.1. The framework relies on technical and economical design parameters, the PVSA cycle, and physio-chemical properties like adsorption isotherms as its inputs. Using these input data, an integrated simulation and costing framework, combined with stochastic optimization, produces the most cost-effective design for the PVSA process. Further elaboration on these individual components is provided in the following sections.

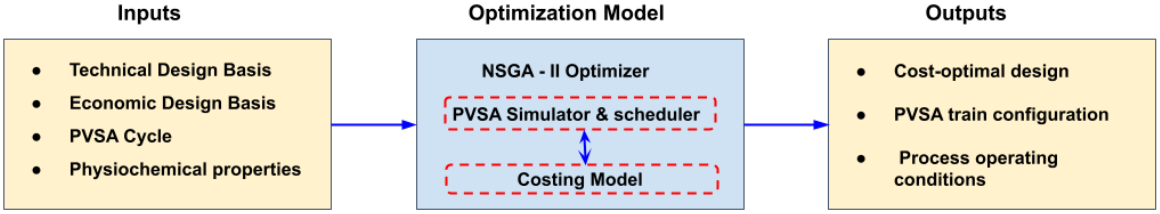

Figure 3.1: Integrated techno-economic optimization framework

3.2.1 Process Layout

A typical adsorption process consists of multiple pieces of equipment that are required to operate the process, such as the feed compressors, heat exchangers, and vacuum pumps and, depending on the size of the plant could contain multiple parallel PVSA trains. The process layout of adsorption-based CO_2 capture is illustrated in Fig. 3.2. Before entering the PVSA unit, the dry flue gas requires compression to overcome the pressure drop within the PVSA columns. Two identical single-stage compressors are employed to achieve the required pressure levels. Following each compression stage, coolers are utilized to lower the temperature of the feed mixture to 298.15 K. A feed header divides the dry flue gas into M identical PVSA trains for processing [56]. The feed mixture to PVSA units is considered to contain a binary mixture of $3.5-30\%$ CO_2 and the balance N_2 was used to simulate the PVSA process. Although other gases, such as oxygen and argon, may be present in the feed mixture, they are substituted with N_2. This assumption is justified by the fact that both O_2 and Ar adsorb weaker than N_2 on zeolite 13X adsorbent, and hence, can be considered to be adequately represented by N_2. Each PVSA unit consists of N identical columns which are scheduled to operate the cycle in order to ensure continuous production.

3.2.2 Four-step LPP Cycle

The particular cycle design considered in this chapter is illustrated in Fig.3.3. The 4-step Light product pressurization (LPP) cycle has four steps; adsorption (ADS),

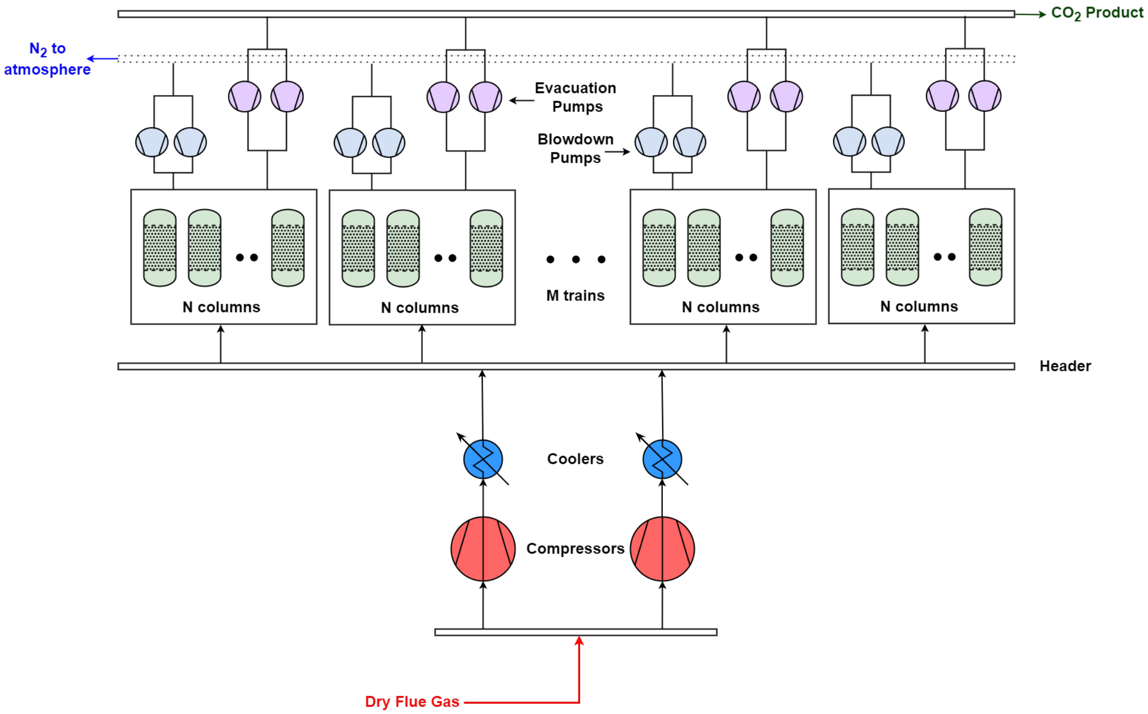

Figure 3.2: PVSA layout for CO$_2$ Capture

co-current blowdown (BLO), counter-current evacuation (EVAC), and light product pressurization (LPP) stages. The separation of feed mixture occurs in the adsorption step at high pressure (P_{H}) where the heavy product CO$_2$ adsorbs in the column, and N$_2$ leaves the column as a light product. The feed mixture must be compressed to a higher pressure (P_{F}) to overcome the pressure drop across the column due to the flow of the feed gas in the adsorption step. In the co-current blowdown step, the column pressure is reduced to an intermediate pressure (P_{I}) to remove N$_2$ left in the column. The column pressure is further reduced to a low vacuum (P_{L}) in the counter-current evacuation step to collect the heavy product CO$_2$ at the feed end of the column. The light product, in this case N$_2$ from the adsorption step, is used to pressurize the column back to the adsorption pressure (P_{H}).

3.2.3 Adsorbent Material

Zeolite 13X is a commercially available adsorbent material, that has been shown to be promising for CO$_2$ capture applications [42, 45]. The adsorption equilibria

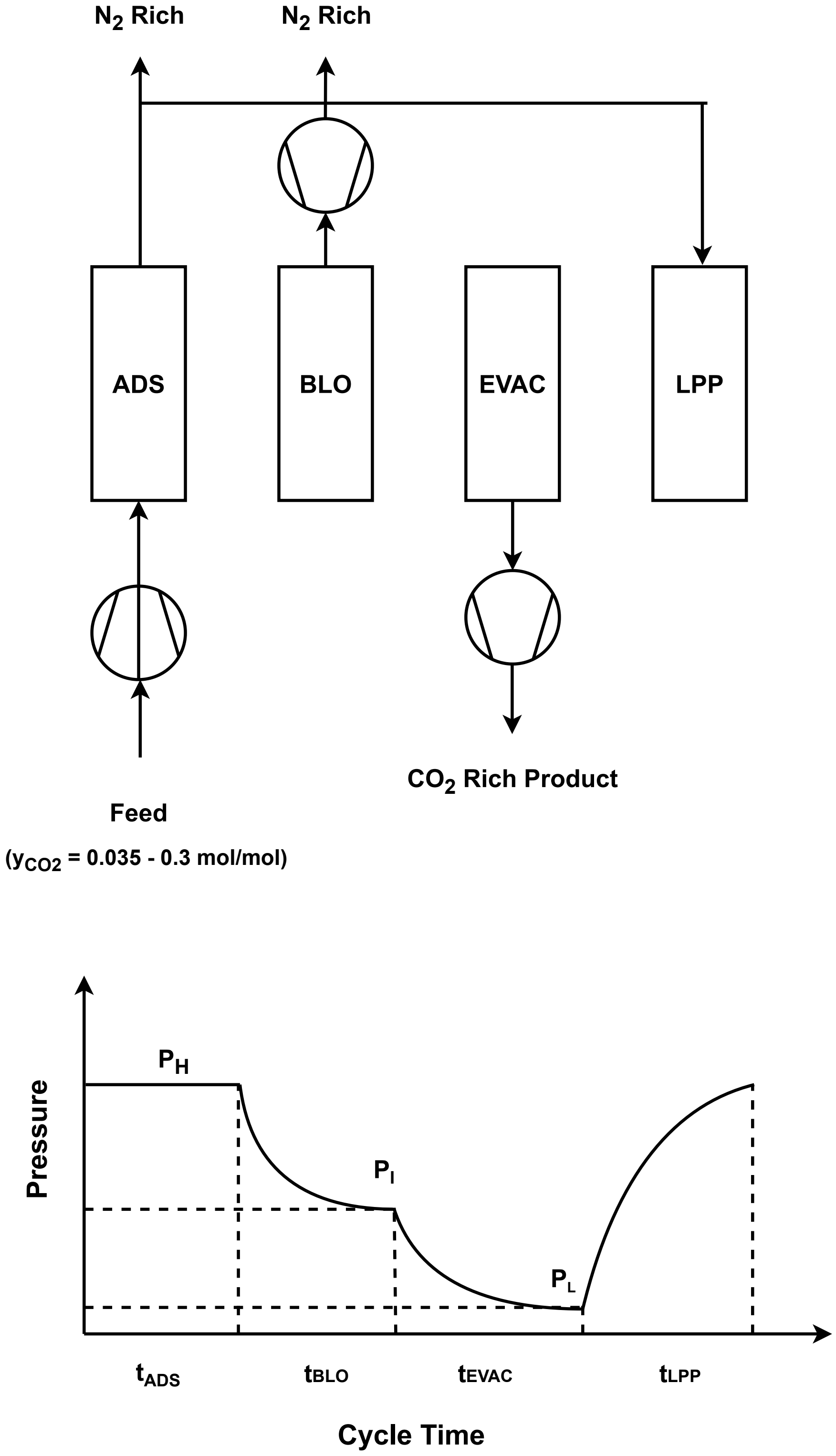

Figure 3.3: Four-step Light Product Pressurization (LPP) PVSA Cycle

for an adsorbent, representing the solid phase loading in equilibrium with the fluid phase composition for this adsorbent, are described using a competitive form dual-site Langmuir (DSL) model (for each component i).

$$q_i^* = \frac{q_{\mathrm{sb},i} b_i c_i}{1 + \sum_i b_i c_i} + \frac{q_{\mathrm{sd},i} d_i c_i}{1 + \sum_i d_i c_i} \tag{3.1}$$

where q_i^* is the solid phase loading of species i, in equilibrium with the fluid phase concentration c_i, $q_{\mathrm{sb},i}$ and $q_{\mathrm{sd},i}$ are the saturation loadings for the two sites and, b_i and d_i are the adsorption equilibrium constants with Vant Hoff temperature dependence as follows:

$$\begin{aligned} b_i &= b_0 e^{\left(-\frac{\Delta U_{\mathrm{b},i}}{RT}\right)} \\ d_i &= d_0 e^{\left(-\frac{\Delta U_{\mathrm{d},i}}{RT}\right)} \end{aligned} \tag{3.2}$$

$\Delta U_{\mathrm{b},i}$ and $\Delta U_{\mathrm{d},i}$ are the internal energies of the two sites, R is the universal gas constant and T is the temperature. The extended dual-site Langmuir isotherm model in Eq. 3.1 explicitly takes into account the competition between CO_2 and N_2. In this chapter, the DSL isotherm's equal energy site (EES) form suggested by Wilkins et. al is used [57]. In this DSL form, the saturation capacity of each site is kept equal for both components and the enthalpy of adsorption for N_2 is kept equal for both sites. This form is supported by experimental evidence for the case of Zeolite 13X [58]. The DSL isotherm parameters for Zeolite 13X pellets were obtained based on experiments conducted by Haghpanah et. al [42]. Figure 3.4 shows the CO_2 and N_2 single component isotherms for Zeolite 13X, and related isotherm parameters are provided in Table 3.1.

3.3 Process Modelling

3.3.1 Modelling of cyclic adsorption processes

A mathematical model, derived by solving mass, momentum, and energy balances in a non-isothermal, one-dimensional framework, was employed for simulating the

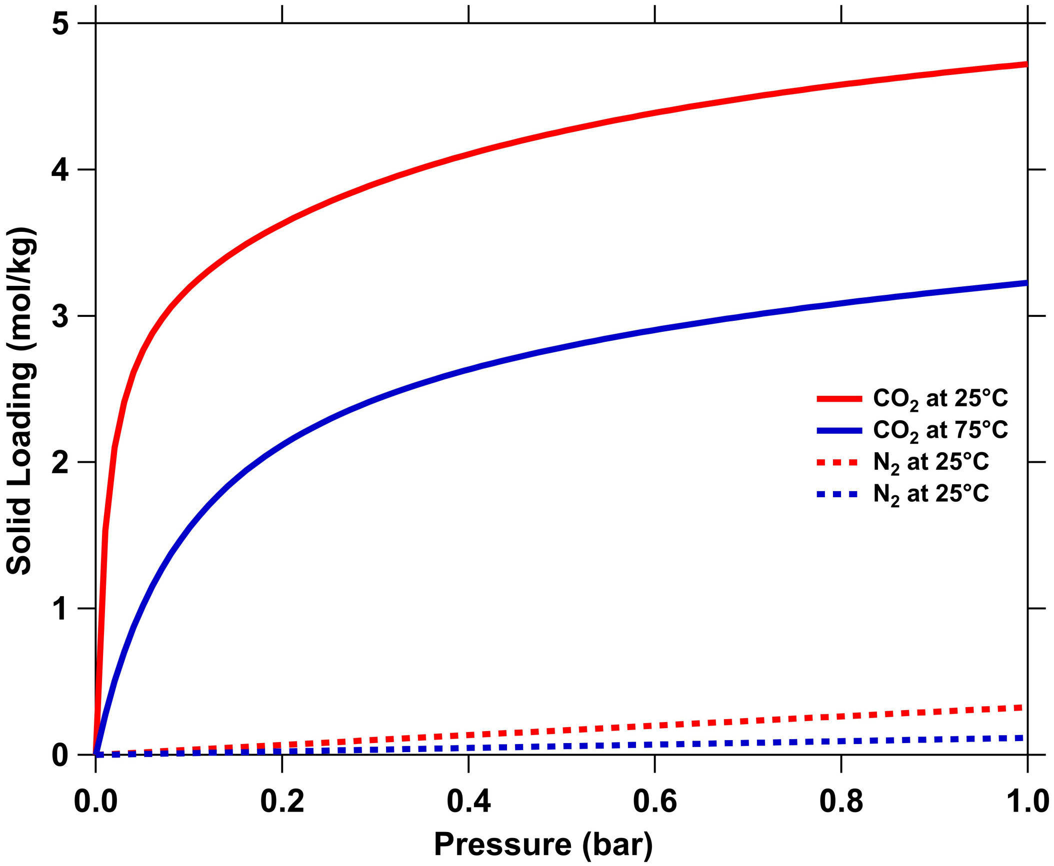

Figure 3.4: CO$_2$ and N$_2$ isotherms on Zeolite 13X at 25°C and 75°C.

PVSA process [42]. The literature includes accounts of experiments conducted at both laboratory and pilot scales to validate the model [59]. The model assumes ideal gas behaviour and employs an axially dispersed plug flow model to depict the bulk flow. It assumes uniformity in composition, pressure, and temperature across the column with no radial gradients. Consistency in adsorbent properties and bed porosity is maintained throughout. Additionally, an instantaneous thermal equilibrium is assumed between the gas and the solid phase. The solid-phase mass transfer is characterized by the linear driving force model, while Ergun's equation is utilized to consider the pressure drop across the column. The assumption of an adiabatic mode of operation, indicating no heat transfer across the walls, remains applicable, especially in large column sizes. The resulting governing equations are provided below.

Table 3.1: Dual-site Langmuir isotherm parameters for zeolite 13X [42]

	CO_2	**N_2**
q_{sb} $\left(\mathrm{mol\ kg^{-1}}\right)$	3.09	3.09
q_{sd} $\left(\mathrm{mol\ kg^{-1}}\right)$	2.54	2.54
b_0 $\left(\mathrm{m^3\ mol^{-1}}\right)$	8.65×10^{-7}	2.69×10^{-6}
d_0 $\left(\mathrm{m^3\ mol^{-1}}\right)$	2.63×10^{-8}	2.69×10^{-6}
ΔU_{b} $\left(\mathrm{J\ mol^{-1}}\right)$	-36641	-15710
ΔU_{d} $\left(\mathrm{J\ mol^{-1}}\right)$	-35690	-15710

3.3.2 Model equations

Based on the above assumptions, the following system of coupled nonlinear partial differential equations based on the conservation of mass, momentum, and energy can be derived:

Component mass balance:

$$\frac{\partial y_i}{\partial t} + \frac{y_i}{T}\frac{\partial P}{\partial t} - \frac{y_i}{P}\frac{\partial T}{\partial t} = \frac{T}{P} D_{\mathrm{L}} \frac{\partial}{\partial z}\left(\frac{P}{T}\frac{\partial y_i}{\partial z}\right) - \frac{T}{P}\frac{\partial}{\partial z}\left(\frac{y_i P}{T} v\right) - \frac{RT}{P}\frac{1-\varepsilon}{\varepsilon}\frac{\partial q_i}{\partial t} \tag{3.3}$$

where, y_i is the fluid phase concentration, t is time, P is the pressure, D_L is the dispersion coefficient, z is the spatial coordinate, v is the interstitial velocity, ϵ the bed voidage and q_i is the solid phase concentration.

Total mass balance:

$$\frac{1}{P}\frac{\partial P}{\partial t} - \frac{1}{T}\frac{\partial T}{\partial t} = -\frac{T}{P}\frac{\partial}{\partial z}\left(\frac{P}{T} v\right) - \frac{RT}{P}\frac{1-\varepsilon}{\varepsilon}\sum_{i=1}^{n_{\mathrm{comp}}}\frac{\partial q_i}{\partial t} \tag{3.4}$$

Column energy balance:

$$\begin{aligned} \left[\tfrac{1-\varepsilon}{\varepsilon}\left(\rho_{\mathrm{s}} C_{\mathrm{p,s}} + C_{\mathrm{p,a}} \textstyle\sum_{i=1}^{n_{\mathrm{comp}}} q_{\mathrm{i}}\right)\right] \tfrac{\partial T}{\partial t} = \tfrac{K_{\mathrm{z}}}{\varepsilon}\tfrac{\partial^2 T}{\partial z^2} - \tfrac{C_{\mathrm{p,g}}}{R}\tfrac{\partial P}{\partial t} - \tfrac{C_{\mathrm{p,g}}}{R}\tfrac{\partial}{\partial z}(vP) \\ -\tfrac{1-\varepsilon}{\varepsilon} C_{\mathrm{p,a}} T \textstyle\sum_{i=1}^{n_{\mathrm{comp}}} \tfrac{\partial q_{\mathrm{i}}}{\partial t} + \tfrac{1-\varepsilon}{\varepsilon}\textstyle\sum_{i=1}^{n_{\mathrm{comp}}} \left((-\Delta H)\tfrac{\partial q_{\mathrm{i}}}{\partial t}\right) \end{aligned} \tag{3.5}$$

where, ρ_s is the solid density, $C_{p,s}$ the specific heat capacity of the solid, $C_{p,a}$ the specific heat capacity of the adsorbed phase, κ_z is the effective thermal conductivity of the bed, $C_{p,g}$ is the specific heat capacity of the fluid phase and ΔH is the heat of adsorption.

Pressure drop (Ergun's equation):

$$-\frac{\partial P}{\partial z} = \frac{150}{4}\frac{1}{r_{\mathrm{p}}^2}\left(\frac{1-\varepsilon}{\varepsilon}\right)^2 \mu v + \frac{1.75}{2}\frac{1}{r_{\mathrm{p}}}\left(\frac{1-\varepsilon}{\varepsilon}\right)\rho|v|v \tag{3.6}$$

where, r_p is the particle radius, μ viscosity of the fluid and ρ is the density of the fluid.

Linear driving force model:

$$\frac{\partial q_i}{\partial t} = k_i\left(q_i^* - q_i\right) \tag{3.7}$$

where, k_i is the lumped mass transfer coefficient.

Mass transfer coefficient (macropore controlled):

$$k_i = \frac{c_i}{q_i^*}\frac{15\varepsilon_{\mathrm{p}}D_{\mathrm{p}}}{r_{\mathrm{p}}^2} \tag{3.8}$$

where, ϵ_p is the particle voidage and D_p is the effective macropore diffusivity.

Adsorption equilibria (generalized form):

$$q_i^* = f\left(c_i, T\right) \tag{3.9}$$

Ideal gas law:

$$c_i = \frac{y_i P}{RT} \tag{3.10}$$

Custom boundary conditions were defined for solving each cycle step. At the column exit, the volumetric flow rate of vacuum pumps was designated as the boundary condition to model blowdown and evacuation steps, as opposed to utilizing predefined exponential pressure profiles. This modification enhances the accuracy of cycle time and allows for reliable estimation of the size and cost of vacuum pumps. Notably, the costs of most vacuum pumps are contingent on volumetric flow rates [60]. Furthermore, recent research indicates that integrating boundary conditions based on the volumetric flow rate of vacuum pumps enhances the overall accuracy of the model in predicting process performance indicators [60]. Hence, the model utilized the volumetric flow rate of vacuum pumps as inputs, and subsequently calculated the durations of blowdown and evacuation.

3.3.3 Initial and boundary conditions

To simulate cyclic adsorption processes, the system of partial differential equations (PDEs) and algebraic equations described above is collectively solved, considering appropriate initial and boundary conditions. To initialize the cycle simulations, a convenient assumption is made: the bed in the first step is equilibrated with a feed mixture at a specified temperature and pressure. Subsequently, the final condition of one step becomes the initial condition for the subsequent step. The boundary conditions in the cyclic adsorption process can be generalized based on the valve positions at the two ends of the adsorbent bed, categorizing them as open-open, open-closed, and closed-open.

Open-open:

In this configuration, both valves are open, constituting a step where an inlet stream flows through the column, and an outlet stream exits from the opposite end. Dankwert's dispersed plug flow system boundary conditions are applied to the mass and energy balances of the components. For the total mass balance, the inlet's flow rate (expressed in terms of velocity) and the exit pressure at the outlet are regulated.

The boundary conditions can be written as,

$$D_{\mathrm{L}} \frac{\partial y_i}{\partial z}\bigg|_{z=0} = -\left. v\right|_{z=0} \left(y_{\mathrm{in}} - \left. y_i\right|_{z=0}\right) \tag{3.11}$$

$$\frac{\partial y_{\mathrm{i}}}{\partial z}\bigg|_{z=L} = 0 \tag{3.12}$$

$$K_z \frac{\partial T}{\partial z}\bigg|_{z=0} = -\varepsilon \tag{3.13}$$

$$\frac{\mathrm{g}}{} C_{\mathrm{p,g}} v\Big|_{z=0} \left(T_{\mathrm{in}} - \left. T\right|_{z=0}\right) \tag{3.14}$$

$$\frac{\partial T}{\partial z}\bigg|_{z=L} = 0 \tag{3.15}$$

$$\left. v\right|_{z=0} = v_{\mathrm{in}} \tag{3.16}$$

$$\left. P\right|_{z=L} = P_{\mathrm{out}} \tag{3.17}$$

Open-closed:

Here, the column inlet is open, and the column outlet is closed. Equations 3.11-3.14 remain valid. Depending on the constituent step, $\left. v\right|_{z=0}$ can be calculated based on either Eq. 3.15 or change in pressure at the column inlet. Equation 3.16 changes to:

$$\frac{\partial P}{\partial z}\bigg|_{z=L} = 0 \tag{3.18}$$

Closed-open:

Here, the column inlet is closed, and the column outlet is open. Equations 3.12, 3.14 remain valid while Eqs. 3.11, 3.13, 3.15 reduce respectively to:

$$
\begin{aligned}
\left.\frac{\partial y_i}{\partial z}\right|_{z=0} &= 0 \\
\left.\frac{\partial T}{\partial z}\right|_{z=0} &= 0 \\
v|_{z=0} &= 0
\end{aligned}
\tag{3.19}
$$

Depending on the dynamics of the step at the column outlet, the boundary condition for the total mass balance can be implemented as either a pressure profile or a constant velocity i.e.,

$$
\begin{aligned}
&P|_{z=L} = P(t) \quad \text{or,} \\
&v|_{z=L} = v_{\text{out}}
\end{aligned}
\tag{3.20}
$$

3.3.4 Numerical solution and model convergence criteria

The numerical solution of the partial differential equations (PDEs) involved discretizing the spatial terms using the finite volume method, employing a weighted essentially nonoscillatory (WENO) scheme as a flux limiter [42]. The partial differential equations (PDEs) were discretized into 30 finite volumes, and the ensuing ordinary differential equations were integrated using a stiff ODE solver, namely *ode23tb*, in MATLAB. The simulations were initialized with the column filled with a feed mixture at P_{L} and followed a unified approach, wherein a single bed sequentially underwent all cycle steps—a commonly employed technique in PVSA simulations. The interlinked cycle steps were simulated using data buffers to store stream information. Blowdown and evacuation steps concluded once the column pressure reached the desired level. The cyclic steady state (CSS) criterion was met when the mass balance error equalled 1% or less for five consecutive cycles. Simulations were conducted over a significant number of cycles to verify the adequacy of this criterion. In cases where the system failed to meet the CSS criterion, simulations were extended up to a maximum of 500 cycles, after which it was assumed that CSS had been achieved. At CSS, the model generated detailed composition, temperature, and pressure profiles crucial for calculating key performance indicators. The parameters used in the simulations are outlined in Table 3.2.

Table 3.2: PVSA fixed simulation parameters

Parameter	**Value**
Column properties	
Column void fraction, $\epsilon_{\mathrm{B}}(-)$	0.37
Tortuosity, $\tau(-)$	3
Length/Diameter Ratio, $L/D(-)$	3
Operating conditions	
Inlet feed temperature, $T_{\mathrm{feed}}(\mathrm{K})$	298.15
Physical properties	
Adsorbent density, $\rho_{\mathrm{s}}\,(\mathrm{kgm}^{-3})$	1130.0
Molecular diffusivity, $D_{\mathrm{m}}\,(\mathrm{cm}^2\ \mathrm{s}^{-1})$	0.16
Fluid viscosity, $\mu(\mathrm{cP})$	0.0172
Specific heat capacity of adsorbent, $C_{\mathrm{p,s}}\left(\mathrm{Jkg}^{-1}\ \mathrm{K}^{-1}\right)$	1070.0
Specific heat capacity of gas phase, $C_{\mathrm{p,g}}\left(\mathrm{Jmol}^{-1}\ \mathrm{K}^{-1}\right)$	30.7
Specific heat capacity of adsorbed phase, $C_{\mathrm{p,a}}\left(\mathrm{Jmol}^{-1}\ \mathrm{K}^{-1}\right)$	30.7
Inside heat transfer coefficient, $h_{\mathrm{in}}\left(\mathrm{Jm}^{-2}\ \mathrm{K}^{-1}\ \mathrm{s}^{-1}\right)$	0
Outside heat transfer coefficient, $h_{\mathrm{out}}\left(\mathrm{Jm}^{-2}\ \mathrm{K}^{-1}\ \mathrm{s}^{-1}\right)$	0
Effective gas thermal conductivity, $K_{\mathrm{z}}\left(\mathrm{Jm}^{-1}\ \mathrm{K}^{-1}\ \mathrm{s}^{-1}\right)$	0.09
Universal gas constant, $\mathrm{R}\left(\mathrm{m}^3\ \mathrm{Pa\ mol}^{-1}\ \mathrm{K}^{-1}\right)$	8.314

3.3.5 Energy calculations

Compressors. Modeling single-stage compressors involves an isentropic compression process, with the assumption of 100% motor efficiency. The calculation of energy consumption is outlined as follows:

$$E_c(J_e) = \frac{1}{\eta_C}\frac{\gamma}{\gamma-1}\int_{t=0}^{t=t_{ADS}} QP\left[\left(\frac{P}{P_{ref}}\right)^{\frac{\gamma}{\gamma-1}} - 1\right] dt \tag{3.21}$$

where, η_C is the compression efficiency which is assumed to be 80%, γ is the adiabatic constant, P is the pressure, P_{ref} is the reference pressure of the flue gas, t_{ADS} is the adsorption step time and Q is the volumetric flow rate of the feed gas mixture.

Vacuum Pumps. The energy consumption of the vacuum pump was modelled as an isoentropic expansion process as given by:

$$E_V(J_e) = \frac{1}{\eta_V}\frac{\gamma}{\gamma-1}\int_{t=0}^{t=t_{step}} QP\left[\left(\frac{P_{atm}}{P}\right)^{\frac{\gamma}{\gamma-1}} - 1\right] dt \tag{3.22}$$

where, t_{step} is the step duration of blowdown/evacuation step, η_V is the vacuum pump efficiency.

3.3.6 Column scheduling

We adopt the column scheduling approach proposed by Khurana and Farooq [60]. This approach ensures that there are enough columns to accept the entire feed in a continuous manner. Dedicated blowdown and evacuation vacuum pumps are needed to allow two or more coupled steps to occur at the same time so that buffer tanks are eliminated. Although the said approach could result in more columns than might be needed, it ensures that the process can be practically accomplished.

Design of a single PVSA train

Each train includes the minimum number of columns and vacuum pumps required for continuous operation. The calculation for the minimum number of columns per train is as follows:

$$N = ceiling(\frac{\sum_{i=steps} t_i}{t_{ADS}}) \tag{3.23}$$

t_i represents the duration of step i in the cycle. The minimum number of blowdowns/evacuation vacuum pumps required are given by,

$$N_{V,j} = ceiling(\frac{t_j}{t_{ADS}}) \qquad j = blowdown/evacuation \tag{3.24}$$

When the sum of individual steps in a cycle is not a multiple of the adsorption time, it is necessary to include an idle step after the evacuation phase to minimize the impact on bed profiles [60]. The calculation for the duration of an idle step is outlined as follows:

$$t_{IDLE} = Nt_{ADS} - \sum_{i=steps} t_i \tag{3.25}$$

A sample column schedule for the 4-step LPP PVSA process is shown in Fig. 3.5.

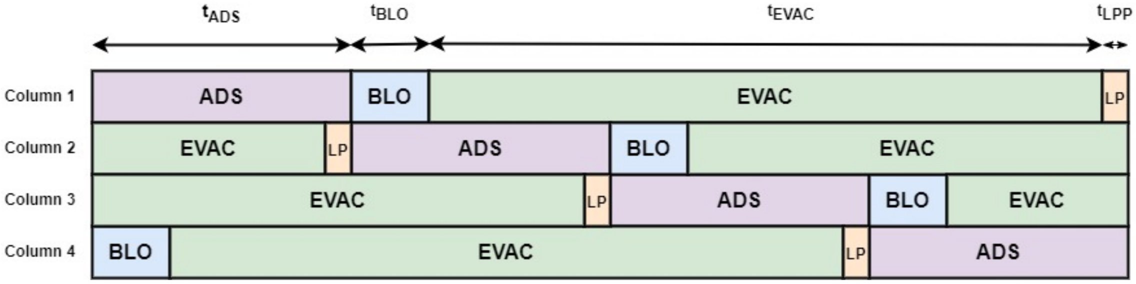

Figure 3.5: Sample column schedule for the 4-step LPP process

Parallel trains

As illustrated in the schematic of the process layout earlier, to treat large flue gas volumes, multiple parallel PVSA unit trains are necessary to achieve a 90% CO_2 capture rate [60]. The calculation for the number of parallel trains is outlined as:

$$M = ceiling(\frac{F_{flue}}{F_{train}}) \tag{3.26}$$

Here, F_{flue} denotes the total flue gas flow rate in kmol/h, and F_{train} represents the average molar flow rate of the feed to each train in kmol/h. It's important to note that the inlet pressure varies during the adsorption step due to the constant velocity boundary condition at the feed end. Consequently, the average molar flow rate of the feed to each train was calculated through an integral average of the molar flow rate throughout the adsorption step. This calculated average was then used to determine the number of parallel trains.

$$F_{train} = \frac{1}{t_{ADS}} \int_0^{t_{ADS}} F dt \tag{3.27}$$

3.3.7 Vacuum pumps

Vacuum pumps are integral to the PVSA process and often represent the largest share of energy consumption. The performance of a vacuum pump depends on the specific flow and pressure conditions. Since the goal of this work is conceptual design we do not care to incorporate actual performance curves - instead, we use an empirical relationship to quantity the efficiency of the vacuum pump solely as a function of the operating pressure. We adopt the following relationship proposed by Maruymana et. al [61].

$$\eta_{\mathrm{V}} = \frac{15.84P}{1 + 19.80P} \tag{3.28}$$

where P (in bar) signifies the suction pressure. The efficiency, denoted as η_{V}, incorporates both the pump and the driver. Figure 3.6 visually illustrates the variation of vacuum pump efficiency with evacuation pressure.

3.4 Cost Assessment

In this work, the costing framework developed by Subraveti et. al is used [55]. The methodology for estimating capital and operating costs is summarized in the following sub-sections.

3.4.1 Capital costs

The purchase and installed cost of process equipment was determined using Aspen Process Economic Analyzer ®. These costs are estimated based on key design parameters such as pressure, diameter, flow rate, etc. Cost functions were developed for each

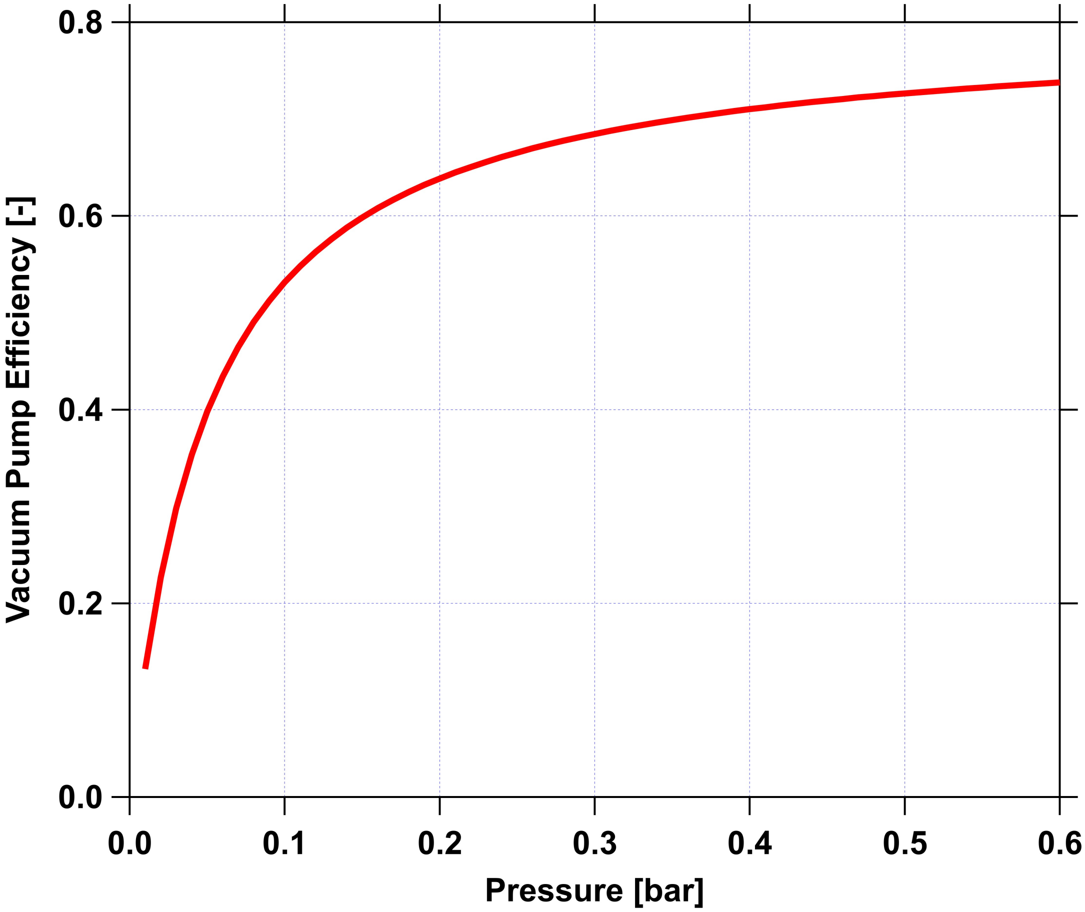

Figure 3.6: Variation of vacuum pump efficiency with evacuation pressure

type of equipment to integrate the capital cost estimation in the techno-economic optimization framework discussed earlier. The correlations developed for estimating the installed cost of major PVSA equipment like compressors, vacuum pumps, columns, heat exchangers, and switching valves are available in the supporting information in the publication by Subraveti et. al. [55].

An overview of the bottom-up approach [62] adopted is illustrated in Fig 3.7. The total direct cost (TDC) was augmented by a process contingency factor amounting to 15% of the TDC without contingencies, in line with NETL guidelines, resulting in the TDC with process contingency (TDCPC) [63]. Following this, indirect costs and project contingencies were added to TDCPC to derive the total plant cost (TPC). Indirect costs, covering engineering expenses, consultancies, service facilities, yard

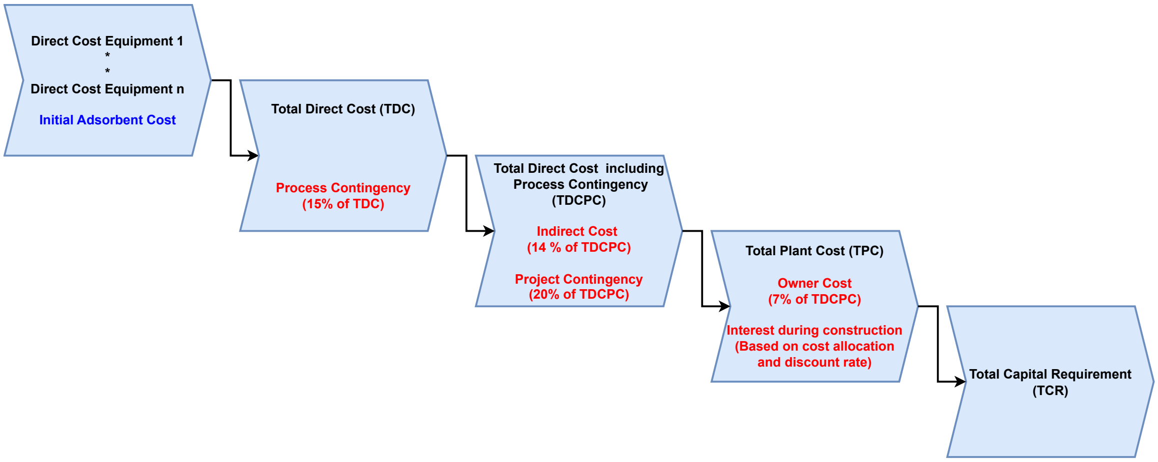

Figure 3.7: Bottom-up approach for calculating capital costs

improvement, building, and sundries, were fixed at 14% of TDCPC. Project contingencies were set at 20% of TDCPC, adhering to NETL guidelines [63]. Finally, owner costs and interest over construction were included in the TPC to calculate the total capital requirement (TCR). Owner costs constituted 7% of TDCPC, and the interest over construction was computed with the assumption that construction costs are spread over a three-year period following a 40/30/30 allocation.

It is important to highlight that the estimation of the direct cost for adsorbents differs from the previously outlined approach due to its specificity. While the cost of an adsorbent holds significance for the design and evaluation of adsorption-based CO_2 capture processes, determining this cost can pose challenges in practice, especially for materials that have not yet been commercialized. In the case of industrially deployed adsorbent Zeolite 13X, its purchase cost was approximated at 1500 USD per tonne [64]. Moreover, beyond adsorbent purchase costs, the expenses related to the transport and installation of adsorbents were uniformly set at 1500 USD per tonne to establish the adsorbent direct cost. Typically, for commercially available adsorbents, transport and installation costs fall within a similar range as the adsorbent purchase cost, aligning with the cost established for Zeolite 13X.

3.4.2 Operating costs

Operating costs are bifurcated into fixed and variable components. The annual fixed operating costs encompass maintenance, labour, insurance, and administrative expenditures. The annual maintenance cost is 2.5% of the total plant cost (TPC), with maintenance labour costs constituting 40% of this aggregate. Yearly disbursements for insurance and location taxes, inclusive of overhead and miscellaneous regulatory fees, are stipulated at 2% of TPC. Labour costs are derived from the assumption that the CO_2 capture unit necessitates five operators (operating in 5 shift patterns, with one operator per shift, given the highly automated nature of adsorption processes), each commanding an annual salary of USD 60000. Administrative costs are established at 30% of the cumulative operating and maintenance labour expenses.

The operating cost corresponding to the periodic replacement of adsorbents due to thermal or mechanical degradation is also considered. The replacement interval for all adsorbents was set at 5 years [65]. Adsorbent replacement costs, covering purchase, transport, and installation expenses, are incurred every five years after the commencement of plant operations for the purpose of renewing the adsorbents.

Variable operating costs include utilities, electricity, cooling water, and adsorbent replacement. The annual utility cost was determined by estimating consumption through process simulations. The unit costs are specified in Table 3.3.

Utility	**Price**
Electricity (USD MWh^{-1})	58.1 [66]
Specific direct emissions (kg.CO_2 MWh^{-1})	38 [67]
Cooling water (USD m^{-3})	0.039 [66]

Table 3.3: Unit costs of utilities

3.5 Performance Metrics

3.5.1 Key technical performance indicators

The definitions for CO_2 purity, CO_2 recovery, overall power consumption, specific energy consumption, and productivity were as follows:

$$CO_2\ Purity\ (\%) = \frac{total\ moles\ of\ CO_2\ in\ the\ product\ step}{total\ moles\ of\ gas\ in\ the\ product\ step} * 100 \tag{3.29}$$

$$CO_2\ Recovery\ (\%) = \frac{total\ moles\ of\ CO_2\ in\ the\ product\ step}{total\ moles\ of\ CO_2\ in\ the\ feed\ step} * 100 \tag{3.30}$$

The overall power consumption (P_{el}) was defined as the sum of the power consumption in each unit train. [60].

$$\begin{split} Overall\ Power\ Consumption,\ P_{el}\ (MW_e) = M * (N_{ADS} * \frac{E_{ADS}(J_e)}{t_{ADS}(s) * 10^6} + \\ N_{BLOW} * \frac{E_{BLOW}(J_e)}{t_{BLOW}(s) * 10^6} + N_{EVAC} * \frac{E_{EVAC}(J_e)}{t_{EVAC}(s) * 10^6}) \end{split} \tag{3.31}$$

In addition to overall power consumption, specific energy consumption was also defined as follows:

$$\begin{split} Specific\ Energy\ Consumption\ (kWh_e\ t_{CO_2}{}^{-1}) = \\ \frac{Overall\ Power\ Consumption\ (kW_e) * Operating\ Hours\ (h\ year^{-1})}{CO_2\ Captured\ (t\ year^{-1})} \end{split} \tag{3.32}$$

Productivity was defined by considering the entire PVSA capture unit as shown below:

$$Productivity\ (TPD\ m^{-3}) = \frac{CO_2\ capture\ rate\ for\ the\ plant\ (TPD)}{total\ adsorbent\ volume\ used\ in\ the\ plant\ (m^3)} \tag{3.33}$$

3.5.2 Key economic performance indicators

The CO_2 avoided cost was deemed the primary economic performance indicator for comparing the cost efficiency of adsorption-based CO_2 capture technology with MEA absorption-based technology. It represents the average discounted CO_2 tax or quota over the project's duration required as income to offset the net present value of additional capital and operating costs arising from CCS infrastructure [68]. The CO_2 avoided cost, expressed in $\mathrm{USD/t_{CO_2\ avoided}}$ (where $\mathrm{t_{CO_2\ avoided}}$ represents metric tonnes of CO_2 avoided), is defined as follows:

$$CO_2\ Avoided\ Cost = \frac{Net\ present\ value\ of\ the\ CCS\ implementation\ cost}{Net\ present\ value\ of\ the\ CO_2\ avoided} \tag{3.34}$$

Or, more specifically,

$$CO_2\ Avoided\ Cost = \frac{\sum_i \frac{TCR_{CCS\ implementation}(i)\ +\ Annual\ OPEX_{CCS\ implementation}(i)}{(1+d)^i}}{\sum_i \frac{Annual\ amount\ of\ CO_2\ emissions\ avoided\ by\ the\ CCS\ implementation\ (i)}{(i+d)^i}} \tag{3.35}$$

where i is the year index (-).

The CO_2 emissions avoided by CCS implementation was defined as the difference between the annual amount of CO_2 captured by CCS implementation and direct emissions due to heat and electricity associated with CCS implementation. Direct emissions due to electricity can be calculated using the following equation:

$$Direct\ Emissions = e_{el}\ * P_{el}(MW_e) * Operating\ hours(h\ year^{-1}) \tag{3.36}$$

Here, e_{el} represents the specific CO_2 emissions associated with each unit of electric power consumed (kg CO_2 $\mathrm{MW_e^{-1}\ h^{-1}}$). By accounting for direct emissions, the equivalent CO_2 avoided reflects the genuine overall reduction in CO_2 emissions from the point source when adsorption capture technology is implemented. This enables a fair comparison with different capture technologies [66]. The economic parameters used to calculate CO_2 avoided cost are detailed in Table 3.4.

Table 3.4: Financial parameters used for calculating CO_2 avoided costs [67]

Parameter	**Value**
Economic lifetime (years)	25
Capacity factor (%)	91.3
CO_2 capture plant construction time (years)	3
Allocation of CO_2 capture construction costs by year (%)	40/30/30
Discount rate (%)	8

The CO_2 capture avoided cost, in $\$/\mathrm{tonne}_{\mathrm{CO_2\ avoided}}$ is defined as follows:

$$CO_2\ Avoided\ Cost = \frac{\sum_i \frac{TCR_{PVSA\ capture\ plant}\ (i)\ +\ Annual\ OPEX_{PVSA\ capture\ plant}\ (i)}{(1+d)^i}}{\sum_i \frac{Annual\ amount\ of\ CO_2\ emissions\ avoided\ by\ the\ PVSA\ capture\ plant\ (i)}{(i+d)^i}} \tag{3.37}$$

3.6 Techno-economic Optimization Framework

The design of the PVSA process was approached with an integrated strategy, emphasizing the optimization of both technological and economic aspects. This included identifying the most favorable design and operational parameters for the process. The multiobjective optimization approach combined considerations of process and material with cost models to achieve the dual objectives of minimizing CO_2 capture expenses while maximizing both CO_2 recovery and CO_2 purity.

The three objective optimizations considered in this work are given below;

1. Objective 1: Maximize Purity

2. Objective 2: Maximize Recovery

3. Objective 3: Minimize CO_2 avoided costs

The variable set includes parameters such as adsorption step duration (t_{ADS}), blowdown vacuum pump capacity (S_B), evacuation vacuum pump capacity (S_E), intermediate vacuum (P_I), evacuation vacuum (P_L), and column diameter (D). In the case of the four-step PVSA cycle under consideration, t_{ADS} can be adjusted during the adsorption step to manage the feed flow rate and control the propagation of the CO_2 front along the column. Since this step operates at atmospheric pressure, the feed pressure can be determined using Ergun's equation. For the blowdown and evacuation stages, the vacuum levels, P_I and P_L, are variable parameters. Additionally, the volumetric flow rates of the blowdown (S_B) and evacuation vacuum pumps (S_E) can be adjusted for their respective stages. To achieve this, S_B and S_E were implicitly modified in terms of the interstitial velocities, v_B and v_E, respectively. This was done to establish a suitable range for vacuum pump sizing for the columns, with an implicit upper limit of 20,000 m^3/h imposed on the maximum vacuum pump size. It is important to note that the model calculates the blowdown and evacuation step durations based on S_B and S_E, respectively. Additionally, the duration of light product pressurization is determined by t_{ADS} and is not treated as a variable in the optimization process. In the context of the scale-up design, the column diameter (D) was included as a variable. Since the column length and diameter can be adjusted simultaneously, the length-to-diameter (L/D) ratio remains constant during the optimization. The specified lower and upper bounds for the variables are detailed in Table 3.5.

The constrained optimization problem was converted into an unconstrained problem by incorporating penalty terms into the objective function. These penalty terms in the objective function impose significant costs when constraints are violated. The problem was then tackled using a non-dominated sorting genetic algorithm II (NSGA-II), a global search method that approaches optimal solutions by simulating the evolutionary process. In simpler terms, the algorithm initiated a distinct set of decision variables within predefined bounds using Latin hypercube sampling. Subsequently, it assessed objective function values based on the integrated PVSA process and cost

Table 3.5: Lower and Upper Bounds used in the optimizations

Decision variable	**Lower bound**	**Upper bound**
Adsorption time, $t_{\mathrm{ADS}}(\mathrm{s})$	50	400
Blowdown vacuum pump flow rate, $S_{\mathrm{B}}\left(\mathrm{m}^3\ \mathrm{h}^{-1}\right)$	1500	20000
Evacuation vacuum pump flow rate, $S_{\mathrm{E}}\left(\mathrm{m}^3\ \mathrm{h}^{-1}\right)$	1500	20000
High pressure, P_{H} (bar)	1	3.6
Intermediate pressure, P_{I} (bar)	$P_{\mathrm{L}}+0.01$	0.99
Low pressure, P_{L} (bar)	0.01	0.2
Column Diameter, $D(\ \mathrm{m})$	2	3
Pellet porosity, $\epsilon_{\mathrm{p}}(-)$	0.2	0.8
Pellet diameter, $d_{\mathrm{p}}(\mathrm{mm})$	1	5

models, forming a generation. NSGA-II iteratively enhanced the objective function values across multiple generations by applying operations such as mutation and crossover. The optimization was implemented using global optimization and parallelization toolboxes in MATLAB 2018b. The population size was established as 24 times the number of variables, and the optimization process was terminated after 50 generations.

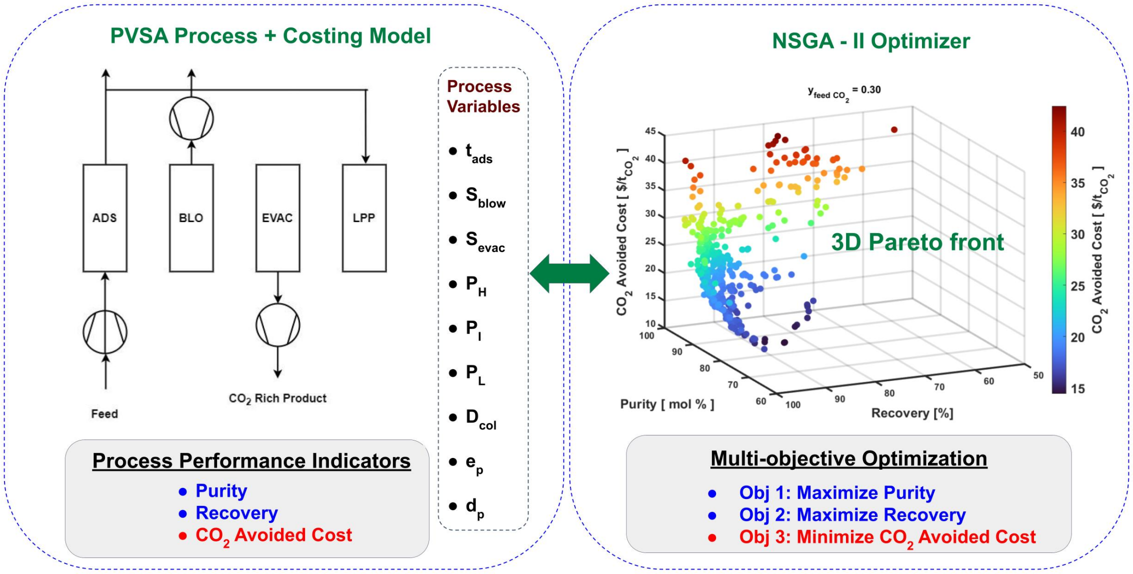

Figure 3.8: Schematic of techno-economic optimization framework

3.7 Results and Discussion

Five different feed CO_2 compositions of flue gases from various point sources ranging from gas turbine power, coal power, SMR, steel and cement industry are considered. Multiple optimizations were carried out to determine the three-dimensional Pareto corresponding to the three objectives considered in the optimization. The results from this optimization were analyzed to determine the Pareto fronts and to study how the process performance and operating parameters vary under different constraints.

3.7.1 CO_2 avoided costs at reduced purity levels

The cost reduction potential of the PVSA process at reduced purity levels but at high recoveries by filtering out data points with recovery > 90 % and purity > 40 % is presented. Key results corresponding to a feed CO_2 composition of 13 mol % are presented as follows. Results for all other compositions are compiled in Appendix B.

Figure 3.9 shows the variation of CO_2 avoided costs at reduced purity levels for a feed flue gas composition of 13 mol %. In this analysis, it is important to note that

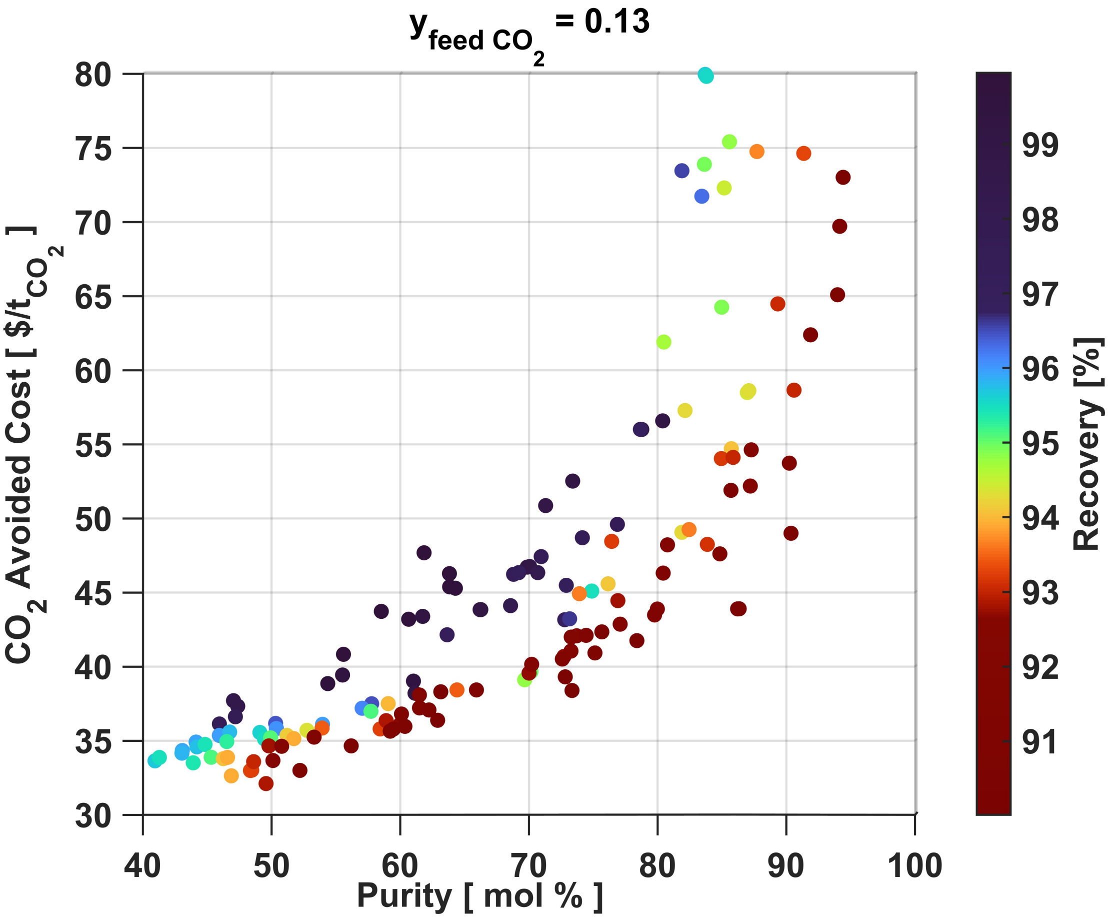

Figure 3.9: Projection of the Pareto surface on the CO_2 avoided cost - Purity plane

high recovery levels in excess of 90% are maintained. As the optimization problem is set up to simultaneously maximize opposing objectives i.e. recovery and purity, for lower purity levels, very high recovery rates in excess of 95% are achievable. A significant reduction in CO_2 avoided costs as low as $32/tonne CO_2 avoided at purity levels of 50-60 % is achievable. For a particular purity, the data points (red coloured) cost corresponds to recoveries close to 90-93 %; however, recoveries > 95 % (blue coloured) are also achievable but at slightly higher costs. A sharp increase can be seen for purities > 75 %. In the region where the purity is in excess of 90%, the CO_2 costs are more than double. Also, at high purity levels, not only are the costs high, but the optimizer struggles to achieve recoveries in excess of 90 % as it hits the lower bound of the evacuation pressure. These results suggest that a PVSA process is economical as a preconcentration unit, as it is able to achieve higher recovery rates at reduced purity levels.

3.7.2 Specific energy consumption at reduced purity levels

The specific energy consumption is another crucial parameter that determines the effectiveness of a separation process. From a CO_2 capture perspective, the energy penalty associated with separating CO_2 has to be as low as possible in order to minimize the operating cost of capture as well as reduce the specific emissions associated with the energy generation. Figure 3.10 illustrates the specific energy consumption of the PVSA process under consideration at reduced purity levels. It is important to note that, the reported energy values correspond to the same data points as for the CO_2 avoided costs. At reduced purity levels, the specific energy consumption tends to reduce significantly to as low as 200 kWh/tonne of CO_2 captured.

3.7.3 Productivity at reduced purity levels

The productivity of the PVSA process is directly related to the size of the capture plant, as it determines the size of the adsorber vessels and the number of parallel PVSA trains required to process a desired throughput of flue gas. Productivity represents the rate at which CO_2 that can be captured from the flue gas per unit volume of adsorbent material used. High productivity values are desirable in order to improve the scalability of a PVSA process. Figure 3.11 illustrates the productivity of the PVSA process under consideration at reduced purity levels. A clear increase in productivity can be seen under reduced purity. The productivity values are almost two to three times higher at the purities of around 40-50 mol % compared to the region with higher purity (90 mol %).

The increase in productivity at reduced purity levels can be explained by analyzing the key process variables such as the evacuation pressure (P_L) i.e., the required vacuum level as well as the total cycle time of the PVSA process. In the four-step

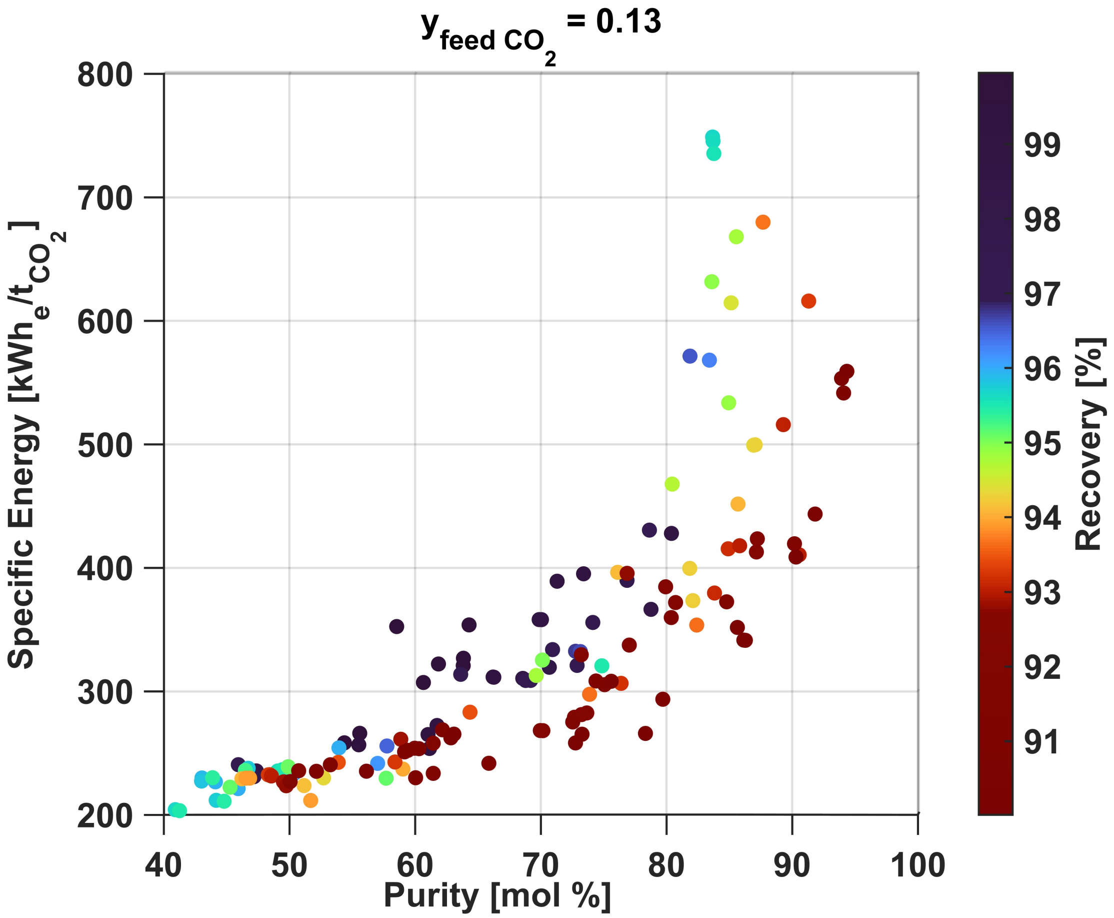

Figure 3.10: Specific energy consumption corresponding to points on the Pareto surface shown in Fig. 3.9

LPP cycle considered in this work, the evacuation step is the longest and, thus, the time-limiting step of the cycle. The evacuation time is determined based on the evacuation vacuum pump capacities, and it is only so fast, that the vacuum pumps can reduce the pressure in the columns to the required evacuation pressure. The lower the evacuation pressure, the more time it takes for the evacuation step to complete. Thus prolonging the total cycle time of the PVSA process.

At reduced purity levels, as illustrated in Fig 3.12, the evacuation pressure required by the process increases, meaning milder vacuum conditions are sufficient. At a purity level of 40-50 mol%, the evacuation pressure is almost ten times higher than that required to achieve a purity level of 95 mol %. Thus at reduced purity levels, the

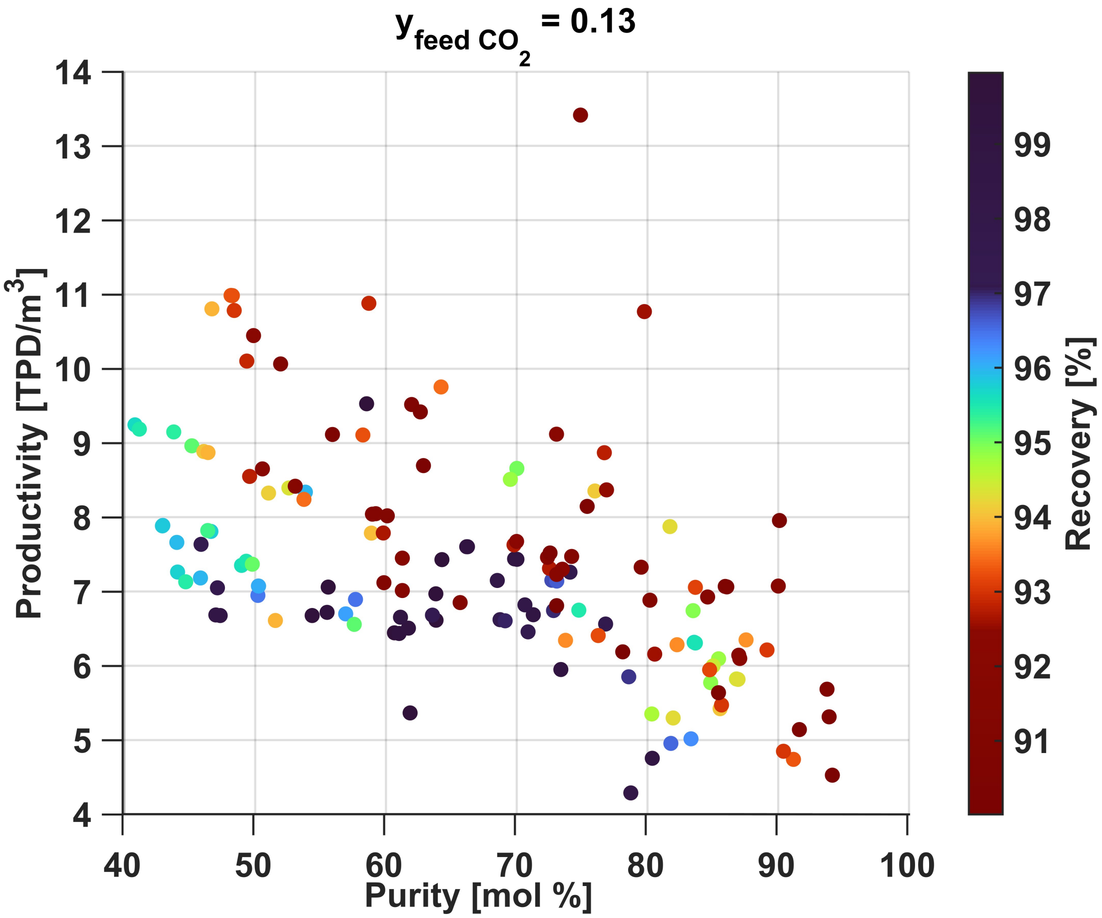

Figure 3.11: Productivity corresponding to points on the Pareto surface shown in Fig. 3.9

evacuation times are significantly shorter in the evacuation step. As discussed earlier, the reduction in the evacuation time results in significantly smaller total cycle times. Figure 3.13 illustrates the variation in total cycle time at reduced purity levels. Cycle times as low as 250 s for purity levels of 40-60 mol % are achievable. This is roughly four times less than that required for high purity levels.

As discussed earlier, the productivity can be increased by reducing the total cycle times. An increased productivity means a unit volume of adsorbent can capture CO_2 at a faster rate or in other words, the the amount of adsorbent required to process a particular throughput of gas reduces and thus translates into a reduction in the total number of parallel PVSA trains required. Figure 3.14 illustrates the reduction in the

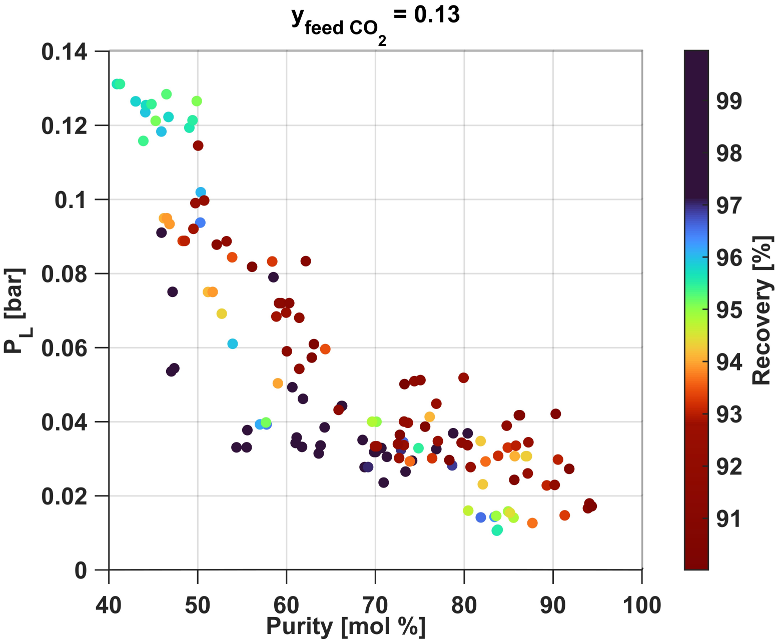

Figure 3.12: Evacuation pressure (P_L) corresponding to the Pareto surface shown in Fig. 3.9

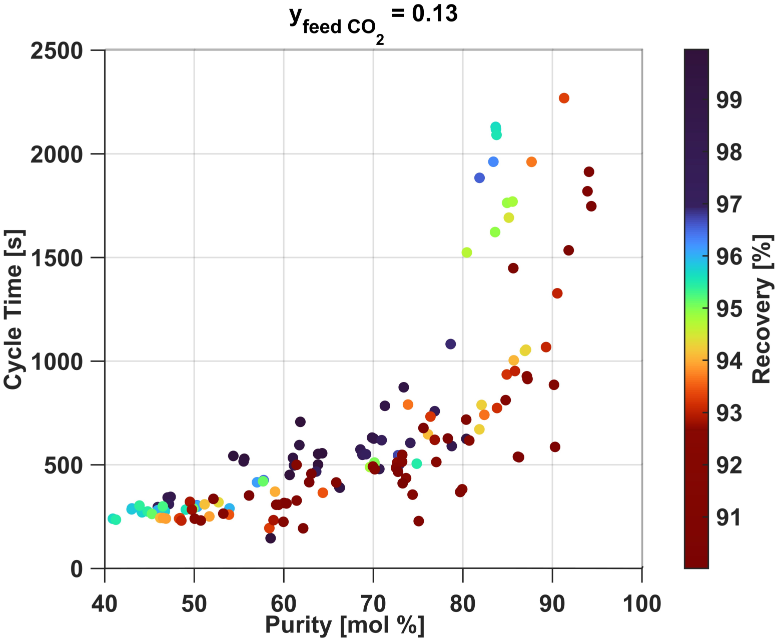

Figure 3.13: Cycle time corresponding to points on the Pareto surface shown in Fig. 3.9

total number of PVSA columns at reduced purity levels.

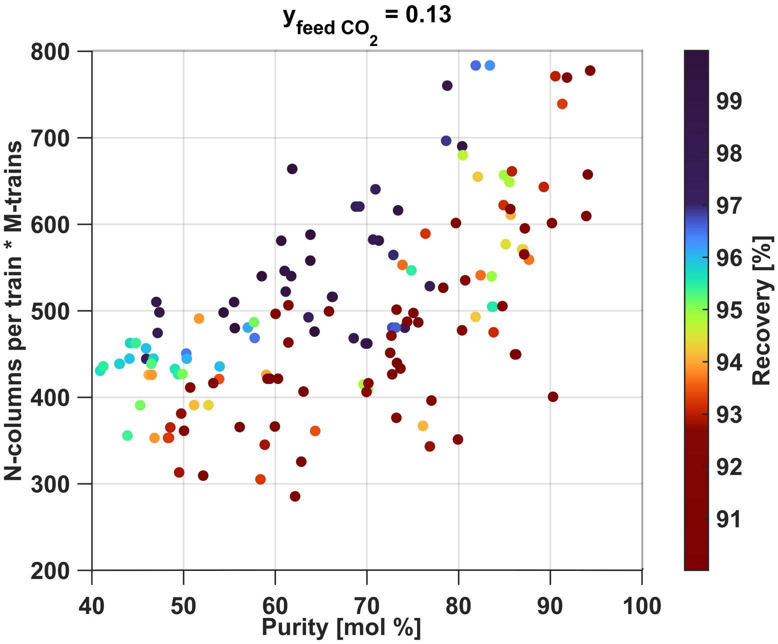

Figure 3.14: Total number of columns in the PVSA unit corresponding to points on the Pareto surface shown in Fig. 3.9

3.7.4 CO_2 avoided cost - purity Pareto

Figure 3.15 shows the CO_2 avoided cost-purity Pareto front for the five different feed compositions considered in this work. It is worth noting that the CO_2 recovery in all the cases is >90%. For all the feed compositions, the CO_2 cost reduces with purity. This trend is more profound for the dilute feed compositions. For instance, for the feed composition of 3.5%, the CO_2 avoided costs at a purity of 45% are as low as \$150/tonne CO_2 avoided. For the feed composition of 7.5%, the costs at a purity level of 40% are half of that at a purity of 90%. For the higher feed composition ranges, i.e. >13%, the CO_2 avoided cost rise steeply after a purity level of 90%. However, the reductions in the costs are gradual, indicating that a PVSA unit is more suited as a pre-concentration block rather than a purification block. It is important to note that for higher feed composition ranges, i.e. >13%, recoveries significantly greater than 90% are achievable when a PVSA unit is operated at reduced purity levels. Other process performance parameters corresponding to the points on the Pareto fronts, such as specific energy consumption, and productivity, are provided in the Appendix B.

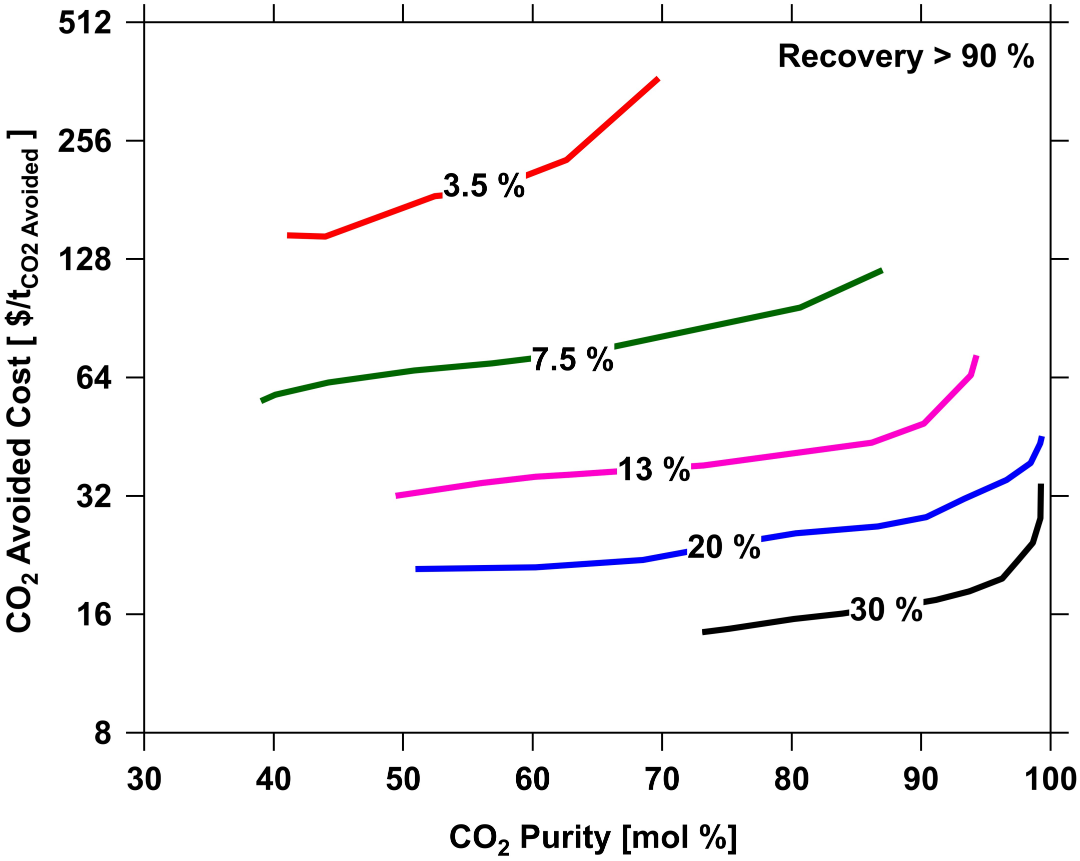

Figure 3.15: The CO_2 avoided cost - purity Pareto for the PVSA process at five different feed compositions

3.8 Conclusion

A techno-economic analysis of the four-step LPP PVSA process for post-combustion CO_2 capture using Zeolite 13X adsorbent is performed using multi-objective optimization to study the cost reduction potential at reduced purity levels. Five different feed CO_2 compositions representative of a wide variety of industrial flue gas streams are studied. The reduction in the costs at lower purity levels is explained by analyzing the specific energy consumption, productivity and pressure levels for the PVSA process under consideration. The specific energy consumption is reduced at lower purities, resulting in lower operating costs. At the same time, productivity is increased, resulting in lower capital costs. Both effects combined explain the reduction in the CO_2 avoided costs at reduced purity levels. This observation is further corroborated by analyzing the adsorption pressure (high pressure) and the evacuation pressure (low pressure) needed in the process, as these process variables are strongly related to specific energy consumption and productivity. At reduced purity levels, the adsorption pressure required is lower, thus reducing the energy spent on feed gas compression. In the case of evacuation pressure, a milder vacuum level is sufficient, meaning less energy is spent by the vacuum pumps as they can be operated at higher efficiencies at milder vacuum levels compared to deep vacuum levels. It is essential to note the strong effect of evacuation pressure on the cycle time of the PVSA process. With practical limits to the capacity of vacuum pumps, deeper vacuum levels result in longer evacuation times and, thus, longer cycle times. Longer cycle times translate into lower productivity, resulting in more parallel PVSA trains to process a desired throughput of flue gas.

Chapter 4

Standalone Liquefaction Process Performance

4.1 Introduction

Liquefaction is a widely popular process in the natural gas industry. Natural gas from underground reservoirs is conditioned and liquified before being shipped long distances. Liquefaction significantly reduces the volume of the product as its density is increased multifold. Liquefaction is also used in the area of gas separations. In the cryogenic distillation of air, the air is compressed and cooled to cryogenic temperatures to separate it into its two primary constituents: nitrogen and oxygen.

In CO_2 capture, liquefaction separates a mixture of primarily CO_2 and N_2 along with gases like oxygen and other impurities. A feed gas mixture containing CO_2 and N_2 is compressed and subjected to sub-ambient temperatures to liquefy CO_2 while the other gases remain in the vapour phase. The condensed CO_2 can then be separated in a vapour-liquid phase separator. The purity and recovery of the liquid CO_2 produced in this process depend on the operating pressure, temperature conditions, and feed gas CO_2 composition. The energy of the pressurized incondensable gases can be recovered by allowing the high-pressure gas to expand in turbo-expanders, which drives a generator that produces electricity. Heat integration is a crucial part of a liquefaction process as it helps reduce the utility consumption in the chiller, thus improving the overall energy efficiency of the process.

The thermodynamic information for liquefaction processes is captured as isothermal binary vapour-liquid equilibrium data. This information helps in determining the operational limits of the liquefaction process. For instance, it helps us determine the minimum pressure required to liquefy a gas stream with a certain CO_2 composition and temperature. What fraction of the gas can be liquified depending on the composition, pressure and temperature? What is the composition of the liquid and vapour phases at a certain temperature and pressure?

A liquefaction process is an attractive option as a purification unit for CO_2 capture applications. It can produce very high-purity CO_2 as a liquid stream, thus potentially eliminating the need for a product compression stage. Liquefaction also allows us to deal with impurities such as oxygen, nitrous and sulphur oxides that may be present in the flue gas in varying quantities. In this chapter, a detailed techno-economic assessment of the liquefaction process is presented.

4.2 Pure Component Phase Diagrams for CO_2 and N_2

The pure component phase diagrams for CO_2 and N_2 hold crucial thermodynamic information related to the phase equilibrium of these chemical species. Figure 4.1a presents the pure component phase diagram for CO_2. The vapour pressure curve shown in green indicates the boundary between the vapour and liquid phase. The melting curve shown in red indicates the boundary between the solid and the liquid phases. The sublimation curve in blue indicates the boundary between the solid and the vapour phases. The intersection of the three curves is the region where all three phases coexist, known as the triple point. The triple-point for CO_2 corresponds to a temperature of -56.4 °C and a pressure of 5.18 bar. Taking the triple-point of CO_2 and the melting curve into consideration is essential in designing the liquefaction process as it determines the lowest operating temperature permissible to avoid issues related to CO_2 freezing in different parts of the process.

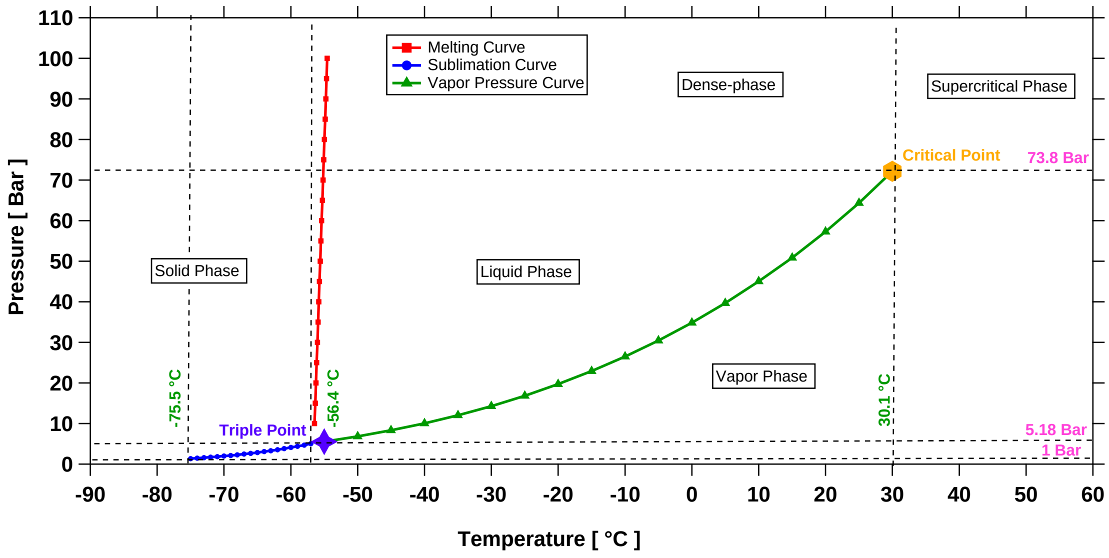

(a) CO_2

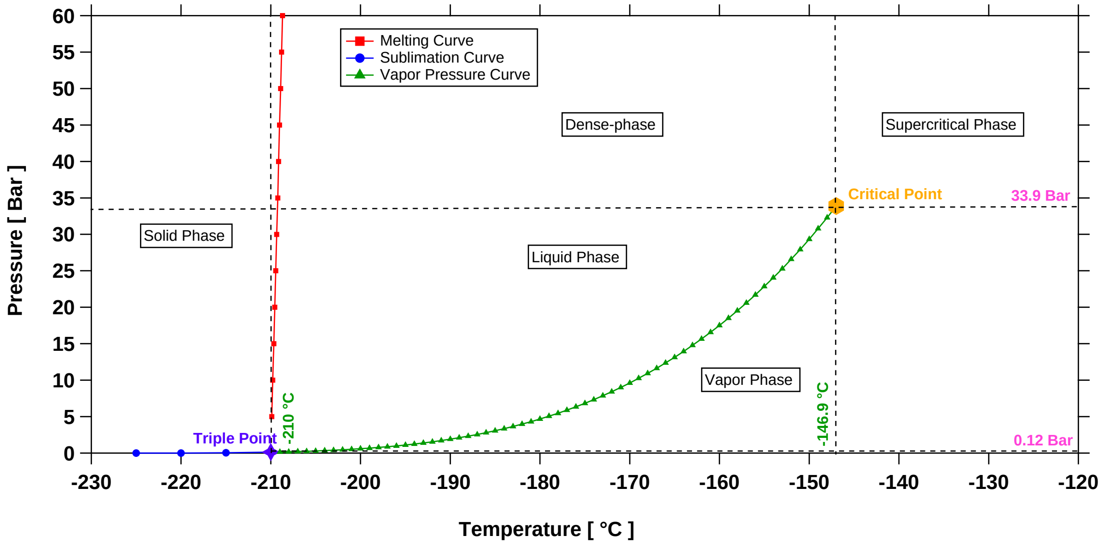

(b) N_2

Figure 4.1: Pure component phase diagrams for CO_2 and N_2 [69]

The critical temperature for CO_2 is 30.1 °C, and the corresponding critical pressure is 73.8 bar. For temperatures higher than the critical temperature and pressures higher than the critical pressure, CO_2 is known to exist in a super-critical phase. In the region above the critical pressure but below the critical temperature, CO_2 exists in a dense phase. This region is important for the CO_2 transport and storage as in this region; the CO_2 density is the highest and the specific volume the lowest.

Figure 4.1b presents the pure component phase diagram for N_2. N_2 has a critical temperature of -146.9 °C, which is much lower than that of CO_2, and explains why it is not condensed much at operating temperature ranges in the liquefaction unit, thus allowing the CO_2 to be drawn as a liquid at high purity. N_2 has a triple point of -210 °C and a critical pressure of 33.9 bar.

4.3 Isothermal Binary Vapor-Liquid Equilibrium Data for CO_2-N_2 System

The pure component phase diagrams are insufficient information to design a liquefaction unit; they do not capture the vapour-liquid equilibrium information for mixtures of CO_2 and N_2 with varying compositions. The dew point and bubble points of mixtures of CO_2 and N_2 vary with composition. Due to the highly non-ideal behaviour of these gas mixtures, estimating the vapour-liquid equilibrium in the form of dew points and bubble points using Raoult's law is not appropriate. Thus, to accurately model their separation by liquefaction, it is critical to experimentally measure the vapour-liquid equilibrium for these mixtures and fit them to appropriate thermodynamic models.

Experimentally measured binary isothermal vapour-liquid equilibrium data at -50 °C and 25 °C for the CO_2-N_2 system reproduced from Westman et. al [70] is presented in Figure.4.2 and Figure. 4.3 respectively. Experimentally measured binary isothermal vapour-liquid equilibrium data at -25 °C for the CO_2-N_2 system reproduced from Lasala et. al [71] is presented in Figure.4.4.

A binary isothermal plot represents the equilibrium composition of the vapour and liquid phases at a fixed temperature. The minimum pressure at which the first dew appears for a particular gas mixture composition is the dew pressure shown in red and the corresponding liquid composition in blue. With further increase in pressure, more gas can be liquefied, and the fraction of the initial gas that gets liquefied can be estimated based on the lever rule. This plot also helps in understanding how

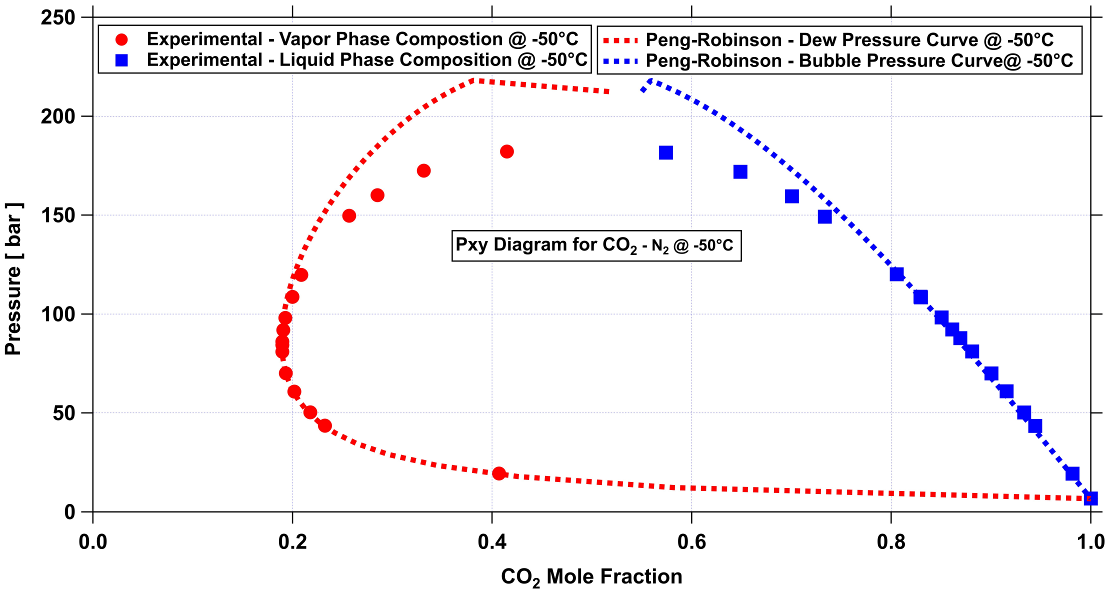

Figure 4.2: Peng-Robinson EOS model fitted to VLE Data at -50°C

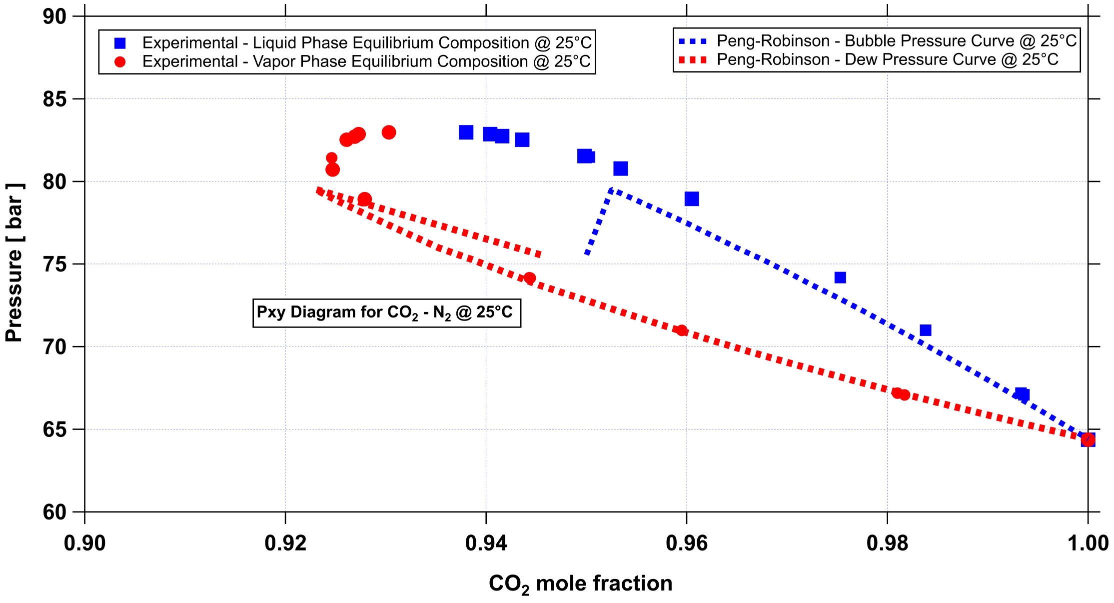

Figure 4.3: Peng-Robinson EOS model fitted to VLE Data at 25°C

pressure affects the recovery of CO_2 as a liquid in the liquefaction unit. As is evident in Figure. 4.2, at -50 °C, if we were to feed a gas mixture of particular composition to the liquefaction unit, the liquid CO_2 recovery can be maximized by pressurizing the gas up to 80 bar, however, the purity of the liquid CO_2 is reduced. It is essential to understand that the minimum CO_2 composition that can be liquified at -50 °C is $\approx$

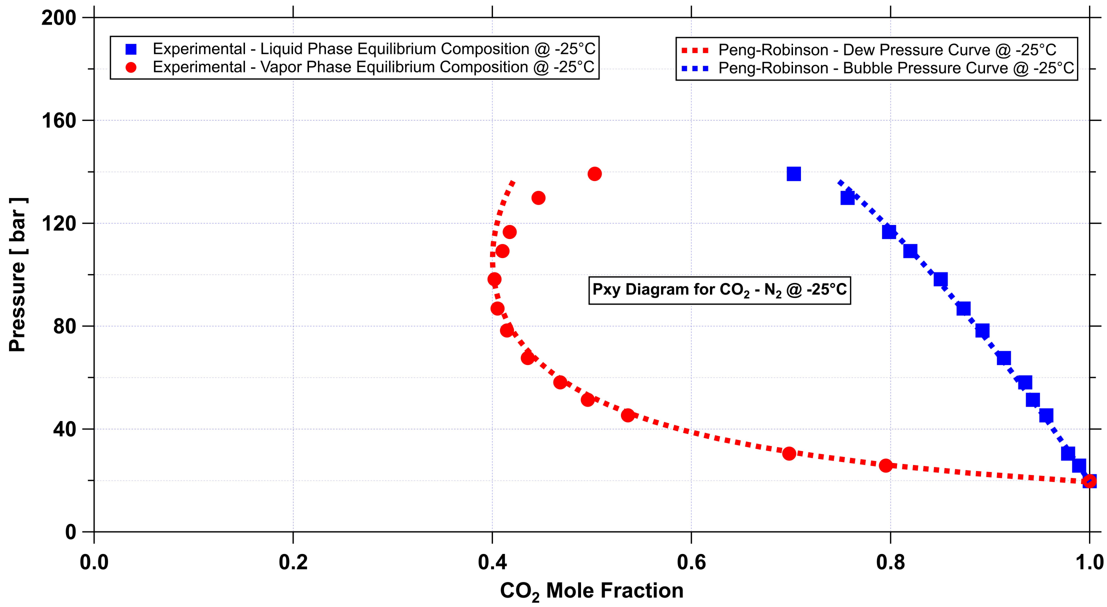

Figure 4.4: Peng-Robinson EOS model fitted to VLE Data at -25°C

18 mol %. This has implications from the process design perspective as it limits the serviceable range of liquefaction as a purification unit to above 18 mol %. Although pushing the operating temperature in the liquefaction unit closer to the triple-point of CO_2 can technically improve the liquid CO_2 recovery and serviceable range, doing so is not recommended to avoid any potential freezing issues.

Figure 4.3 presents binary isothermal VLE data for the system at 25 °C. As indicated earlier, this temperature condition is relevant to the transport and storage sections. With typical purities over 95 mol %, the minimum transport and storage pressure essential to keep the captured CO_2 in a dense phase and prevent phase separation is more than 85 bar.

Thermodynamic Model for CO_2-N_2 Liquefaction

Modelling the Pressure-Volume-Temperature (PVT) relationship and the phase equilibrium behaviour of the CO_2-N_2 system accurately is crucial in process simulation as it significantly affects the performance of the separation process. Liquefing the gas involves compressing the feed gas mixture to high pressures, which implies that the gas mixture can no longer be assumed to behave ideally and thus limits the use of the ideal gas law and Raoult's law. Hence, more advanced equations of state are required to estimate important thermodynamic properties such as the volumetric flow rates of gas and liquid phases along with the phase behaviour with reasonable accuracy. This allows us to adequately size process equipment and make better cost estimates.

The Peng-Robinson equation of state with the standard alpha function is the recommended property method for hydrocarbon processing applications such as gas processing, refinery, and petrochemical processes. This work considers the Peng-Robinson equation of state, Eq. 4.1 to predict the PVT relationship of pure gases and mixtures. It is coupled with appropriate mixing rules and binary interaction parameters for modelling gas mixtures accurately [72].

$$P = \frac{RT}{V_m - b} - \frac{a}{V_m(V_m + b) + b(V_m - b)} \tag{4.1}$$

where, P is the pressure, T is the temperature, V_m is the molar volume, b is a parameter relating to the volume occupied by one-mole molecules, and a is a parameter related to the attractive forces between the molecules

$$b = \sum_i x_i b_i \tag{4.2}$$

where, x_i is the mole fraction of component i and b_i the parameter relating to the volume occupied by one-mole molecules of component i.

$$a = \sum_i \sum_j x_i x_j (a_i a_j)^{0.5}(1 - k_{ij}) \tag{4.3}$$

where, a_i, and a_j are the parameters related to the attractive forces between the molecules of components i and j, respectively. k_{ij} is the binary interaction parameter.

$$a_i = \alpha_i 0.45724 \frac{R^2 T_{ci}^2}{P_{ci}} \tag{4.4}$$

where, α_i is a temperature-dependent parameter, T_{ci} is the critical temperature of component i, P_{ci} is the critical pressure of component i.

$$b_i = 0.07780 \frac{RT_{ci}}{P_{ci}} \tag{4.5}$$

$$\alpha_i(T) = [1 + m_i(1 - T_{ri}^{1/2})]^2 \tag{4.6}$$

where, T_{ri} is the reduced temperature defined as

$$T_{ri} = \frac{T}{T_c} \tag{4.7}$$

$$m_i = 0.37464 + 1.5422 w_i - 0.26992 w_i^2 \tag{4.8}$$

where, ω_i is acentric factor of component i.

$$k_{ij} = k_{ij}^{(1)} + k_{ij}^{(2)} T + \frac{k_{ij}^{(3)}}{T} \tag{4.9}$$

$$k_{ij} = k_{ji} \tag{4.10}$$

Eq.4.10, means that the interaction between component i and j is the same as the interaction between component j and i, which is a reasonable assumption for many systems. This assumption simplifies the model without sacrificing accuracy in many practical applications. The symmetry of k_{ij} is a common feature in many equations of state, including the Peng-Robinson EOS, and it helps to reduce the number of parameters that need to be determined or estimated when dealing with multi-component systems.

In Eq. 4.1, $i = CO_2, N_2$ are the two species under consideration. The parameters a, b in Eq. 4.1 are calculated from Eq. 4.2 through Eq. 4.8. Eq. 4.3 is the standard quadratic mixing term, where k_{ij} has been made temperature-dependent and is calculated using Eq. 4.9. For accurately modelling the vapour-liquid equilibrium behaviour, the binary interaction parameters $k_{ij}^{(1)}, k_{ij}^{(2)}, k_{ij}^{(3)}$ are obtained by regressing experimentally measured isothermal VLE data at multiple temperatures to predict the phase behaviour over a wide temperature range closely.

Table 4.1 presents the pure component parameters used in the above-described calculation method. Table 4.2 shows the binary interaction parameters for the CO_2-N_2 pair obtained from fitting experimental VLE data. These parameters were retrieved from Aspen's physical property database APV140 EOS-LIT.

Table 4.1: Pure component parameters used in the standard Peng-Robinson EOS

	Parameters		
	T_c (°C)	P_c (bar)	ω (-)
CO_2	31.06	73.83	0.231
N_2	-146.95	34	0.0425

Table 4.2: Binary interaction parameters used in the standard Peng-Robinson EOS

Parameters	**Value**
$k_{ij}^{(1)}$	-0.017
$k_{ij}^{(2)}$	0
$k_{ij}^{(3)}$	0

At -50°C, the Peng-Robinson EOS predicts the dew and bubble compositions for up to 125 bar with reasonably good accuracy. However, at higher pressures closer to the super-critical region, it underestimates the dew compositions and overestimates the bubble compositions. A similar trend is observed at -25°C; however, the deviation occurs at pressures above 90 bar. At 25°C, the dew compositions are predicted with reasonable accuracy up to 75 bar. However, the bubble compositions can be underestimated even at lower pressures.

It is important to note that despite deviations at higher pressures, the Peng-Robinson EOS fairly accurately predicts the phase behaviour in the operating range of interest for the liquefaction unit, i.e. in the pressure range of 1 bar to 60 bar and the temperature range of -50 °C to 25°C. Thus, the Peng-Robinson EOS can be relied on for simulating all the unit operations in the liquefaction unit.

4.4 Model flow sheeting and heat integration

This section discusses the flow-sheeting details of the liquefaction unit. The entire liquefaction unit is simulated using the Peng-Robinson thermodynamic package in the Aspen Plus© simulation environment. In the properties environment, initially, the Peng-Robinson property method is selected, and the program is set up to use this property method in all the unit operations to be used in the simulation environment.

As mentioned earlier in this chapter, the liquefaction unit compresses feed gas from the PVSA unit. Then, it chills it to cryogenic temperatures to facilitate the recovery of liquid CO_2 as the separation product. The compression train consists of a series of compressors wherein the feed gas pressure is increased in stages by maintaining a practical pressure ratio of 1.8 - 2.2. A reasonable isoentropic and mechanical efficiency of 85% are assumed for both. As the gas is pressurized, it heats up, and its temperature increases and thus must be cooled before feeding to the next compression stage. This is done using inter-stage cooling where the gas is cooled to 35°C using cooling water as the cooling utility. In the penultimate compression stage, the gas is pressurized up to 35 bar, and the stream is combined with an internal recycle from the downstream purification separator. This combined stream is then fed to the last compression stage, compressed up to 60 bar before being sent to the chilling section.

The compressed gas is cooled down to -50°C in a series of heat exchangers. A significant portion of CO_2 is liquefied in the multistream heat recovery exchanger through heat integration. This considerably reduces the refrigeration load on the

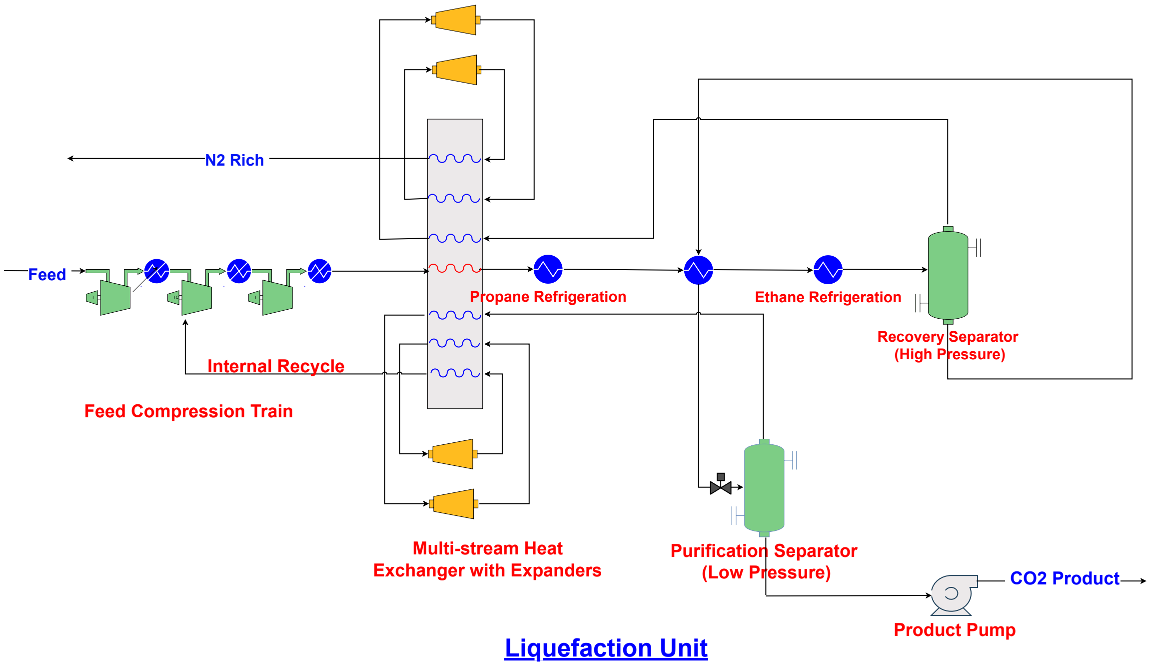

Figure 4.5: Process Flow Diagram of Liquefaction Process

downstream chillers. It is accomplished by allowing the cold N_2 rich stream to exchange heat with the hot compressed feed gas in the heat recovery exchanger. The cold N_2 rich steam from the recovery separator is at high pressure, and thus, its pressure energy can be recovered as shaft work by allowing it to expand in a series of turbo expanders. The shaft work can be used to drive an electrical generator and thus generate electrical power. Depending on the feed gas composition, multiple stages of expansion may be required for this, as with each expansion stage, the gas cools due to the Joule-Thomson effect, and thus, the pressure ratio in each expansion stage has to be adjusted such that the outlet temperature remains well above the triple-point of CO_2. The partially condensed feed gas is fed to the main refrigeration chiller and cooled to the lowest temperature of -50°C. Ethane can be used as a cooling utility in this chiller.

The compressed, chilled and partially liquefied feed gas stream is taken to the first phase separator vessel, the recovery separator. The recovery separator separates all the condensed liquid from the uncondensed gas. The uncondensed gas stream rich in N_2 is recycled to the PVSA unit after passing through the heat integration blocks explained above. The condensed liquid is rich in CO_2 but may not be at the desired purity level of 95 mol % CO_2 or more. Hence, this stream is taken to the second phase separator vessel, the purification separator. In the purification separator, the liquid CO_2 is flashed by reducing its pressure to about 37 bar, and then the phases are separated. The liquid stream from the purification separator is now at the desired purity and thus drawn out as the product stream. Since this stream is now at a low pressure, it has to be pumped to the desired final pressure suitable for transport and storage using a centrifugal pump. This high-pressure dense phase stream can exchange heat with the feed gas for heat integration before being transported and stored.

In the sample flowsheet shown in Fig. 4.6, a feed stream shown in magenta with a CO_2 composition of 60 mol % is fed to the liquefaction unit. The captured CO_2 product stream with a purity of 95 mol % is shown in green and the N_2 rich stream with a roughly 18-20 mol % composition is shown in blue. The feed stream is obtained from the upstream PVSA unit in the hybrid process, as presented in the following chapter. The N_2 rich stream will be recycled to the PVSA unit to improve the recovery of the overall hybrid process. Table 4.4 lists important streams' flow rates, compositions, and conditions in the liquefaction flowsheet.

Table 4.3: Block specifications used in the simulation

Block	Block Specification	Unit	Value
Feed Compressor			
STAGE1			
STAGE2	Pressure ratio	-	2.2
STAGE3	Isentropic efficiency	-	0.85
STAGE4	Mechanical efficiency	-	0.85
STAGE5			
Inter-Stage Coolers			
INTCOOL1	Hot stream outlet temperature	°C	35
INTCOOL2	Pressure drop	bar	0.1
INTCOOL3	Overall heat transfer coefficient	$Wm^{-2}K^{-1}$	850
INTCOOL4			
Heat Recovery Exchanger (HTRC)			
CO_2-PROD	Cold side streams - outlet temperature	°C	25
INTRECYL			35
EXP1IN			100
EXP2IN			100
EXP3IN			100
N2RICH			25
Turbo-Expanders			
EXPAND1	Pressure ratio	-	0.3
EXPAND2	Isentropic efficiency	-	0.85
EXPAND3	Mechanical efficiency	-	0.85
Main Chiller			
ETH-VAP	Hot stream outlet temperature	°C	-52
	Pressure drop	bar	0.3
	Overall heat transfer coefficient	$Wm^{-2}K^{-1}$	1350
Recovery Separator			

Table 4.3 continued from previous page

Block	Block Specification	Unit	Value
SEP1	Heat duty	GJh^{-1}	0
	Pressure drop	bar	0
Purification Separator			
SEP2	Pressure	bar	37
	Heat duty	GJh^{-1}	0
Product Pressurization Pump			
PUMP	Discharge pressure	bar	150

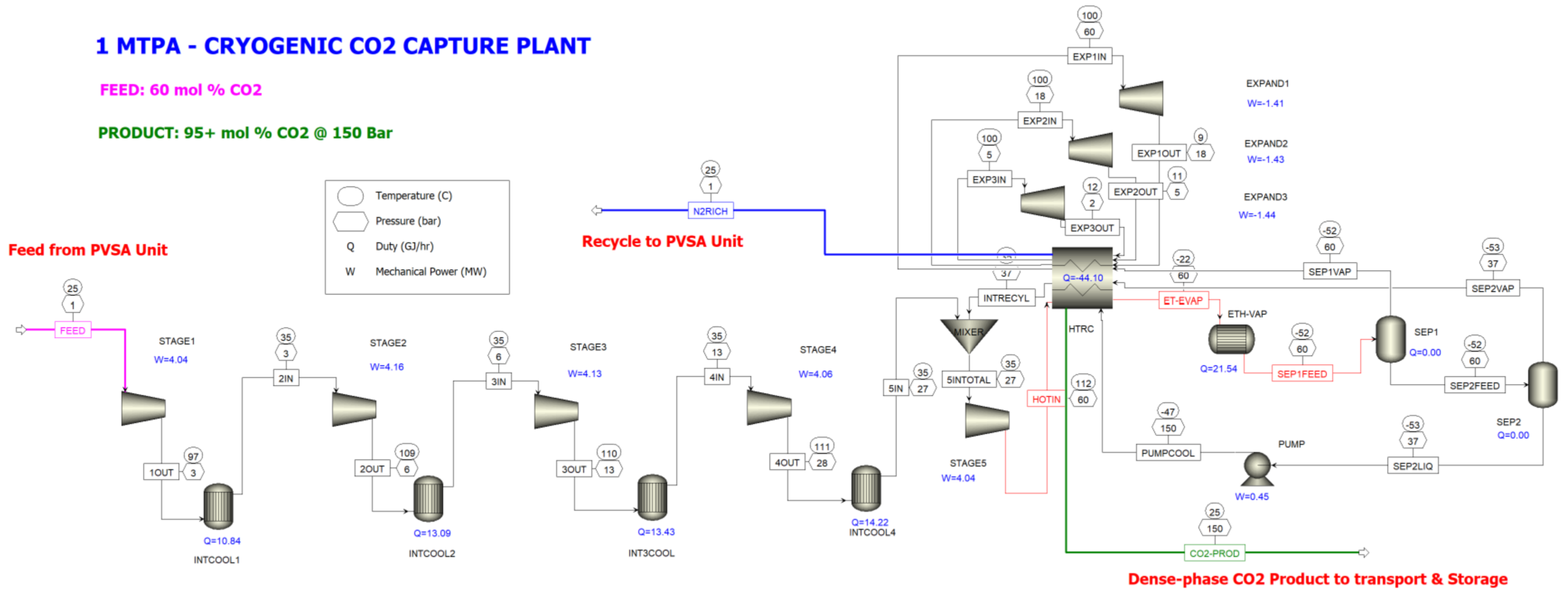

Figure 4.6: Aspen Plus© flowsheet for liquefaction unit

4.5 Energy Analysis and Cost Estimation

Techno-economic assessment is performed to design liquefaction processes for CO_2 capture from post-combustion flue gas streams. Most liquefaction studies for CO_2 capture deal with process optimizations involving energy reduction. While energy consumption can be used as a proxy for operating costs, in a realistic scenario, one must also consider the capital costs. The scale of the capture plant is an important economic consideration; in this study, all the estimates are done by considering a basis of 1 million tonnes of CO_2 captured per annum.

4.5.1 Cost Assessment

Costs are assessed using the N^{th} of a Kind (NOAK) approach. This approach assumes that the liquefaction technology is mature for CO_2 capture and has passed commercial-scale demonstration targets [68]. The cost methodology followed assesses both capital cost (CAPEX) and operating cost (OPEX). Costs are reported in USD_{2022} price levels.

Capital Costs

To estimate capital costs, a bottom-up approach is considered [62]. The workflow implemented for cost estimation is shown in Fig.4.7. With a fully converged Aspen Plus flowsheet for the liquefaction unit, utilities and their respective costs are configured. The utility unit cost is also shown in Fig. 4.7. Next, the activated economics is enabled in the simulation environment to initiate capital cost evaluation through the Aspen Process Economic Analyzer (APEA). Capital cost evaluation in APEA involves three stages. In the first stage, all the unit operations in the Aspen Plus flowsheet are mapped with appropriate process equipment. Default mapping is used to map unit operations against standard process equipment available in the Aspen database. After successfully mapping all critical unit operations, the second stage involves sizing the mapped process equipment using process information from

Table 4.4: Stream table indicating properties of critical streams for the Aspen Plus Flowsheet

Stream Name	Units	FEED	HOTIN	ET-EVAP	SEP1FEED	SEP2LIQ	N2RICH	CO_2-PROD
Phase		Vapor	Vapor			Liquid	Vapor	Vapor
Temperature	**°C**	**25**	**111**	**-21**	**-52**	**-52**	**25**	**25**
Pressure	**bar**	**1.25**	**60.3**	**60.2**	**60.1**	**37**	**1.4**	**149.9**
Vapor Fraction		1	1	0.700	0.446	0	1	1
Liquid Fraction		0	0	0.299	0.553	1	0	0
Mole Flows	**kmol/hr**	**4900**	**5045**	**5045**	**5045**	**2646**	**2253**	**2646**
CO_2	kmol/hr	2940	2973	2973	2973	2514	425	2514
N_2	kmol/hr	1960	2072	2072	2072	131	1828	131
Mole Fractions								
CO_2		0.6	0.589	0.589	0.589	0.950	0.188	0.950
N_2		0.4	0.41	0.410	0.410	0.049	0.811	0.049
Vapor Phase								
Mole Fractions								
CO_2		0.6	0.589	0.446	0.188		0.188	0.950
N_2		0.4	0.410	0.553	0.811		0.811	0.049
Liquid Phase								
Mole Fractions								
CO_2				0.924	0.912	0.950		
N_2				0.075	0.087	0.049		

the Aspen Plus environment. The program considers all relevant design standards and codes for sizing process equipment. In the final stage, the comprehensive vendor database information evaluates equipment capital and installed costs. The sum of all the capital costs for all equipment is referred to here as the total direct cost (TDC).

A 15% process contingency factor, consistent with NETL guidelines, was incorporated into the total direct cost to determine the total direct cost with process contingency (TDCPC), excluding any contingencies [73]. Subsequently, the total direct cost with process contingencies was augmented by both indirect costs and project contingencies to arrive at the total plant cost (TPC). Indirect costs, encompassing engineering expenses, consulting fees, service infrastructure, yard enhancements, building expenses, and miscellaneous costs, were allocated at 14% of TDCPC. Project contingencies were determined at 20% of TDCPC, in adherence to NETL guidelines [73]. The total capital requirement (TCR) is computed by adding owner costs and interest over construction to the TPC. Owner costs are estimated at 7% of TDCPC [62]. The interest accrued during construction is determined based on the assumption that construction costs are distributed evenly over a three-year construction period using a 40/30/30 allocation.

Operating Costs

Operating costs encompass both fixed and variable components. The annual fixed operating expenses encompass maintenance, labour, insurance, and administrative outlays. Specifically, the yearly maintenance cost equates to 2.5% of the total plant cost (TPC), with maintenance labour expenses constituting 40% of this figure. Additionally, insurance and location taxes, including overhead and miscellaneous regulatory fees, have been established at 2% of TPC. Labour costs were computed on the premise that the CO_2 capture unit necessitates five operators, each working a shift pattern, with one operator per shift, considering the high level of automation in the liquefaction processes. These operators receive an annual salary of 60,000 USD each. Administrative costs have been allocated at 30% of the combined operating

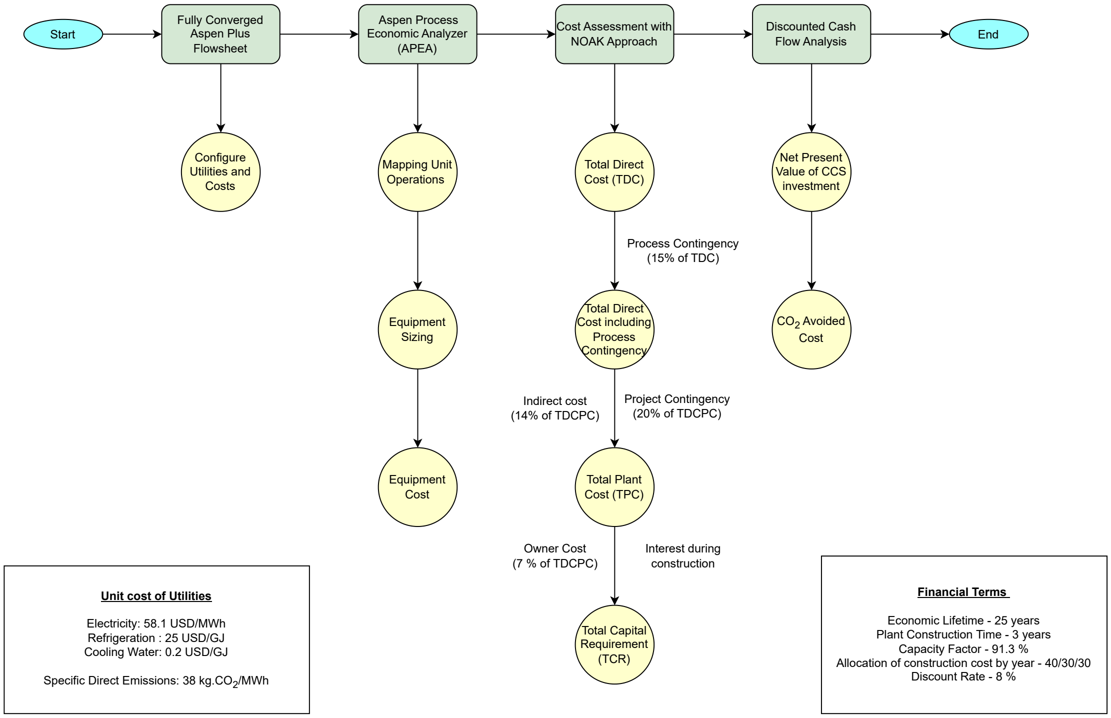

Figure 4.7: Liquefaction Costing Work flow

and maintenance labour expenses.

The variable operating expenses encompass utilities, electricity, cooling water, and refrigeration. The annual utility costs were derived from process simulations, and the unit costs of these utilities can be found in Table 4.5.

4.5.2 Key Performance Indicators

Key technical performance indicators for liquefaction

The CO_2 purity, CO_2 recovery and specific energy consumption are defined as follows:

$$CO_2\ Purity\ (\%) = \frac{total\ moles\ of\ CO_2\ in\ the\ product\ stream}{total\ moles\ of\ gas\ in\ the\ product\ stream} * 100 \tag{4.11}$$

Table 4.5: Unit cost of utilities

Utility	**Price**
Electricity (USD MWh^{-1})	58.1 [66]
Refrigeration at -65°C (USD GJ^{-1})	25 [74]
Cooling Water (USD GJ^{-1})	0.2 [66]
Specific Direct Emissions (kg.CO_2 MWh^{-1})	38 [67]

$$CO_2\ Recovery\ (\%) = \frac{total\ moles\ of\ CO_2\ in\ the\ product\ stream}{total\ moles\ of\ CO_2\ in\ the\ Feed\ stream\ to\ Liquefaction} * 100 \tag{4.12}$$

$$Specific\ Energy\ (kWh_e\ t^{-1}_{CO_2}) = \frac{Overall\ Power\ (kW_e) * Operating\ hours\ (h\ year^{-1})}{CO_2\ Captured\ (t\ year^{-1})} \tag{4.13}$$

Key economic performance indicators for liquefaction

The key economic performance indicator is the CO_2 avoided cost. It represents the mean discounted CO_2 tax throughout the project necessary to match the net present value (NPV) of the CCS investment costs [75]. The CO_2 avoided cost, in $USD/t_{CO_2\ avoided}$ is calculated as follows:

$$CO_2\ avoided\ cost = \frac{Net\ Present\ Value\ of\ the\ CCS\ implementation\ cost}{Net\ Present\ value\ of\ the\ CO_2\ avoided} \tag{4.14}$$

In terms of the financial terms, it can be written as:

$$CO_2\ avoided\ cost = \frac{\sum_i \frac{TCR_{CCS\ implementation}(i) + Annual\ OPEX_{CCS\ implementation}(i)}{(1+d)^i}}{\sum_i \frac{Annual\ amount\ of\ CO_2\ emissions\ avoided\ by\ the\ CCS\ implementation\ (i)}{(1+d)^i}} \tag{4.15}$$

where i is the year index (-).

Table 4.6: Economic parameters used in calculating CO_2 avoided costs

Parameters	**Value**
Economic lifetime (years)	25
Capacity factor (%)	91.3
CO_2 capture plant construction time (years)	3
Allocation of CO_2 capture construction costs by year (%)	40/30/30
Discount rate (%)	8

The quantity of CO_2 emissions prevented through CCS implementation is determined by the contrast between the annual CO_2 capture achieved by CCS implementation and the direct emissions originating from the heat and electricity consumed during CCS implementation. The direct emissions due to electricity can be computed using the following formula:

$$Direct\ Emissions = e_{el} * P_{el}(MW_e) * Operating\ hours\ (h/year) \tag{4.16}$$

Here, e_{el} signifies the specific CO_2 emissions linked to every unit of electric power used; the equivalent CO_2 avoided measurement reflects the genuine overall reduction in CO_2 emissions achieved by power plant when employing liquefaction capture technology. This method facilitates an equitable comparison with diverse capture technologies [66]. The financial parameters used to compute the cost of CO_2 avoided are provided in Table 4.6.

4.6 Results and Discussion

Considering the thermodynamic limits of liquefaction for the CO_2-N_2 system, the range of feed compositions to be evaluated is fixed to be 40-75 mol % CO_2. Separate simulations were performed to study this composition range, and the performance indicators were analyzed to study the process performance; thus, the CO_2 avoided cost and its distributions.

4.6.1 Specific Energy Consumption Vs. Recovery in Liquefaction Unit

Figure 4.8 shows the variation of CO_2 recovery and the specific energy consumption with feed composition in the liquefaction unit. The CO_2 recovery shown in red increases from 72 % to 93% as the feed gas CO_2 composition increases from 40 mol % to 75 mol%. This observation can be explained based on the phase equilibrium behaviour of this system at -50°C and 60 bar with the help of the lever rule. As the feed compositions increase, the fraction of CO_2 that can be liquefied increases, thus allowing more liquid CO_2 to be drawn as the product. The specific energy consumption shown in blue, on the other hand, decreases. As the feed gas is compressed to about the same pressure for all the compositions to maximize recovery, the compression energy is about the same for all cases. However, since more liquid CO_2 can be drawn at higher compositions, the energy consumption per tonne CO_2 decreases.

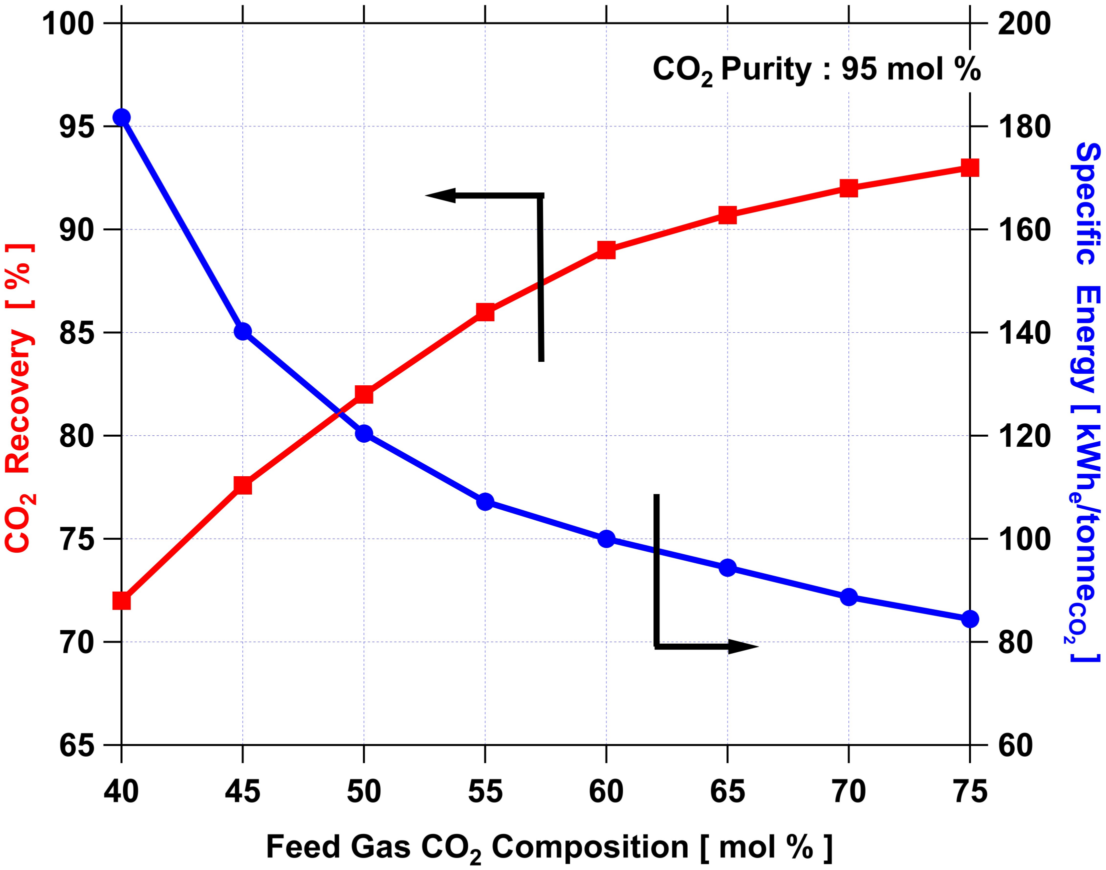

Figure 4.8: CO$_2$ Recovery and Specific Energy Consumption

4.6.2 Capital Cost Correlations

The Aspen Economic Process Analyzer® (APEA) was utilized to estimate the capital costs of individual process equipment. Multiple economic assessments were conducted for each piece of equipment, considering a diverse set of key design characteristics. MATLAB was used to carry out the power-law model regression. This approach was undertaken to establish reliable capital cost correlations. Figure 4.9 provides the correlations for estimating capital costs for four major equipment in the liquefaction process along with the coefficients for the power-law model.

Multi-stage Centrifugal Compressor: In the liquefaction process, multi-stage compressors are required to pressurize the feed to high pressures. The capital cost of centrifugal compressors is a strong function of their volumetric inlet capacity. The discharge pressure also influences the capital cost to some extent; however, in the case of the liquefaction process, since the maximum compression feed pressure is more or else constant, only the cost variation with the inlet flow rate is considered here, assuming a five-stage compressor with a stage pressure ratio of 2.2 is required to compress the feed to 60 bar. A single variable cost correlation is shown in Eq. 4.17.

$$Multistage\ compressor\ cost\ (USD) = 90.41 *\ [Inlet\ flow\ rate\ (L\ min^{-1})]^{0.8668} \tag{4.17}$$

Heat Recovery Exchanger: The heat recovery exchanger is a multi-stream heat exchanger used for heat integration. Multi-stream exchangers are vendor-specific items, and hence estimating their costs is not straightforward. In this work, the cost of this exchanger is estimated based on the area required and the design pressure. A design pressure of 156 bar is considered to enable heat integration between the cold purified CO_2 product at 150 bar and the compressed feed stream. A single variable cost correlation is shown in Eq. 4.18.

$$Heat\ recovery\ exchanger\ cost\ (USD) = 900 * [heat\ transfer\ area\ (m^2)]^{1.025} \tag{4.18}$$

Turbo-expanders: The turbo-expanders are a series of gas expansion equipment using which the pressure energy of the uncondensed N_2 rich gas is recovered in the form of shaft work. The capital cost of turbo-expanders is a strong function of the amount of shaft work they can produce. In this work, the capital cost of turbo-expanders is estimated based on their output brake horsepower. A single variable cost correlation is shown in Eq.4.19.

$$Turbo-expander\ cost\ (USD) = 2244\ *\ [Output\ power\ (kW)]^{0.8099} \tag{4.19}$$

Main Chiller: The main chiller is a heat exchanger which cools the compressed feed to cryogenic temperatures, thus liquefying the CO_2. The main chiller is cooled

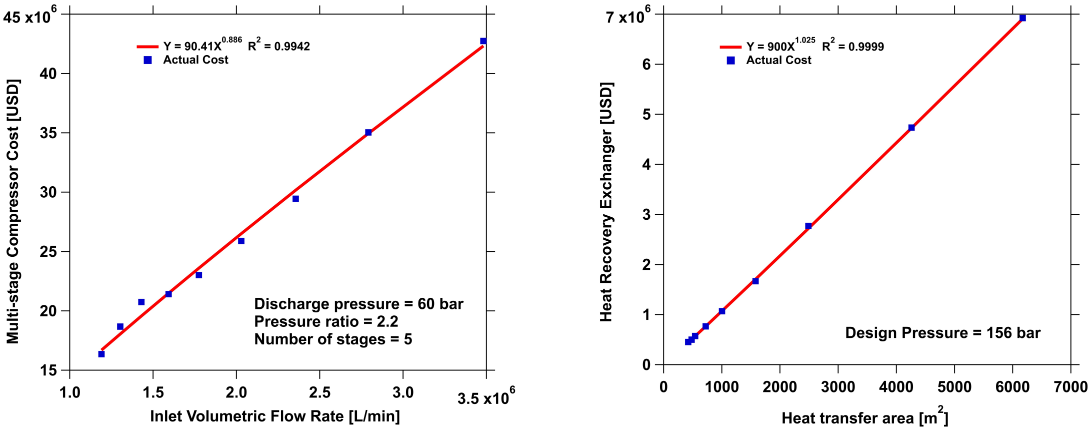

(a) Multi-stage compressor (b) Heat recovery exchanger

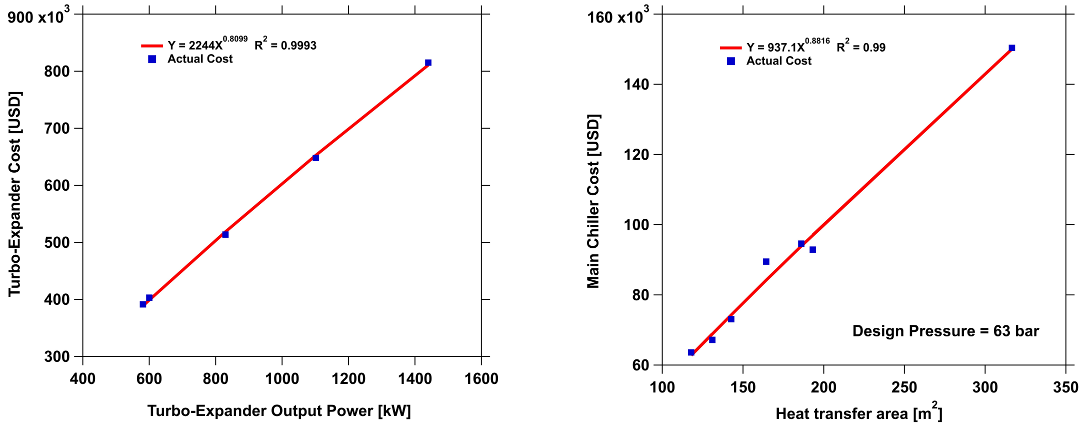

(c) Turbo-expander (d) Main refrigeration chiller

Figure 4.9: Correlations for estimating capital costs for major equipment in the liquefaction process

using an external refrigeration system. The capital cost of heat exchangers is a strong function of their heat transfer area and the design pressure. In this work, the design pressure is fixed at 63 bar. A single variable cost correlation is shown in Eq. 4.20.

$$Main\ chiller\ cost\ (USD) = 937.1\ *\ [heat\ transfer\ area\ (m^2)]^{0.8816} \tag{4.20}$$

4.6.3 CO_2 Avoided Costs and Distribution

Figure 4.10 shows the variation of CO_2 avoided costs with feed gas composition to the liquefaction. Costs decrease with an increase in composition. The cost flattens out beyond 60 mol % up to 75 mol %. Thus a relatively small variation is seen in the liquefaction process. Figure 4.11a shows the distribution of the total CO_2 avoided costs in terms of capital (CAPEX) costs and operating (OPEX) costs. Fig. 4.11b shows the capital distribution (CAPEX) regarding the equipment CAPEX and indirect costs. Figure 4.11c shows the distribution of equipment CAPEX. A large portion of the equipment CAPEX is attributed to compressors in purple, the heat recovery exchanger in pink, and the turbo expanders in blue. Figure 4.11d shows the distribution of the variable OPEX in the utilities in the liquefaction unit. The contribution of electrical power has a reducing trend while the refrigeration increases as the feed composition increases. The refrigeration load is expected to increase as the condensable load increases with increasing CO_2 composition.

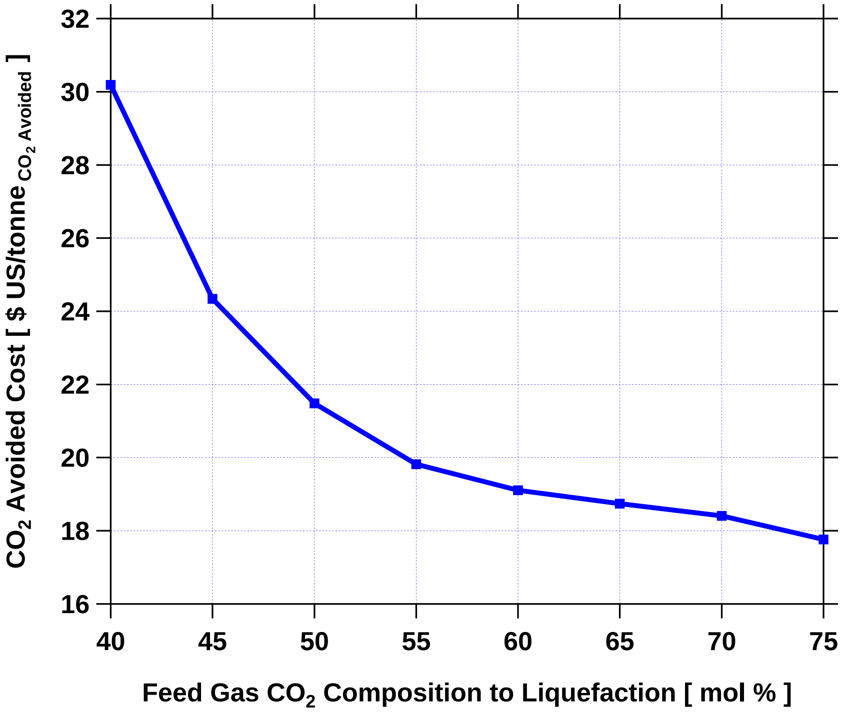

Figure 4.10: CO_2 Avoided Costs for the liquefaction process

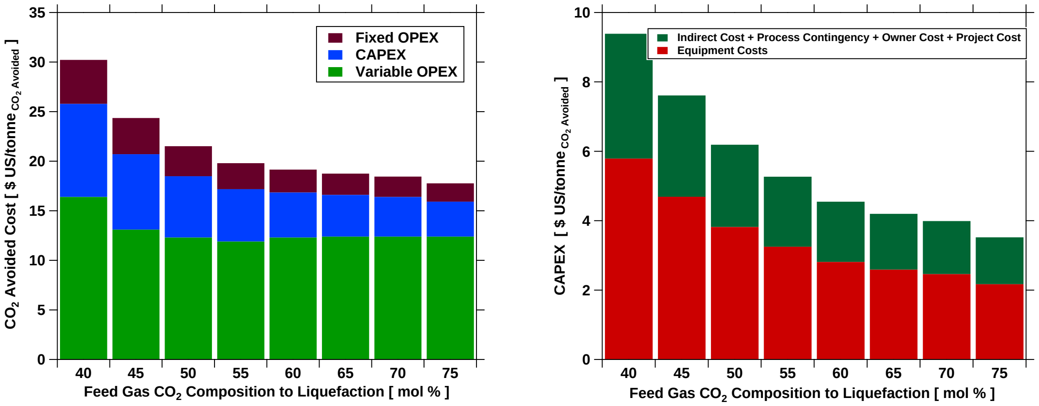

(a) Distribution of CO$_2$ Avoided costs (b) Distribution of total CAPEX

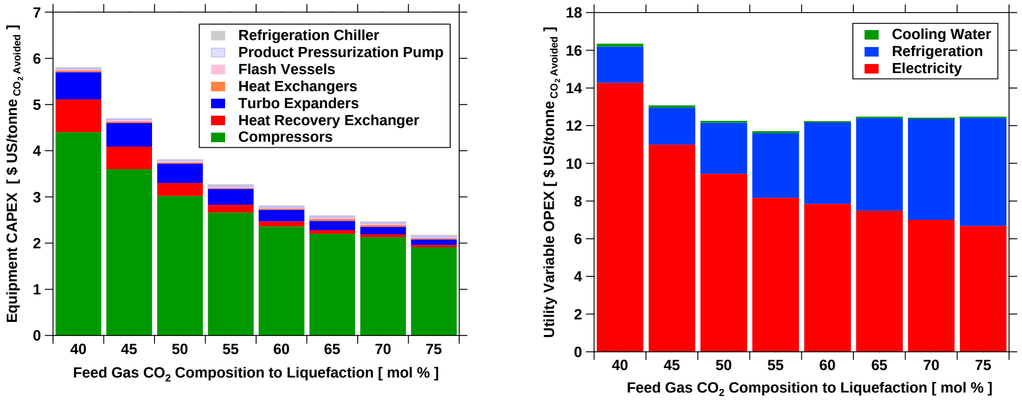

(c) Distribution of Equipment CAPEX (d) Distribution of Variable OPEX

Figure 4.11: Breakdown of Liquefaction Cost

4.7 Conclusion

The effectiveness of a liquefaction process for post-combustion CO$_2$ is discussed using process simulation and techno-economic assessment. The thermodynamics of a liquefaction process for post-combustion CO$_2$ capture is presented using pure component and binary phase equilibrium data. The suitability of the Peng-Robinson equation of state for high-pressure, low-temperature applications is established by regressing isothermal experimental binary CO$_2$-N$_2$ data at cryogenic and ambient temperatures. Detailed process simulations are performed to study the recovery limits and the associated specific energy consumption using the commercial process simulator Aspen Plus. Capital costs are estimated using the Aspen Process Economic Analyzer corresponding to a CO_2 capture plant scale of 1 MTPA. Key economic performance indicators such as CO_2 avoided costs and its distribution are estimated using a discounted cash flow analysis.

The temperature and pressure conditions required for the transport and storage of captured CO_2 are highlighted using a pure component phase diagram for CO_2. The regression analysis suggests that the Peng-Robinson equation of state accurately models the phase equilibrium behaviour for the CO_2-N_2 system over a wide pressure and temperature range. The process simulation model for the liquefaction process consists of the feed compression, heat integration, chilling and phase separation section. The low-temperature limit in the liquefaction process is imposed by the freezing point of CO_2; this limits the recovery of liquid CO_2 beyond a certain point. Multiple simulations are carried out to estimate the specific energy consumption of the process for which the recovery is maximized. Detailed costing studies suggest the CO_2 avoided costs fall in the range of \$ 18-30/tonne of CO_2 captured for the feed gas composition range of 40-75 mol% CO_2.

A detailed breakdown of the CO_2 costs indicates that there is only a slight variability in the total operating costs (OPEX); this is primarily due to the same order of the feed compression required in order to maximize the liquid CO_2 recovery. Using the turbo-expanders it is possible to recover $\approx 20\%$ of the energy consumed by the compressors.

In summary, a liquefaction process can serve as an effective separation process. In the context of post-combustion CO_2 capture, where the flue gas compositions are low, the liquefaction process can best serve as a purification block as it has the potential to produce high CO_2 purities. A drawback of the liquefaction process is that the feed gas has to be moisture-free in order to prevent it from freezing in the narrow tubes of the heat exchanger network.

Chapter 5

Hybrid Adsorption + Liquefaction Process Performance

In this chapter, we compare a standalone PVSA process with zeolite 13X adsorbent and a hybrid PVSA + liquefaction process based on detailed techno-economic assessments. The advantages of a hybrid process over a standalone PVSA process are provided in terms of cost, energy, and footprint savings.

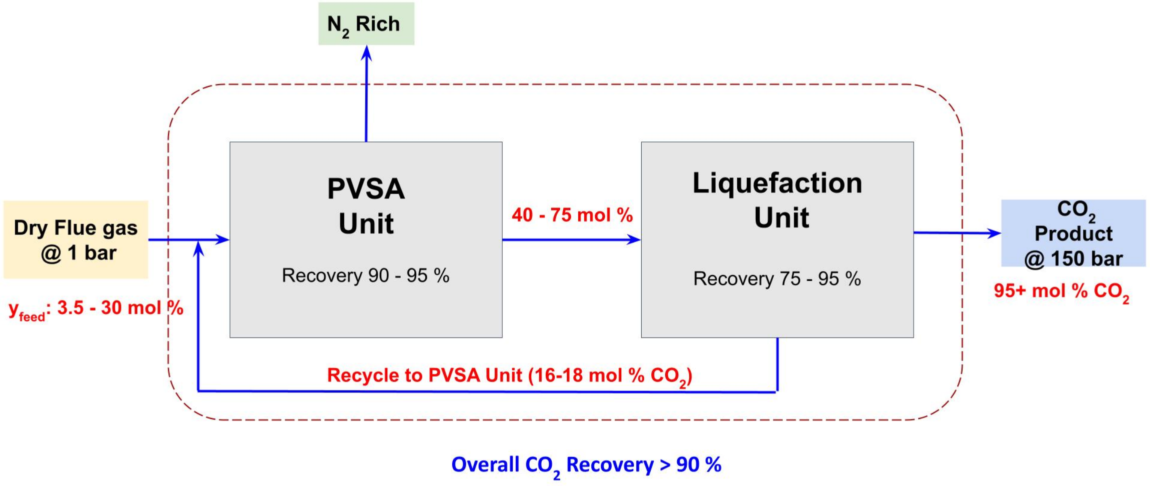

Figure 5.1: Block flow diagram of hybrid adsorption + liquefaction process

5.1 Proposed Hybrid Process

A block flow diagram of the proposed hybrid process is illustrated in Fig 5.1. Dried flue gas at atmospheric pressure from an upstream dehydration unit enters as feed to the hybrid process. It is first sent to the PVSA-based adsorption unit, where the CO_2 in the feed gas is pre-concentrated to a purity of 40 - 75 %, depending on the feed gas composition at a high recovery rate. The N_2 rich stream rejects most of the N_2 from the process in the PVSA unit. It is either vented to the atmosphere directly or could be utilized to some extent in the upstream dehydration stage. The partially purified stream containing the recovered CO_2 is sent to the liquefaction unit downstream of the PVSA unit for further purification to the desired sequestration concentration of at least 95 %. Since the CO_2 recovery in the liquefaction is limited by thermodynamic phase equilibrium, a stream with a CO_2 composition of 16-18 mol % is recycled back to the PVSA unit. This helps ensure the overall recovery is at least 90 %. The liquefaction unit can produce a high-purity CO_2 product as a supercritical liquid or gas, depending on transportation and storage requirements.

The adsorption process employed in the PVSA unit is studied in earlier chapters. In this work, the chosen PVSA process is the four-step LPP cycle; however, more advanced cycle design configurations, such as the six-step dual reflux (DR) cycle, could also be used to further improve the adsorption-based process's performance. Also, the adsorbent material in this work is considered commercially available Zeolite 13X. Other potential adsorbents could potentially enhance the performance of the PVSA unit, which in turn upgrades the performance of the hybrid process.

5.2 Modelling approach for Hybrid Processes

The mode of operation for the two processes used in the hybrid is different; adsorption processes such as PVSA are inherently dynamic, while the liquefaction processes can be modelled as a steady-state process. The modelling of both processes as one block is not straightforward. Hence, it was decided to model these two processes independently using appropriate simulation tools.

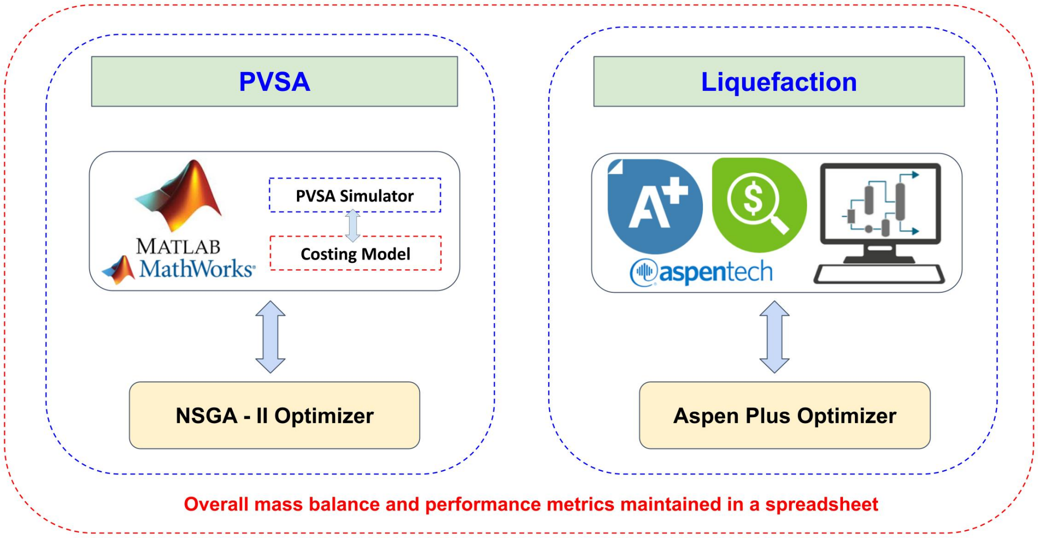

Figure 5.2: Modelling approach used to study the hybrid process

Figure 5.2 illustrates the overview of the modelling approach used in this work. It is important to note that since the modelling is done independently, the optimal operating conditions and the corresponding performance metrics from both models were maintained together in a spreadsheet to verify overall mass balances and account for total energy and total costs in the hybrid process. The technical modelling details for both processes are presented in separate chapters in the earlier part of this thesis.

5.3 Hybrid Process Performance Vs. Standalone Processes

This section compares the performance of hybrid adsorption and a liquefaction process with standalone processes. Key performance indicators such as CO_2 avoided costs, specific energy consumption, and footprint of the PVSA unit are compared, along with critical operating variables in the PVSA unit.

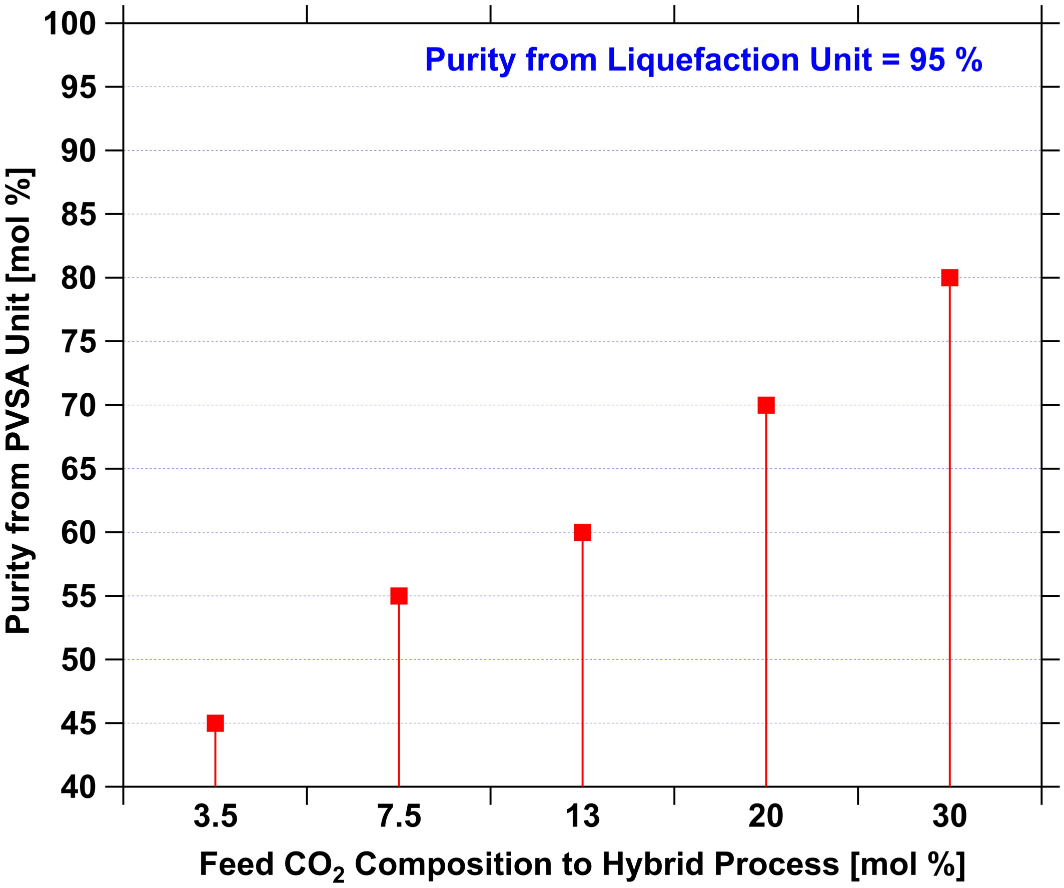

Figure 5.3: Purity from the PVSA unit of the hybrid process.

In the hybrid process, the PVSA unit pre-concentrates the CO_2 in the flue gas to intermediate purities with high recovery. This partially concentrated gas is then fed to the liquefaction unit for further purification. The variation of the intermediate purities with different feed compositions is presented in Fig 5.3.

In Fig 5.4a, CO_2 avoided costs are presented for a standalone PVSA process with product CO_2 compression, the hybrid process and a standalone amine absorption process with MEA as the solvent with product CO_2 compression. These costs are estimated for a 2004 tonne/hr capture scale of incoming flue gas. Five flue gas compositions ranging between 3.5-30 mol % are presented. It is important to note that the adsorbent material is the same for the standalone PVSA and hybrid processes, i.e., Zeolite 13X. The hybrid process demonstrates superior performance over a standalone

PVSA process across all compositions studied. The cost savings are as high as 50 % for a 3.5 mol % feed compared to a standalone PVSA process. However, the cost savings were reduced to 12 % for a 30 mol % feed compared to a standalone PVSA process. The reduction in cost savings at higher feed compositions is because although the cost of the PVSA unit in the hybrid reduces to some extent, the cost of the liquefaction varies only marginally. Compared to the amine absorption process, the standalone PVSA and hybrid processes are competitive at feed compositions greater than 13 mol %. However, the costs are higher for dilute feed compositions, i.e. less than 13 mol %, than for the amine absorption process.

In Figure 5.4b, the total number of PVSA columns required in the standalone PVSA process is compared to that in the PVSA unit of the hybrid process. A more than 60 % reduction is seen for the 3.5 mol % feed, which is a significant improvement in the footprint of the PVSA unit of the capture plant. Reducing the number of columns also means a corresponding reduction in the blowdown and evacuation pumps and the associated piping network.

The process-wise breakdown of CO_2 avoided cost is presented in Fig. 5.5. For the dilute feed compositions, the cost contribution to the PVSA is high ($> 90\%$ of the total cost). However, for higher feed compositions, since there is a significant reduction in the costs of the PVSA unit with feed composition, the costs are divided approximately equally between the PVSA and liquefaction units. As discussed in Chapter 4, there is only a small variation in the cost of the liquefaction unit with composition, hence the cost contribution of the liquefaction unit remains almost constant for all the feed compositions considered in the analysis of the hybrid process.

The savings in the CO_2 avoided costs in the hybrid process are strongly influenced by the savings in the specific energy consumption. Fig 5.6a shows the savings in the specific energy consumption for the hybrid process compared to the standalone PVSA process. Savings as high as 45 % are expected for a 3.5 mol % feed composition; however, the savings in energy are reduced at higher feed compositions to about

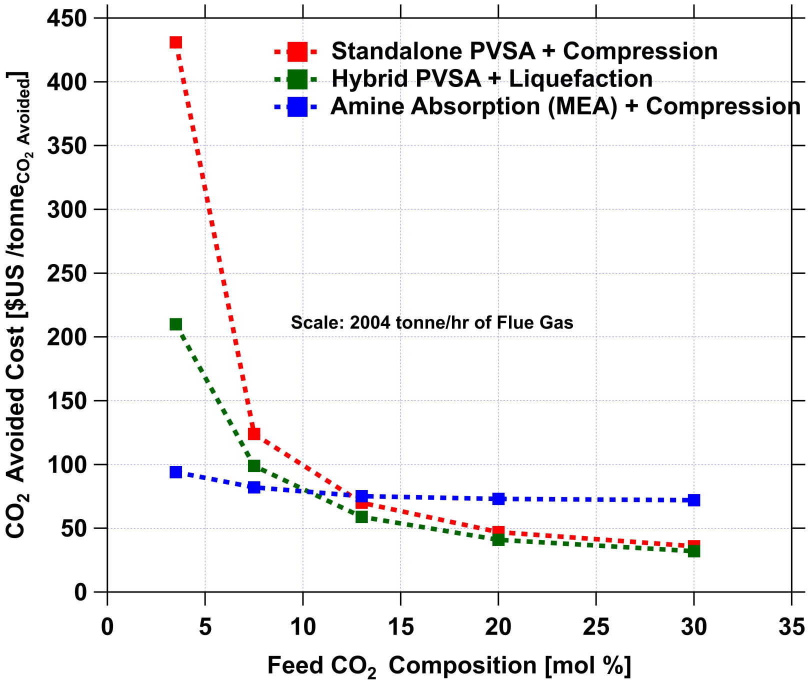

(a) CO_2 avoided cost

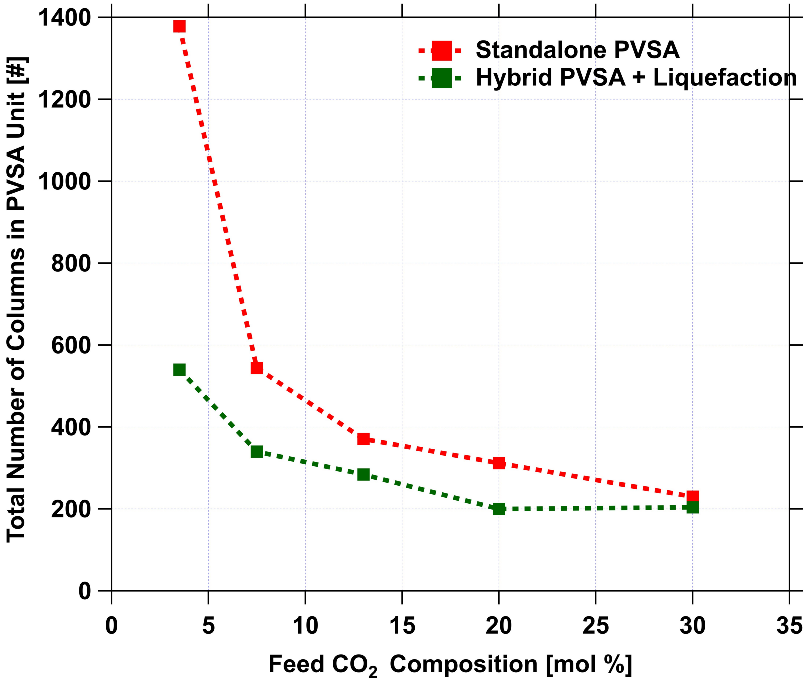

(b) Total number of columns in the PVSA unit required to process 2004 tonne/hr of flue gas

Figure 5.4: Hybrid adsorption + liquefaction process performance v/s. standalone PVSA process

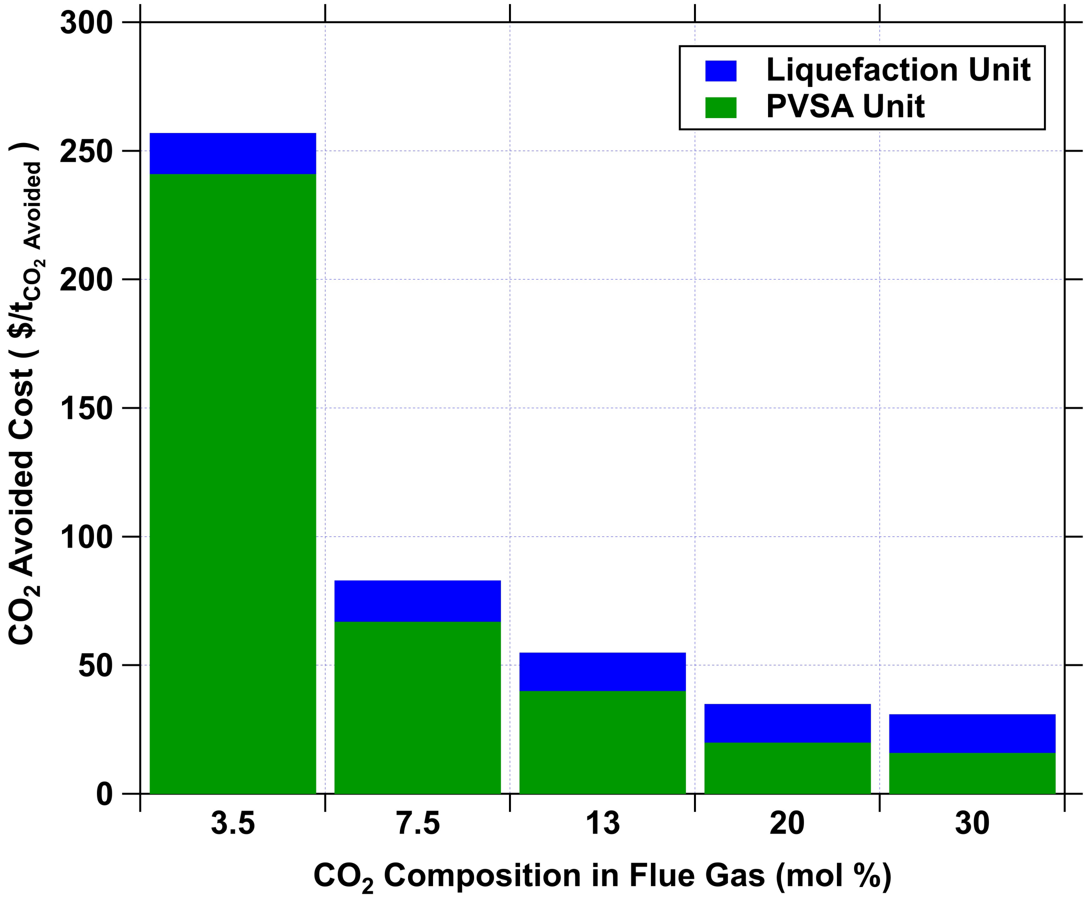

Figure 5.5: Process-wise cost distribution in the hybrid process

29 % for a 30 mol % feed composition. When comparing with the amine absorption, it is important to note that the amine absorption is a thermally driven process different from the electrically driven standalone PVSA and hybrid process. Hence, to compare them, the thermal specific energy consumption for the amine absorption process, which ranges between 4.9 - 4 GJ/tonneCO_2, is converted to equivalent electrical units by assuming a 50 % thermal to electrical energy conversion efficiency. The hybrid process is competitive with the amine absorption process for feed gas composition greater than 7.5 mol %. However, for dilute compositions, the hybrid process consumes significantly more energy.

The reduction in the number of columns required to treat the same amount of flue gas can be explained by analyzing the improvement in the productivity values of the

PVSA unit as shown in Fig 5.6b. A higher productivity means reducing the amount of adsorbent volume required to capture the same amount of CO_2. The increase in the PVSA productivity for the hybrid process can be explained by analyzing the vacuum level required in the PVSA cycle's evacuation steps. As shown in Fig 5.6d, the evacuation pressure is higher in the hybrid process. Higher evacuation pressures result in shorter evacuation step times and, thus, shorter total cycle times. With shorter cycle times, one PVSA train can capture CO_2 at a high rate, thus increasing its productivity. The increased productivity per PVSA train translates into fewer parallel PVSA trains required to process a desired flue gas throughput, reducing the total number of columns needed for the PVSA unit.

The operating conditions, process performance and the breakdown of their respective CO_2 avoided costs for the PVSA unit and the liquefaction unit, for the five compositions studied in this work are presented in Table 5.1. All costs are reported in \$/tonne CO_2 avoided. It is important to note that the PVSA unit is operated in such a way that intermediate purity levels in the range of 45 - 80 mol% are obtained at a high CO_2 recovery (>91%). Thus, in this hybrid process, the PVSA unit works as a preconcentration unit. Lowering the purity level obtained from the PVSA unit results in a significant reduction in specific energy consumption compared to a PVSA unit that is operated as a standalone unit producing both high purity and high recovery. In the PVSA unit, the total CO_2 avoided costs are dominated by operating consistently across all the compositions. For instance, for the feed compositions of 3.5 - 7.5 %, the PVSA OPEX contributes >70% to the total PVSA CO_2 avoided costs. This is due to the steep increase in the specific energy consumption with the decrease in CO_2 composition. In terms of the CAPEX, the feed compressors and the columns contribute the most to the PVSA CAPEX, followed by the vacuum pumps. The partially purified gas from the PVSA unit is sent as feed to the liquefaction unit. In the liquefaction unit, in order to maximize the recovery of liquid CO_2, irrespective of the composition fed to the liquefaction unit, the gas is first compressed to a pressure of 60 bar and then chilled to a temperature of -50°C. The liquified CO_2 is sent to a purification separator, where it is flashed by reducing the pressure of the stream to 37 bar. This ensures the final purity of the liquified CO_2 is >95%. Since the energy from the pressurized uncondensed gas is recovered through turbo-expanders, the net electrical energy consumption in the liquefaction unit is the difference between the electrical energy consumption by the compressors and the electrical power generated from the turbo-expanders. In other words, the turbo-expanders offset a portion of the electricity required by the compressors. The liquefaction unit has net specific electrical energy in the range of 80.8 - 140 kWh_e/tonne CO_2 captured. Refrigeration is required to chill the feed gas to -50°C; thus, a refrigeration load is associated with the liquefaction unit in addition to the electrical load. The specific energy of refrigeration lies in the range of 38.53 - 101.2 MJ/tonne of CO_2 captured. The compressors and the heat recovery exchanger contribute the highest to the CAPEX of the liquefaction unit. As discussed earlier, the distribution of the process-wise CO_2 avoided costs varies significantly with feed composition to the hybrid process. For dilute compositions, the PVSA unit contributes majorly to the total CO_2 avoided costs. The costs are more evenly divided for feed compositions >20 mol %, this is because the liquefaction costs remain almost constant with an increase in composition, but the PVSA costs reduce significantly.

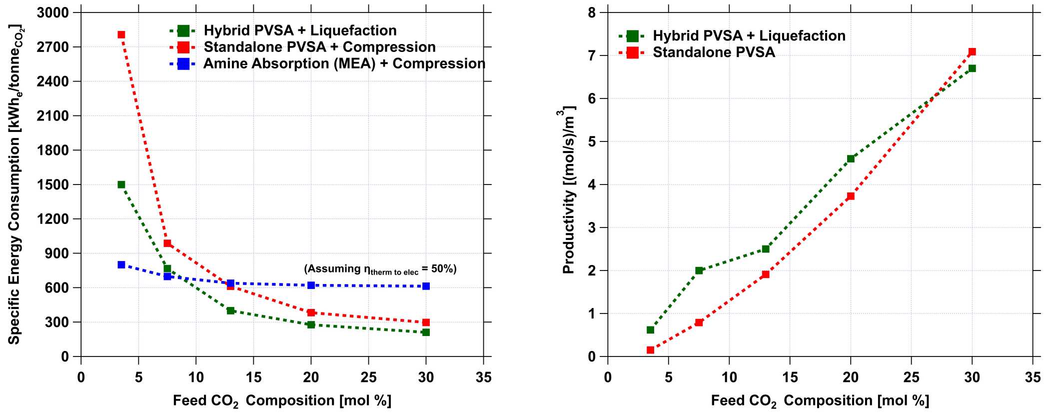

(a) Specific Energy Consumption (b) Productivity

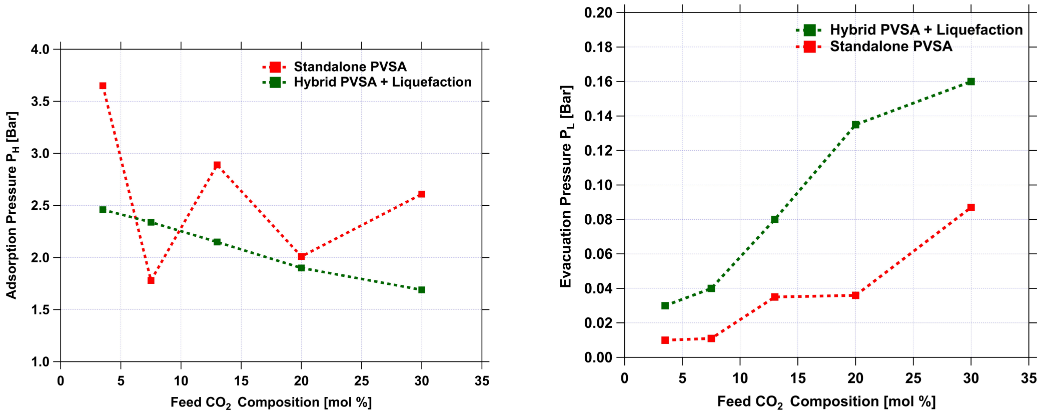

(c) P_H - Adsorption Pressure (d) P_L - Evacuation Pressure

Figure 5.6: Specific energy consumption, productivity, adsorption pressure and desorption pressure corresponding to the data points in Fig. 5.4

Table 5.1: Operating conditions and breakdown of CO_2 avoided costs for the PVSA unit and the liquefaction unit in the hybrid process.

	3.5%	**7.5%**	**13%**	**20%**	**30%**
PVSA operating conditions					
Adsorption time (s)	131	127	102	75	94
Blowdown flow rate (m^3 h^{-1})	9179	8815	7063	8669	6668
Evacuation flow rate (m^3 h^{-1})	8721	12922	10627	11698	18929
Adsorption pressure (bar)	2.5	2.34	2.2	1.8	1.7
Blowdown pressure (bar)	0.29	0.4	0.49	0.69	0.88
Evacuation pressure (bar)	0.03	0.04	0.08	0.14	0.16

Table 5.1 continued from previous page

	3.5%	**7.5%**	**13%**	**20%**	**30%**
Feed velocity (m s^{-1})	0.92	1.05	1.12	1.1	1.21
Column diameter (m)	2.65	2.55	2.74	2.7	2.74
Particle porosity (-)	0.69	0.46	0.54	0.48	0.49
Particle diameter (mm)	3.5	2.5	2.5	3	3
PVSA process performance					
Purity (%)	45	55	60	70	80
Recovery (%)	91.5	91.6	91.5	91.6	97
Productivity (mol m^{-3} s^{-1})	0.56	2.01	2.48	4.61	6.69
Specific energy (kWh_e/t_{CO_2})	1207	561	228	173	124
Cost breakdown ($\$/t_{CO_2\ avoided}$)					
PVSA CAPEX	44.9	20.1	14.3	7.1	5.2
Total direct cost	25.4	11.3	8.1	4.0	2.94
Column cost	9.3	3.7	3.3	1.3	0.93
Compressor cost	7.4	3.4	1.9	1.3	0.86
Vacuum pump cost	6.7	3.2	1.9	1.0	0.87
Heat Exchanger cost	0.2	0.09	0.04	0.03	0.02
Valves cost	0.85	0.35	0.3	0.12	0.08
Initial adsorbent cost	0.86	0.57	0.5	0.2	0.15
Total indirect costs	19.5	8.74	6.2	3.1	2.26
PVSA OPEX	104	49	22.3	14.9	10.38
Fixed OPEX	21.6	9.7	6.9	3.4	2.5
Electricity cost	80.3	38	14.5	11	7.57
Adsorbent cost	1.3	0.88	0.8	0.3	0.24
Cooling water cost	0.7	0.32	0.1	0.11	0.05
PVSA CO_2 avoided cost	149	69	36.6	22	15.6
Liquefaction operating conditions					
Feed CO_2 composition (%)	45	55	60	70	80

Table 5.1 continued from previous page

	3.5%	**7.5%**	**13%**	**20%**	**30%**
Feed compression pressure (bar)	60	60	60	60	60
Feed Chilling temperature (°C)	-50	-50	-50	-50	-50
Purification separator pressure (bar)	37.5	37.5	37.5	37.5	37.5
Product pump discharge pressure (bar)	150	150	150	150	150
Liquefaction process performance					
Purity (%)	95	95	95	95	95
Recovery (%)	78	85	89	92	95
Specific energy - refrigeration ($\mathrm{MJ/t_{CO_2}}$)	101.2	84.3	62.7	51.76	38.53
Specific energy - electrical ($\mathrm{kWh_e/t_{CO_2}}$)	140	107	100	88.7	80.8
Cost breakdown ($\$/t_{\mathrm{CO_2\ avoided}}$)					
Liquefaction CAPEX	7.6	5.28	4.5	4.0	3.07
Total direct cost	4.7	3.3	2.81	2.5	1.9
Compressors	3.6	2.6	2.3	2.13	1.68
Heat exchangers	0.03	0.02	0.02	0.04	0.02
Turbo-expanders	0.5	0.34	0.25	0.16	0.08
Flash vessels	0.03	0.03	0.03	0.03	0.03
Heat recovery exchanger	0.49	0.17	0.11	0.06	0.05
Chillers	0.01	0.01	0.01	0.02	0.01
Product Pump	0.03	0.03	0.03	0.03	0.03
Total Indirect costs	2.9	2.0	1.7	1.5	1.2
Liquefaction OPEX	13.9	12.4	12.55	12.64	12.46
Fixed OPEX	3.65	2.63	2.3	2.06	1.65
Electricity cost	8.18	6.24	5.84	5.16	4.7
Refrigeration cost	1.95	3.43	4.32	5.35	6.04
Cooling water	0.13	0.09	0.08	0.07	0.06
Liquefaction CO_2 avoided cost	21.52	17.7	17.1	16.6	15.5
CO_2 avoided cost of hybrid process	**214.8**	**98.9**	**58.6**	**40.5**	**31.8**

5.4 Conclusion

In this chapter, a hybrid adsorption + liquefaction process is proposed, and its performance is compared to standalone processes like PVSA and MEA absorption in terms of specific energy consumption, and the CO_2 avoided costs. The proposed process is a combination of a PVSA process with Zeolite 13X adsorbent and a liquefaction process. The PVSA process serves as a preconcentration unit, while the liquefaction unit takes on the load of purifying the CO_2 and delivers the capture CO_2 at conditions suitable for transport and storage. The cost reduction potential of the PVSA process under reduced purity levels is leveraged in the hybrid process, thus making it a more cost-efficient option over standalone processes. Due to the differences in the mode of operation of the two processes considered, PVSA operates in a dynamic mode, while liquefaction can be operated as a steady-state process; both processes were modelled and optimized separately and the results reconciled. The process models are combined with costing models to arrive at CO_2 costs for both processes independently.

Five different feed compositions are studied for the hybrid process. The hybrid process performs better than the standalone PVSA process across all compositions. The hybrid process seems to be the most effective for dilute flue gas compositions. Significant savings in energy, cost, and footprint can be seen for the hybrid process when compared with the standalone PVSA process with the same adsorbent. At high feed compositions, though, the savings are reduced as the adsorption process becomes more energy efficient. The hybrid process improves the scalability of the PVSA process by reducing the total number of PVSA columns required to process a desired throughput of flue gas. This is possible due to the increase in the productivity of the PVSA process when operated at reduced purity levels.

Chapter 6

Conclusions

6.1 Summary

The techno-economic performance of a four-step light product pressurization (LPP) PVSA process with Zeolite 13X adsorbent is analyzed for a wide range of feed flue gas compositions. Three objective optimization studies are conducted to study the variation of CO_2 avoided costs at reduced purity levels and to obtain Pareto-optimal operating conditions corresponding to the objectives optimized. A similar trend is observed for all the five different feed compositions studied wherein the CO_2 avoided costs reduced with purity level. The cost reduction is justified by analyzing the variation of specific energy consumption, productivity and required pressure levels at reduced purity levels.

With the potential for significant cost reduction at reduced purity levels, the PVSA process can be leveraged to recover CO_2 at high rates, even from dilute flue gases, using commercially available adsorbent Zeolite 13X. Along with cost reduction, other important practical considerations, such as the higher evacuation pressure and reduced plot footprint, create an opportunity for PVSA to be employed as a preconcentration unit in hybrid processes such as that discussed in this thesis.

The techno-economic performance of a liquefaction process is analyzed for a wide range of feed gas CO_2 compositions while considering thermodynamic and practical limitations. Experimental binary phase equilibrium data is regressed to obtain appropriate binary interaction parameters for the Peng-Robinson thermodynamic property package used in the simulation. A liquefaction process is developed and simulated in Aspen Plus, along with a costing framework based on capital costs estimated using the Aspen Process Economic Analyzer. The simulation flowsheet is optimized for maximizing liquid CO_2 recovery and minimizing specific capture costs. The cost variation with feed gas CO_2 compositions is analyzed, and a detailed costing breakdown is provided. The variable OPEX is the major contributor to the CO_2 avoided cost but only slightly with composition. The small variation in the variable OPEX costs is explained based on the same level of feed compression required to maximize liquid CO_2 recovery.

The effectiveness of hybrid adsorption combined with liquefaction is studied using a techno-economic assessment. The cost-saving potential of a PVSA process under reduced purity constraints is leveraged in the hybrid process. Significant cost, energy, and footprint savings are established for the range of flue gas compositions studied. The hybrid process is effective in the dilute flue gas composition ranges. The high purities possible in the liquefaction create the potential for treating other impurities that come along with flue gas, which are not addressed in detail in this study.

6.2 Outlook

Despite the improvements over a standalone PVSA process, for dilute flue gases, the costs are significantly higher when compared to a standalone MEA-based absorption process. It is also important to note that the footprint of the PVSA unit, even in the hybrid process, is way too large to be industrially implementable.

To further bring down the costs of PVSA units, more advanced cycle design along with better adsorbent material needs to be evaluated in order to establish the true potential of a hybrid PVSA + liquefaction process. To increase the productivity of the PVSA unit, a horizontal bed configuration rather than vertical beds could be a practical option.

The biggest challenge with post-combustion capture is to deal with the moisture present in the flue gas effectively; the current notion of the high energy requirements for TSA-based process for drying the flue gas needs attention and quantification. Alternate potential drying options, such as membrane-based drying, must be studied in detail and compared with TSA-based drying.

Bibliography

[1] I. P. on Climate Change (IPCC), *Climate Change 2021 – The Physical Science Basis: Working Group I Contribution to the Sixth Assessment Report of the Intergovernmental Panel on Climate Change*. Cambridge University Press, 2023. DOI: 10.1017/9781009157896.

[2] U. N. F. C. on Climate Change (UNFCCC), *Adoption of the Paris Agreement. United Nations Framework Convention on Climate Change*. 2015. [Online]. Available: https://unfccc.int/documents/184656.

[3] B. Metz, O. Davidson, H. De Coninck, M. Loos, and L. Meyer, *IPCC special report on carbon dioxide capture and storage*. Cambridge: Cambridge University Press, 2005.

[4] Z. H. Liang *et al.*, "Recent progress and new developments in post-combustion carbon-capture technology with amine-based solvents," *International Journal of Greenhouse Gas Control*, vol. 40, pp. 26–54, 2015.

[5] H. C. Mantripragada, H. Zhai, and E. S. Rubin, "Boundary Dam or Petra Nova–Which is a better model for CCS energy supply?" *International Journal of Greenhouse Gas Control*, vol. 82, pp. 59–68, 2019.

[6] S. Giannaris *et al.*, "SaskPower's Boundary Dam Unit 3 Carbon Capture Facility-The Journey to Achieving Reliability," in *Proceedings of the 15th Greenhouse Gas Control Technologies Conference*, 2021, pp. 15–18.

[7] M. E. Boot-Handford *et al.*, "Carbon capture and storage update," *Energy & Environmental Science*, vol. 7, no. 1, pp. 130–189, 2014.

[8] E. S. Rubin, C. Chen, and A. B. Rao, "Cost and performance of fossil fuel power plants with CO_2 capture and storage," *Energy policy*, vol. 35, no. 9, pp. 4444–4454, 2007.

[9] A. Samanta, A. Zhao, G. K. Shimizu, P. Sarkar, and R. Gupta, "Post-combustion CO_2 capture using solid sorbents: a review," *Industrial & Engineering Chemistry Research*, vol. 51, no. 4, pp. 1438–1463, 2012.

[10] S. G. Subraveti, S. Roussanaly, R. Anantharaman, L. Riboldi, and A. Rajendran, "How much can novel solid sorbents reduce the cost of post-combustion [formula omitted] capture? A techno-economic investigation on the cost limits of pressure–vacuum swing adsorption," 2022.

[11] A. Wright, Personal Communication.

[12] A. A. Abd, S. Z. Naji, A. S. Hashim, and M. R. Othman, "Carbon dioxide removal through physical adsorption using carbonaceous and non-carbonaceous adsorbents: a review," *Journal of Environmental Chemical Engineering*, vol. 8, no. 5, p. 104 142, 2020.

[13] J. Elfving, C. Bajamundi, J. Kauppinen, and T. Sainio, "Modelling of equilibrium working capacity of PSA, TSA and TVSA processes for CO_2 adsorption under direct air capture conditions," *Journal of CO_2 Utilization*, vol. 22, pp. 270–277, 2017.

[14] A. H. Berger and A. S. Bhown, "Comparing physisorption and chemisorption solid sorbents for use separating CO_2 from flue gas using temperature swing adsorption," *Energy Procedia*, vol. 4, pp. 562–567, 2011.

[15] M. T. Ho, G. W. Allinson, and D. E. Wiley, "Reducing the cost of CO_2 capture from flue gases using pressure swing adsorption," *Industrial & Engineering Chemistry Research*, vol. 47, no. 14, pp. 4883–4890, 2008.

[16] N. Álvarez-Gutiérrez, M. Gil, F Rubiera, and C Pevida, "Kinetics of CO_2 adsorption on cherry stone-based carbons in CO_2/CH_4*separations*," *Chemical engineering journal*, vol. 307, pp. 249–257, 2017.

[17] F. Raganati, M. Alfe, V. Gargiulo, R. Chirone, and P. Ammendola, "Kinetic study and breakthrough analysis of the hybrid physical/chemical CO_2 adsorption/desorption behavior of a magnetite-based sorbent," *Chemical Engineering Journal*, vol. 372, pp. 526–535, 2019.

[18] C. Chao, Y. Deng, R. Dewil, J. Baeyens, and X. Fan, "Post-combustion carbon capture," *Renewable and Sustainable Energy Reviews*, vol. 138, p. 110 490, 2021.

[19] S. Kumar, R. Srivastava, and J. Koh, "Utilization of zeolites as CO_2 capturing agents: Advances and future perspectives," *Journal of CO_2 Utilization*, vol. 41, p. 101 251, 2020.

[20] F Raganati, P Ammendola, and R Chirone, "CO_2 capture performances of fine solid sorbents in a sound-assisted fluidized bed," *Powder technology*, vol. 268, pp. 347–356, 2014.

[21] G. Férey, "Hybrid porous solids: past, present, future," *Chemical Society Reviews*, vol. 37, no. 1, pp. 191–214, 2008.

[22] K. S. Walton, M. B. Abney, and M. D. LeVan, "CO_2 adsorption in Y and X zeolites modified by alkali metal cation exchange," *Microporous and mesoporous materials*, vol. 91, no. 1-3, pp. 78–84, 2006.

[23] A. Zukal, J. Pawlesa, and J. Čejka, "Isosteric heats of adsorption of carbon dioxide on zeolite MCM-22 modified by alkali metal cations," *Adsorption*, vol. 15, pp. 264–270, 2009.

[24] D. Newsome, S. Gunawan, G. Baron, J. Denayer, and M.-O. Coppens, "Adsorption of CO 2 and N 2 in Na–ZSM-5: effects of Na+ and Al content studied by Grand Canonical Monte Carlo simulations and experiments," *Adsorption*, vol. 20, pp. 157–171, 2014.

[25] M. Younas *et al.*, "Recent progress and remaining challenges in post-combustion CO_2 capture using metal-organic frameworks (MOFs)," *Progress in Energy and Combustion Science*, vol. 80, p. 100 849, 2020.

[26] M. Bui *et al.*, "Carbon capture and storage (CCS): the way forward," *Energy & Environmental Science*, vol. 11, no. 5, pp. 1062–1176, 2018.

[27] T. Ghanbari, F. Abnisa, and W. M. A. W. Daud, "A review on production of metal organic frameworks (MOF) for CO_2 adsorption," *Science of The Total Environment*, vol. 707, p. 135 090, 2020.

[28] Z. Yuan, M. R. Eden, and R. Gani, "Toward the development and deployment of large-scale carbon dioxide capture and conversion processes," *Industrial & Engineering Chemistry Research*, vol. 55, no. 12, pp. 3383–3419, 2016.

[29] J.-B. Lin *et al.*, "A scalable metal-organic framework as a durable physisorbent for carbon dioxide capture," *Science*, vol. 374, no. 6574, pp. 1464–1469, 2021.

[30] S. T. Inc. "Mof sorbent on a roll – a scalable solution for gigaton scale carbon capture." (2021), [Online]. Available: https://www.svanteinc.com/news/a-scalable-solution-for-carbon-capture/.

[31] P. Hovington, O. Ghaffari-Nik, L. Mariac, A. Liu, B. Henkel, and S. Marx, "Rapid cycle temperature swing adsorption process using solid structured sorbent for co2 capture from cement flue gas," in *Proceedings of the 16th Greenhouse Gas Control Technologies Conference (GHGT-16)*, 2022, pp. 23–24.

[32] S. T. Inc. "Svante secures commercial supply of mof advanced sorbent materials with basf for carbon capture market." (2023), [Online]. Available: https://www.svanteinc.com/news/svante-secures-commercial-supply-of-mof-advanced-sorbent-materials-with-basf-for-carbon-capture-market/.

[33] J. Abanades *et al.*, "Emerging CO_2 capture systems," *International Journal of Greenhouse Gas Control*, vol. 40, pp. 126–166, 2015.

[34] C. Dhoke, A. Zaabout, S. Cloete, and S. Amini, "Review on reactor configurations for adsorption-based CO_2 capture," *Industrial & Engineering Chemistry Research*, vol. 60, no. 10, pp. 3779–3798, 2021.

[35] Z. Liu, L. Wang, X. Kong, P. Li, J. Yu, and A. E. Rodrigues, "Onsite CO_2 capture from flue gas by an adsorption process in a coal-fired power plant," *Industrial & engineering chemistry research*, vol. 51, no. 21, pp. 7355–7363, 2012.

[36] W.-C. Yang and J. Hoffman, "Exploratory design study on reactor configurations for carbon dioxide capture from conventional power plants employing regenerable solid sorbents," *Industrial & Engineering Chemistry Research*, vol. 48, no. 1, pp. 341–351, 2009.

[37] F. Rezaei and P. Webley, "Structured adsorbents in gas separation processes," *Separation and Purification Technology*, vol. 70, no. 3, pp. 243–256, 2010.

[38] G. Mondino, C. A. Grande, R. Blom, and L. O. Nord, "Moving bed temperature swing adsorption for CO_2 capture from a natural gas combined cycle power plant," *International Journal of Greenhouse Gas Control*, vol. 85, pp. 58–70, 2019.

[39] T. Okumura, T. Ogino, S. Nishibe, Y. Nonaka, T. Shoji, and T. Higashi, "CO_2 capture test for a moving-bed system utilizing low-temperature steam," *Energy Procedia*, vol. 63, pp. 2249–2254, 2014.

[40] M. K. Verma, "Fundamentals of carbon dioxide-enhanced oil recovery (co 2-eor): A supporting document of the assessment methodology for hydrocarbon recovery using co 2-eor associated with carbon sequestration," US Geological Survey, Tech. Rep., 2015.

[41] R. Haghpanah, R. Nilam, A. Rajendran, S. Farooq, and I. A. Karimi, "Cycle synthesis and optimization of a VSA process for postcombustion CO_2 capture," *AIChE Journal*, vol. 59, no. 12, pp. 4735–4748, 2013.

[42] R. Haghpanah *et al.*, "Multiobjective optimization of a four-step adsorption process for postcombustion CO_2 capture via finite volume simulation," *Industrial & Engineering Chemistry Research*, vol. 52, no. 11, pp. 4249–4265, 2013.

[43] J. Zhang, P. A. Webley, and P. Xiao, "Effect of process parameters on power requirements of vacuum swing adsorption technology for CO_2 capture from flue gas," *Energy Conversion and Management*, vol. 49, no. 2, pp. 346–356, 2008.

[44] J. Zhang and P. A. Webley, "Cycle development and design for CO_2 capture from flue gas by vacuum swing adsorption," *Environmental science & technology*, vol. 42, no. 2, pp. 563–569, 2008.

[45] P. Xiao, J. Zhang, P. Webley, G. Li, R. Singh, and R. Todd, "Capture of CO 2 from flue gas streams with zeolite 13X by vacuum-pressure swing adsorption," *Adsorption*, vol. 14, pp. 575–582, 2008.

[46] A. Agarwal, L. T. Biegler, and S. E. Zitney, "A superstructure-based optimal synthesis of PSA cycles for post-combustion CO_2 capture," *AIChE journal*, vol. 56, no. 7, pp. 1813–1828, 2010.

[47] Z. Liu, C. A. Grande, P. Li, J. Yu, and A. E. Rodrigues, "Multi-bed vacuum pressure swing adsorption for carbon dioxide capture from flue gas," *Separation and Purification Technology*, vol. 81, no. 3, pp. 307–317, 2011.

[48] M. Ramezan *et al.*, "Carbon dioxide capture from existing coal-fired power plants," *National Energy Technology Laboratory, DOE/NETL Report*, vol. 401, p. 110 907, 2007.

[49] C. Song *et al.*, "Alternative pathways for efficient CO_2 capture by hybrid processes—A review," *Renewable and Sustainable Energy Reviews*, vol. 82, pp. 215–231, 2018.

[50] “Hybrid membrane-absorption CO_2 capture process, author=Freeman, Brice and Hao, Pingjiao and Baker, Richard and Kniep, Jay and Chen, Eric and Ding, Junyuan and Zhang, Yue and Rochelle, Gary T,” *Energy Procedia*, vol. 63, pp. 605–613, 2014.

[51] J. C. L. Y. Fong, C. J. Anderson, G. Xiao, P. A. Webley, and A. F. Hoadley, “Multi-objective optimisation of a hybrid vacuum swing adsorption and low-temperature post-combustion CO_2 capture,” *Journal of Cleaner Production*, vol. 111, pp. 193–203, 2016.

[52] B. Belaissaoui, Y. Le Moullec, D. Willson, and E. Favre, “Hybrid membrane cryogenic process for post-combustion CO_2 capture,” *Journal of Membrane Science*, vol. 415, pp. 424–434, 2012.

[53] H. Salih *et al.*, “Feed study for retrofitting holcim us cement facility with co2 capture plant using air liquide adsorption assisted cryogenic technology,” *Available at SSRN 4291335*, 2022.

[54] L. Plc. “Adsorption-based carbon capture.” (), [Online]. Available: https://www.linde-engineering.com/en/process-plants/adsorption-and-membrane-plants/adsorption-based-carbon-capture-and-co2-recovery/index.html?creative=674348543958&keyword=carbon%20capture%20linde&matchtype=b&network=g&device=c&utm_medium=paid&utm_source=Google+Ads&utm_campaign=HISELECT_ContactForm&utm_term=carbon%20capture%20linde&gad_source=1&gclid=Cj0KCQiAyKurBhD5ARIsALamXaEtFyu8F5h4B8DOW8pzQ
g2wJGSUaAheZEALw_wcB.

[55] S. G. Subraveti, S. Roussanaly, R. Anantharaman, L. Riboldi, and A. Rajendran, “Techno-economic assessment of optimised vacuum swing adsorption for post-combustion CO_2 capture from steam-methane reformer flue gas,” *Separation and Purification Technology*, vol. 256, p. 117 832, 2021.

[56] N. Susarla *et al.*, “Energy and cost estimates for capturing CO_2 from a dry flue gas using pressure/vacuum swing adsorption,” *Chemical Engineering Research and Design*, vol. 102, pp. 354–367, 2015.

[57] N. S. Wilkins and A. Rajendran, “Measurement of competitive co2 and n2 adsorption on zeolite 13x for post-combustion co2 capture,” *Adsorption*, vol. 25, no. 2, pp. 115–133, 2019.

[58] L. E. Perez, P. Sarkar, and A. Rajendran, “Experimental validation of multi-objective optimization techniques for design of vacuum swing adsorption processes,” *Separation and Purification Technology*, vol. 224, pp. 553–563, 2019.

[59] S. Krishnamurthy *et al.*, “CO_2 capture from dry flue gas by vacuum swing adsorption: a pilot plant study,” *AIChE Journal*, vol. 60, no. 5, pp. 1830–1842, 2014.

[60] M. Khurana and S. Farooq, “Integrated Adsorbent Process Optimization for Minimum Cost of Electricity Including Carbon Capture by a VSA Process,” *AIChE Journal*, vol. 65, no. 1, pp. 184–195, 2019.

[61] R. T. Maruyama, K. N. Pai, S. G. Subraveti, and A. Rajendran, "Improving the performance of vacuum swing adsorption based CO_2 capture under reduced recovery requirements," *International Journal of Greenhouse Gas Control*, vol. 93, p. 102 902, 2020.

[62] M. Haaf, R. Anantharaman, S. Roussanaly, J. Ströhle, and B. Epple, "CO_2 capture from waste-to-energy plants: Techno-economic assessment of novel integration concepts of calcium looping technology," *Resources, Conservation and Recycling*, vol. 162, p. 104 973, 2020.

[63] K. Gerdes, W. M. Summers, and J. Wimer, "Quality Guidelines for Energy System Studies: Cost Estimation Methodology for NETL Assessments of Power Plant Performance," National Energy Technology Laboratory (NETL), Pittsburgh, PA, Morgantown, WV ..., Tech. Rep., 2011.

[64] D. Danaci, M. Bui, N. Mac Dowell, and C. Petit, "Exploring the limits of adsorption-based CO 2 capture using MOFs with PVSA–from molecular design to process economics," *Molecular Systems Design & Engineering*, vol. 5, no. 1, pp. 212–231, 2020.

[65] K. T. Leperi, R. Q. Snurr, and F. You, "Optimization of two-stage pressure/-vacuum swing adsorption with variable dehydration level for postcombustion carbon capture," *Industrial & Engineering Chemistry Research*, vol. 55, no. 12, pp. 3338–3350, 2016.

[66] S. O. Gardarsdottir *et al.*, "Comparison of technologies for CO_2 capture from cement production—Part 2: Cost analysis," *Energies*, vol. 12, no. 3, p. 542, 2019.

[67] S. Roussanaly, R. Anantharaman, and C. Fu, "Low-carbon footprint hydrogen production from natural gas: A techno-economic analysis of carbon capture and storage from steam-methane reforming," 2020.

[68] S. Roussanaly, R. Anantharaman, K. Lindqvist, H. Zhai, and E. Rubin, "Membrane properties required for post-combustion CO_2 capture at coal-fired power plants," *Journal of membrane science*, vol. 511, pp. 250–264, 2016.

[69] E. W. Lemmon, I. H. Bell, M. L. Huber, and M. O. McLinden, *NIST Standard Reference Database 23: Reference Fluid Thermodynamic and Transport Properties-REFPROP, Version 10.0, National Institute of Standards and Technology*, 2018. DOI: https://doi.org/10.18434/T4/1502528. [Online]. Available: https://www.nist.gov/srd/refprop.

[70] S. F. Westman *et al.*, "Vapor–liquid equilibrium data for the carbon dioxide and nitrogen (CO_2+ N_2) system at the temperatures 223, 270, 298 and 303 K and pressures up to 18 MPa," *Fluid Phase Equilibria*, vol. 409, pp. 207–241, 2016.

[71] S. Lasala, P. Chiesa, R. Privat, and J.-N. Jaubert, "VLE properties of CO_2–Based binary systems containing N_2, O_2 and Ar: Experimental measurements and modelling results with advanced cubic equations of state," *Fluid Phase Equilibria*, vol. 428, pp. 18–31, 2016.

[72] D.-Y. Peng and D. B. Robinson, "A new two-constant equation of state," *Industrial & Engineering Chemistry Fundamentals*, vol. 15, no. 1, pp. 59–64, 1976.

[73] J. Theis, "Quality Guidelines for Energy Systems Studies: Cost Estimation Methodology for NETL Assessments of Power Plant Performance - Feb 2021," Feb. 2021. DOI: 10.2172/1567736. [Online]. Available: https://www.osti.gov/biblio/1567736.

[74] W. L. Luyben, "Estimating refrigeration costs at cryogenic temperatures," *Computers & Chemical Engineering*, vol. 103, pp. 144–150, 2017.

[75] N. B. R. Anantharaman O. Bolland, "D1.4.3 European best practice guidelines for assessment of CO_2 capture technologies (DECARBit project)," 2011. [Online]. Available: https://www.sintef.no/globalassets/project/decarbit/d-1-4-3_euro_bp_guid_for_ass_CO$_{2}$_cap_tech_280211.pdf.

Appendix A: Unconstrained optimization results for PVSA process

A.1 For 13 mol % : Three objective Optimizations for PVSA Process

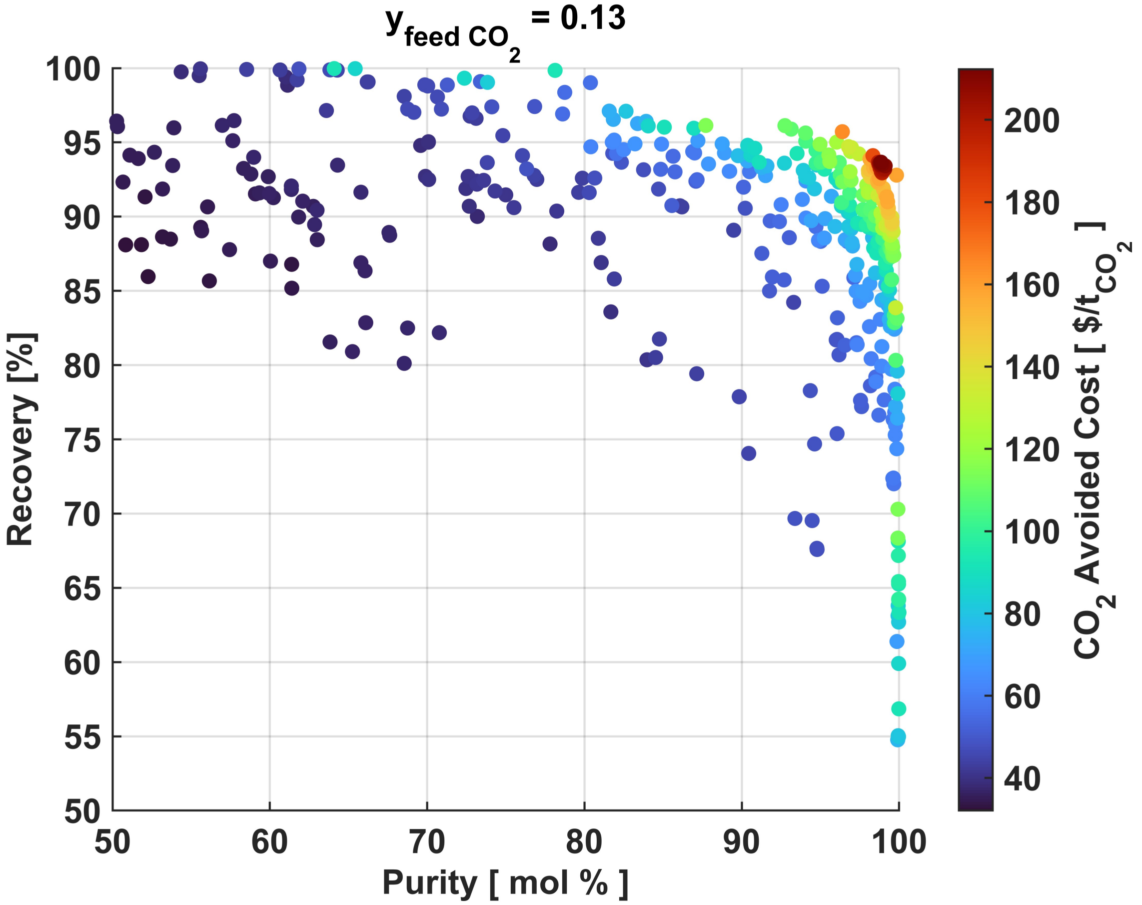

Figure A.1: Unconstrained optimization results for minimizing capture cost while maximizing purity and recovery with Zeolite 13X adsorbent

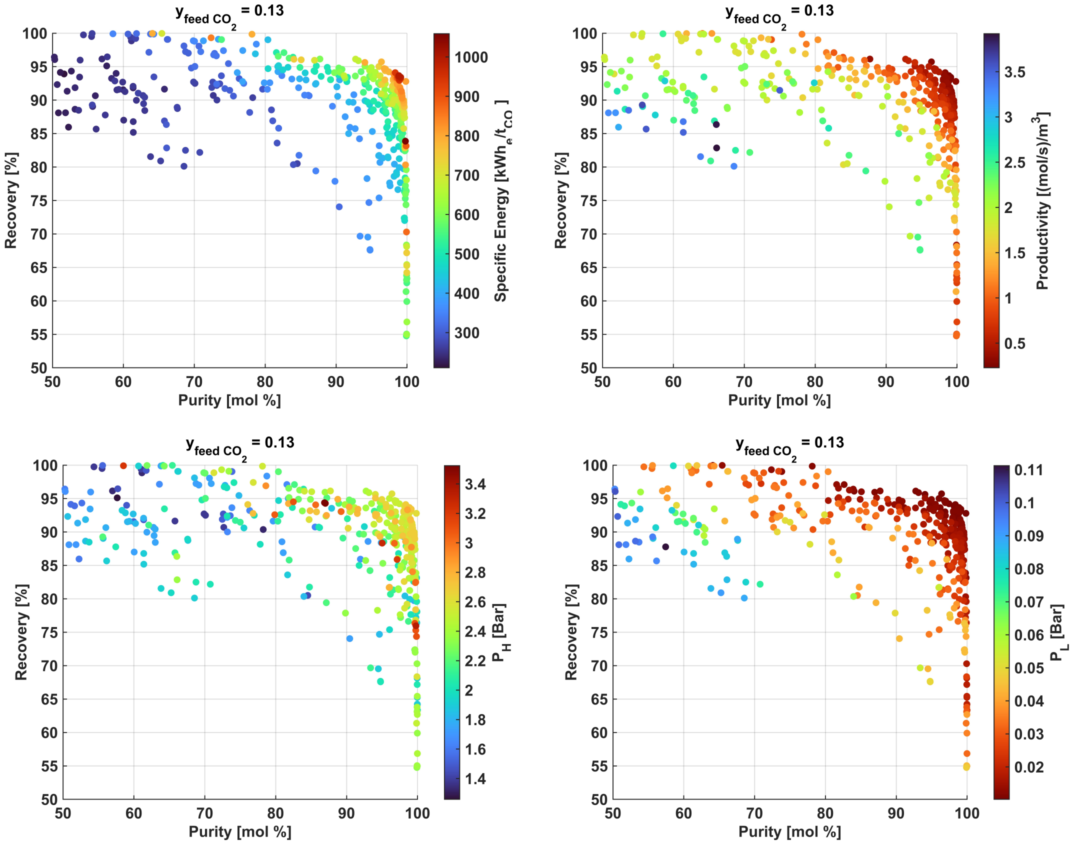

(c) P_H - Adsorption Pressure

(d) P_L - Evacuation Pressure

Figure A.2: Specific Energy Consumption, Productivity, adsorption pressure and desorption pressure corresponding to the data points in Fig. A.1

A.2 For 20 mol % : Three objective Optimizations for PVSA Process

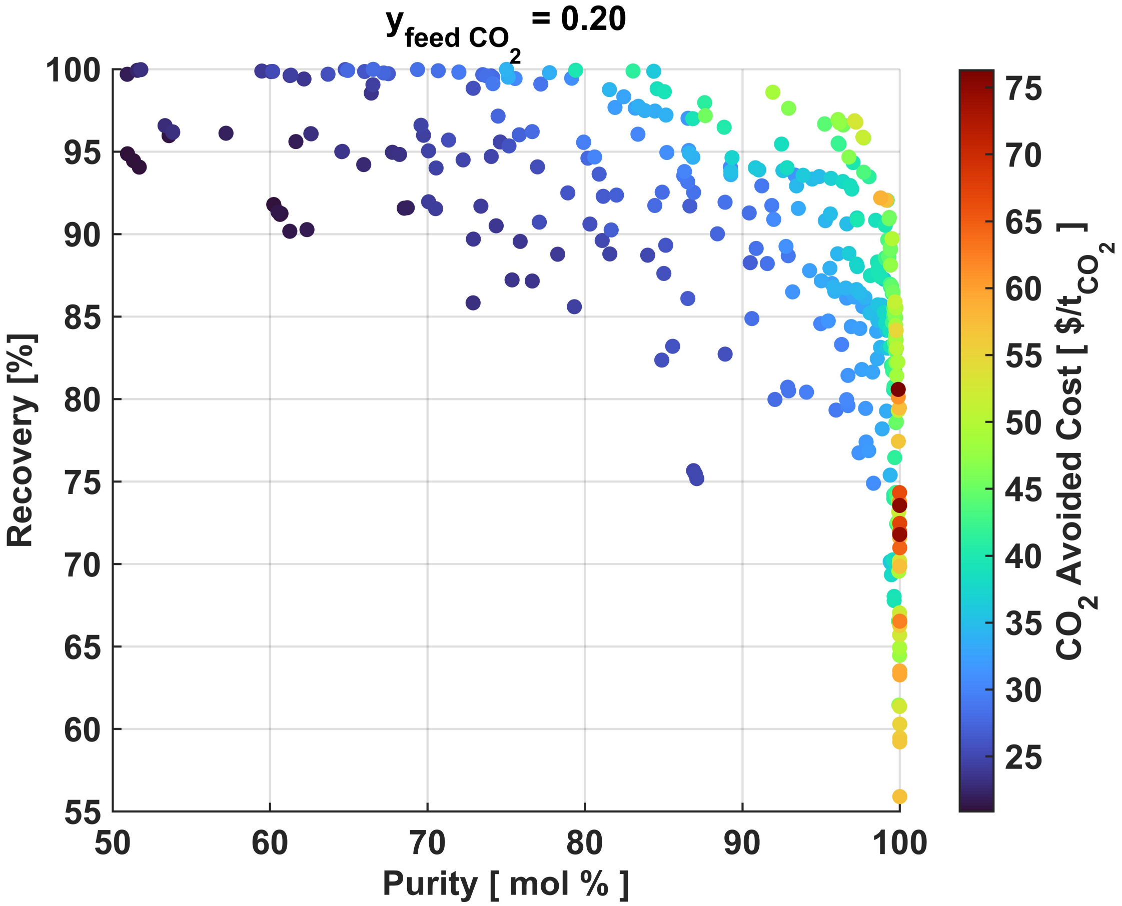

Figure A.3: Unconstrained optimization results for minimizing capture cost while maximizing purity and recovery with Zeolite 13X adsorbent

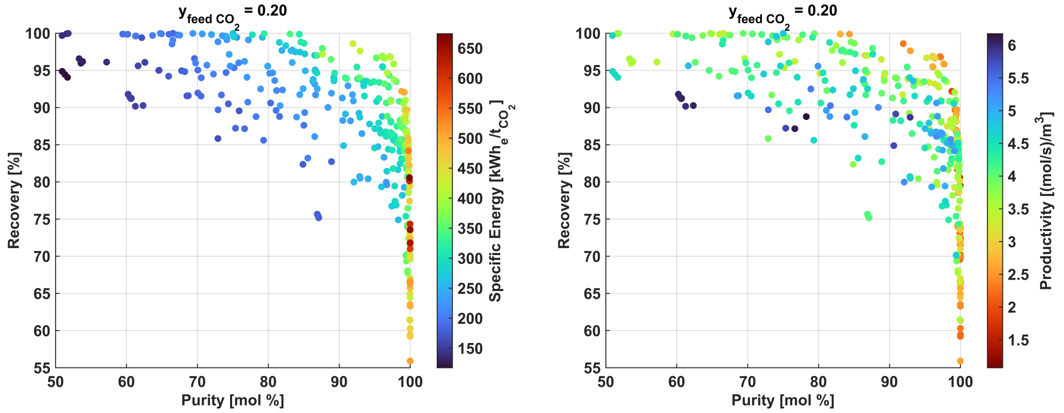

(a) Specific Energy Consumption (b) Productivity

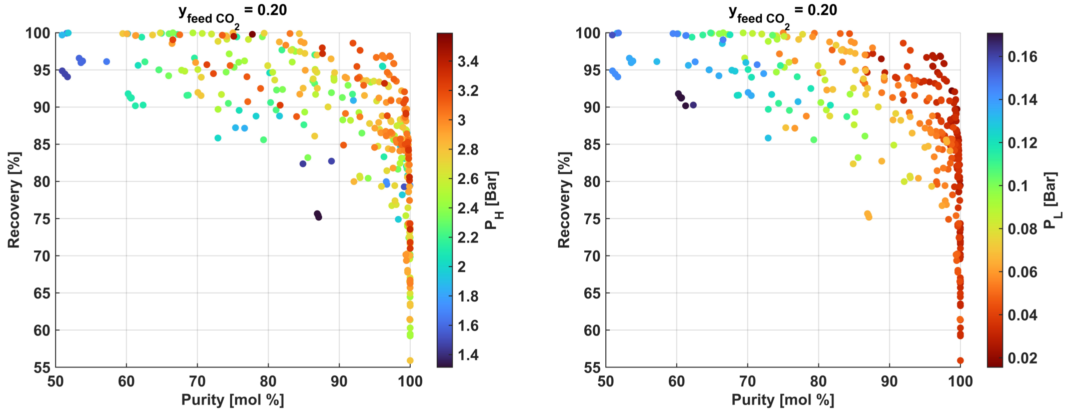

(c) P_H - Adsorption Pressure (d) P_L - Evacuation Pressure

Figure A.4: Specific Energy Consumption, Productivity, adsorption pressure and desorption pressure corresponding to the data points in Fig. A.3

A.3 For 30 mol % : Three objective Optimizations for PVSA Process

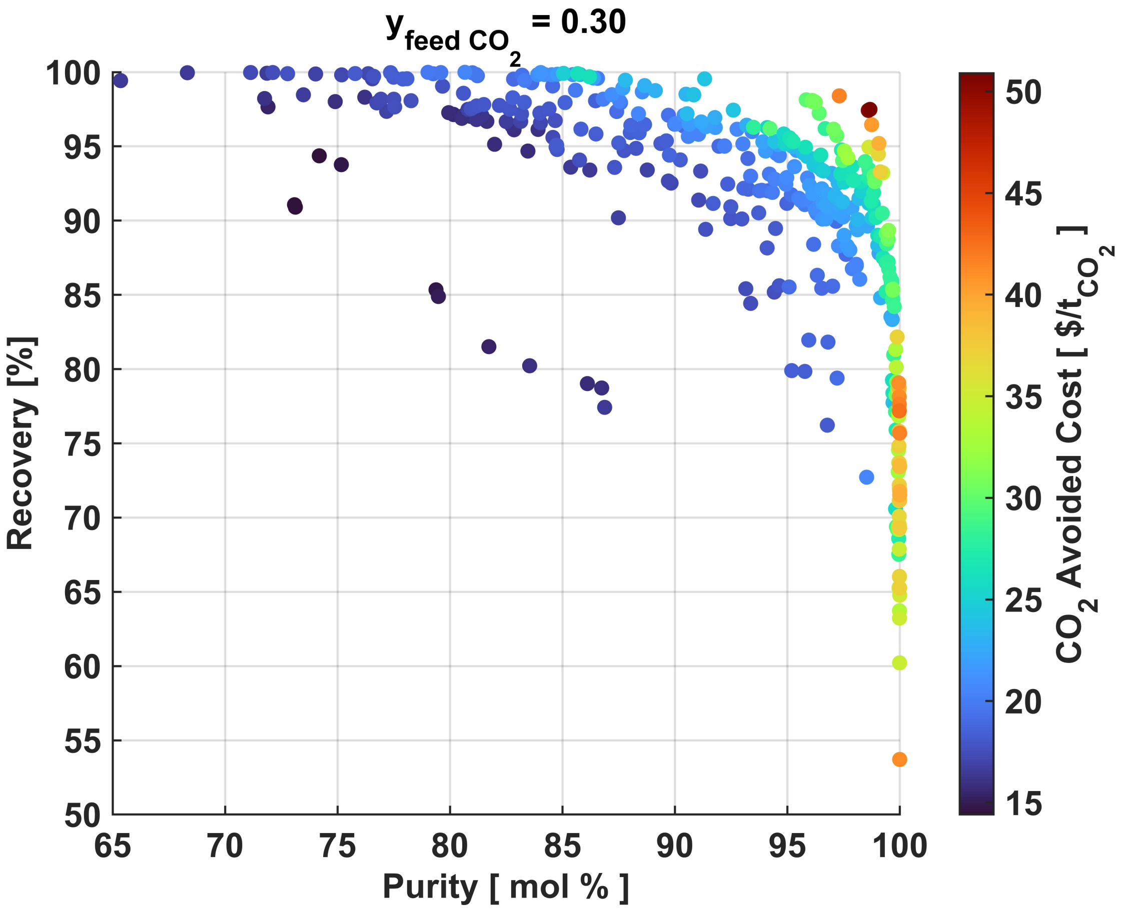

Figure A.5: Unconstrained optimization results for minimizing capture cost while maximizing purity and recovery with Zeolite 13X adsorbent

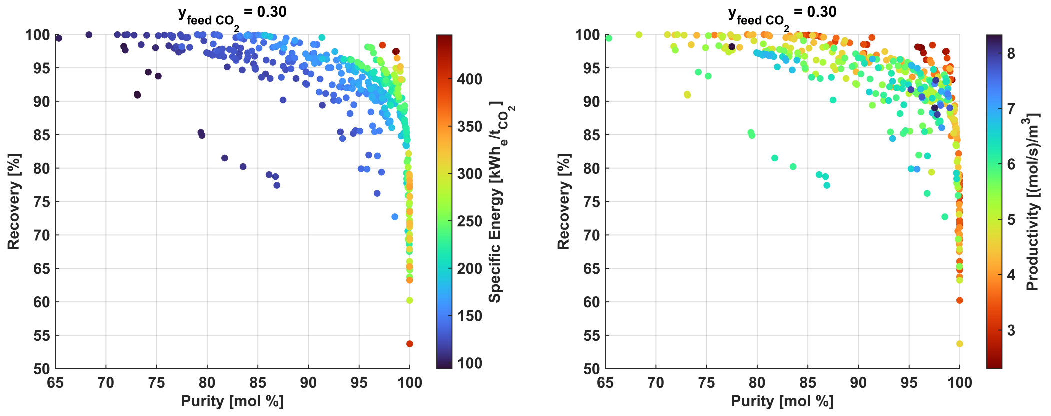

(a) Specific Energy Consumption (b) Productivity

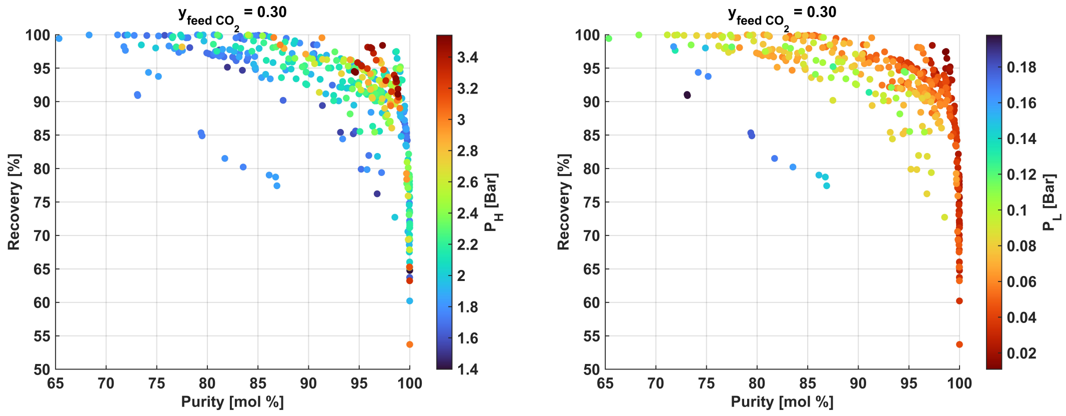

(c) P_H - Adsorption Pressure (d) P_L - Evacuation Pressure

Figure A.6: Specific Energy Consumption, Productivity, adsorption pressure and desorption pressure corresponding to the data points in Fig. A.5

Appendix B: PVSA performance under reduced purity constraints

B.1 7.5 mol % feed composition

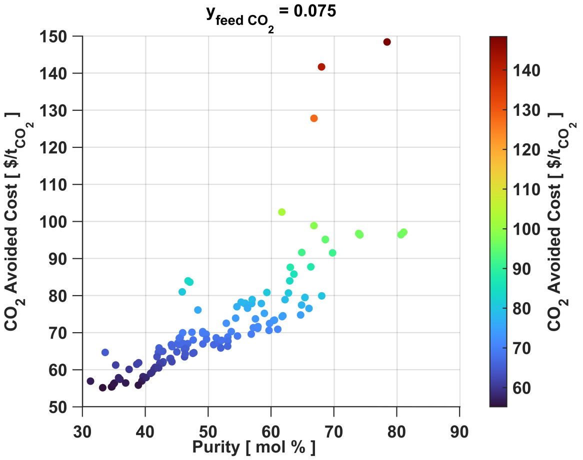

(a) CO_2 avoided cost

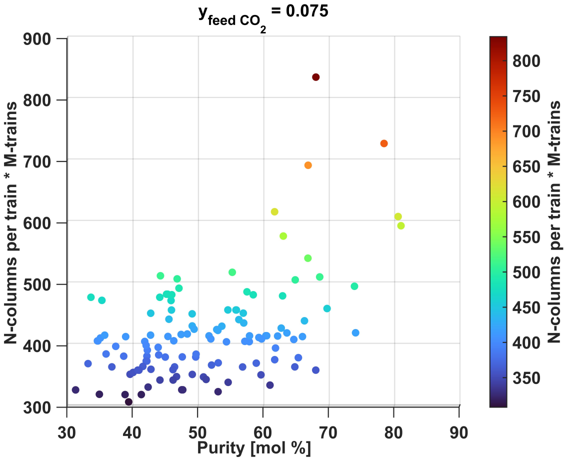

(b) Total columns in the PVSA unit

Figure B.1: Optimization results for minimizing capture cost under reduced purity constraints with Zeolite 13X adsorbent

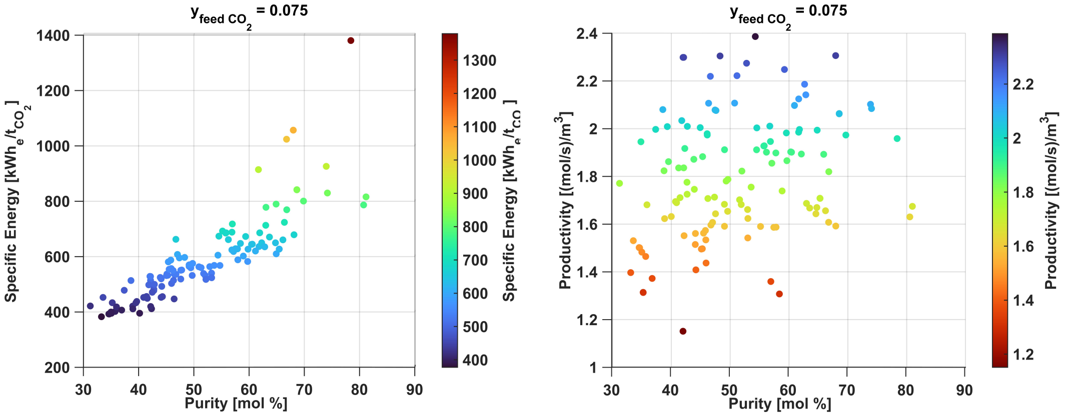

(a) Specific Energy Consumption (b) Productivity

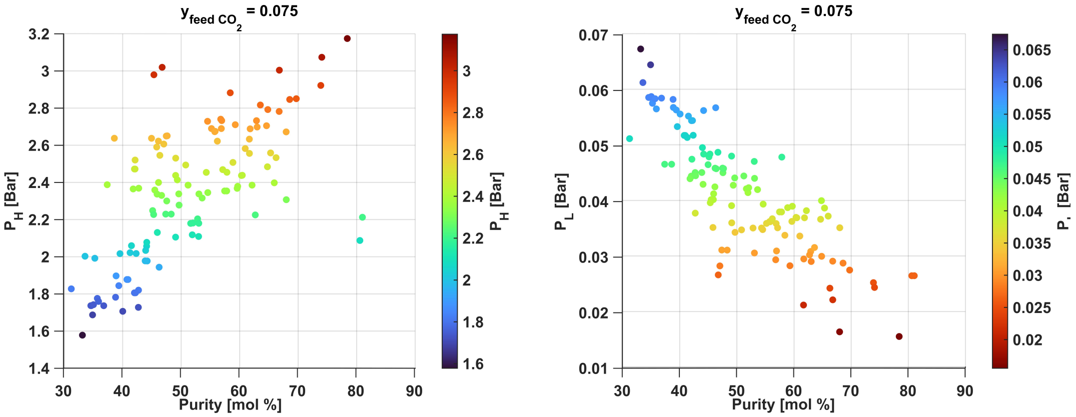

(c) P_H - Adsorption Pressure (d) P_L - Evacuation Pressure

Figure B.2: Specific Energy Consumption, Productivity, adsorption pressure and desorption pressure corresponding to the data points in fig. B.1

B.2 20 mol % feed composition

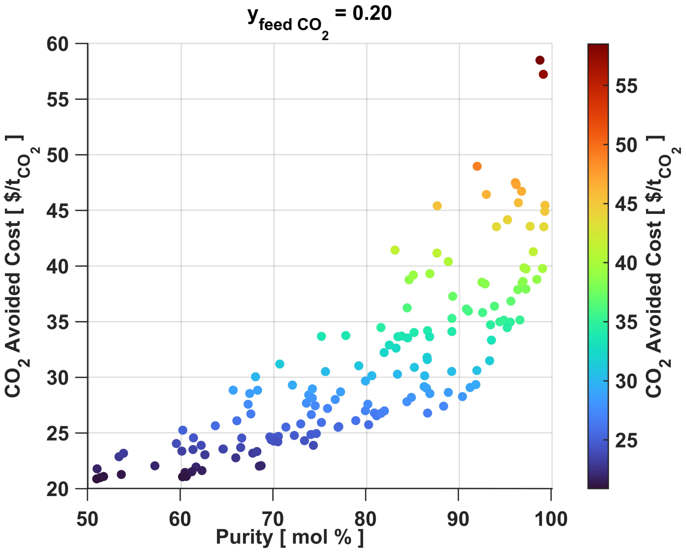

(a) CO_2 avoided cost

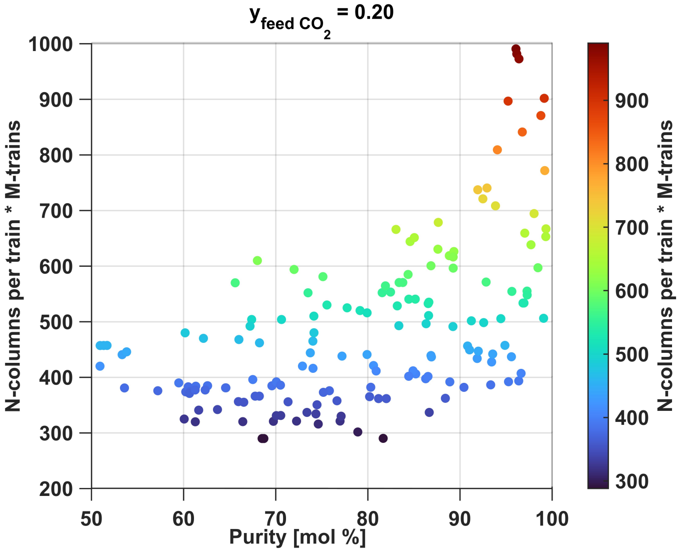

(b) Total Number of Columns in the PVSA unit

Figure B.3: Optimization results for minimizing capture cost under reduced purity constraints with Zeolite 13X adsorbent

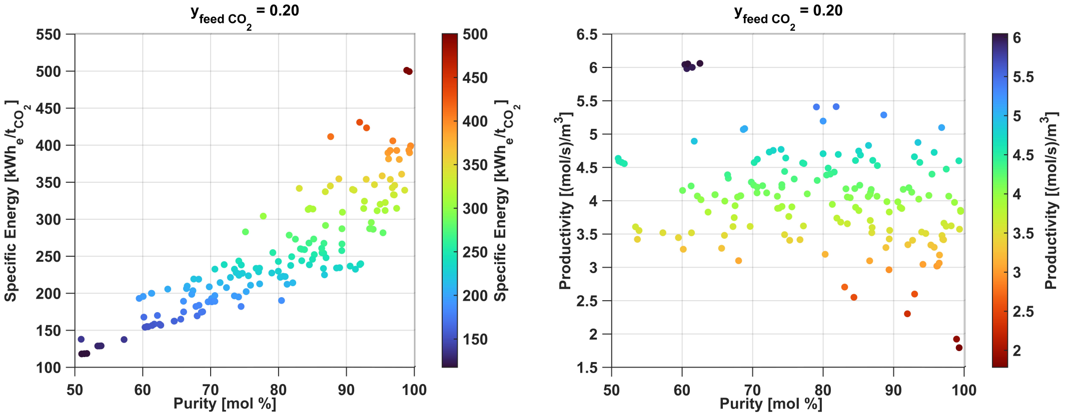

(a) Specific Energy Consumption (b) Productivity

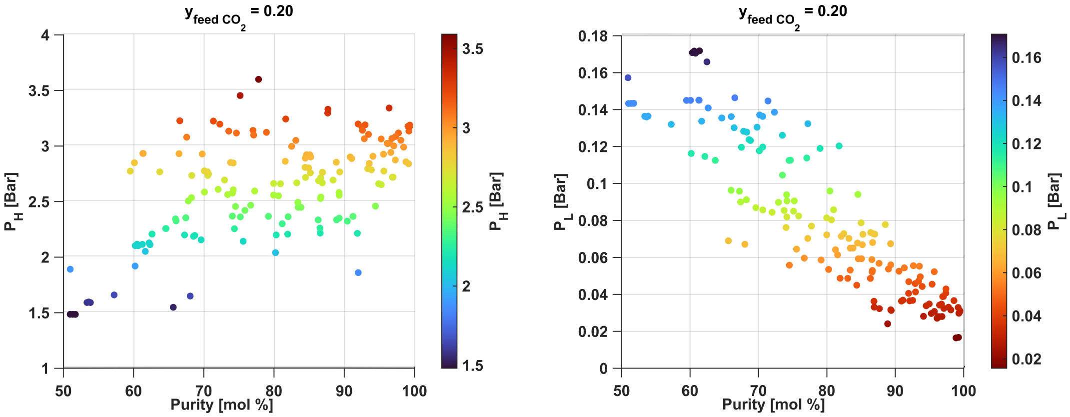

(c) P_H - Adsorption Pressure (d) P_L - Evacuation Pressure

Figure B.4: Specific Energy Consumption, Productivity, adsorption pressure and desorption pressure corresponding to the data points in fig. B.3

B.3 30 mol % feed composition

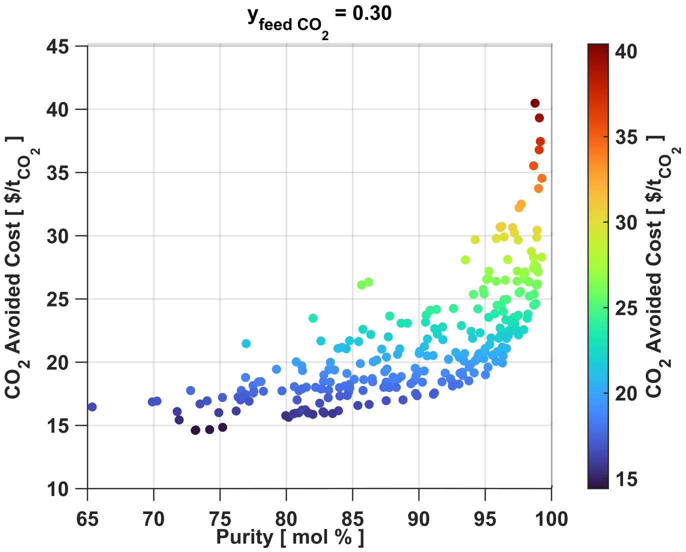

(a) CO_2 avoided cost

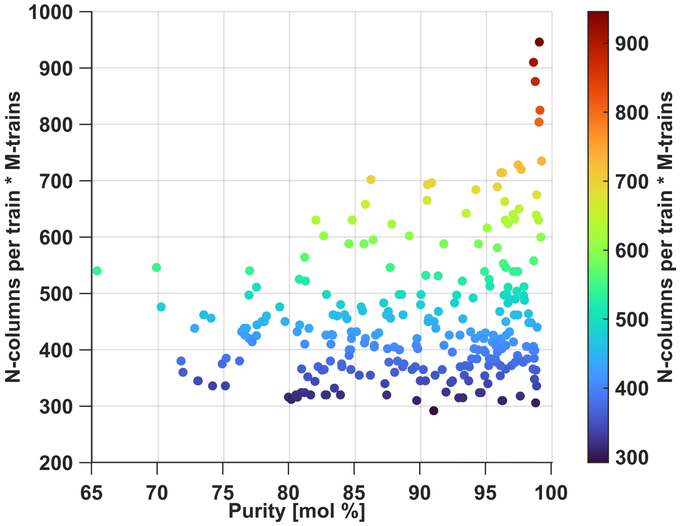

(b) Total Number of Columns in the PVSA unit

Figure B.5: Optimization results for minimizing capture cost under reduced purity constraints with Zeolite 13X adsorbent

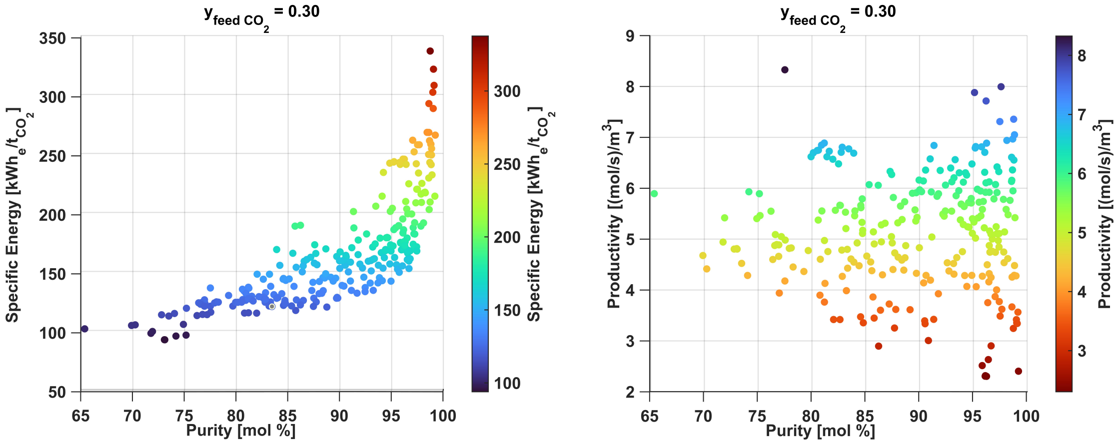

(a) Specific Energy Consumption

(b) Productivity

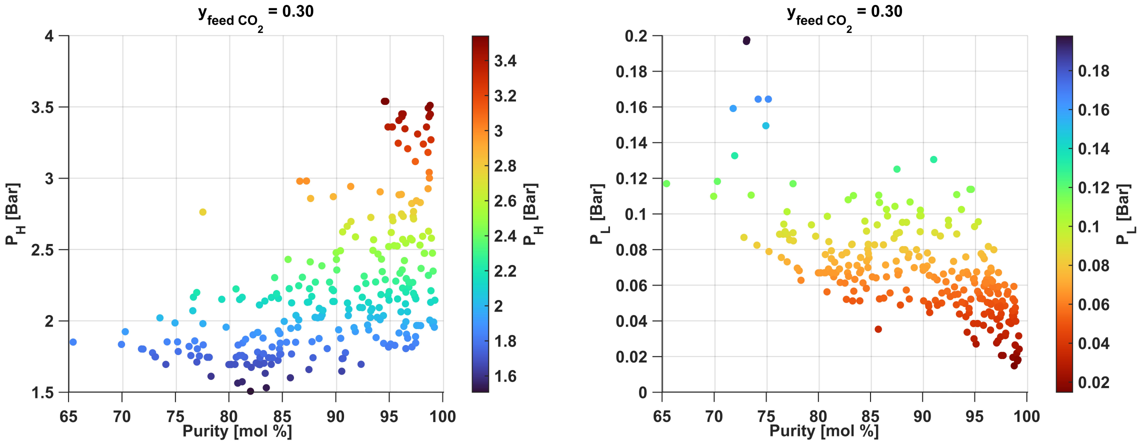

(c) P_H - Adsorption Pressure

(d) P_L - Evacuation Pressure

Figure B.6: Specific Energy Consumption, Productivity, adsorption pressure and desorption pressure corresponding to the data points in Fig. B.5